Master of Science Thesis

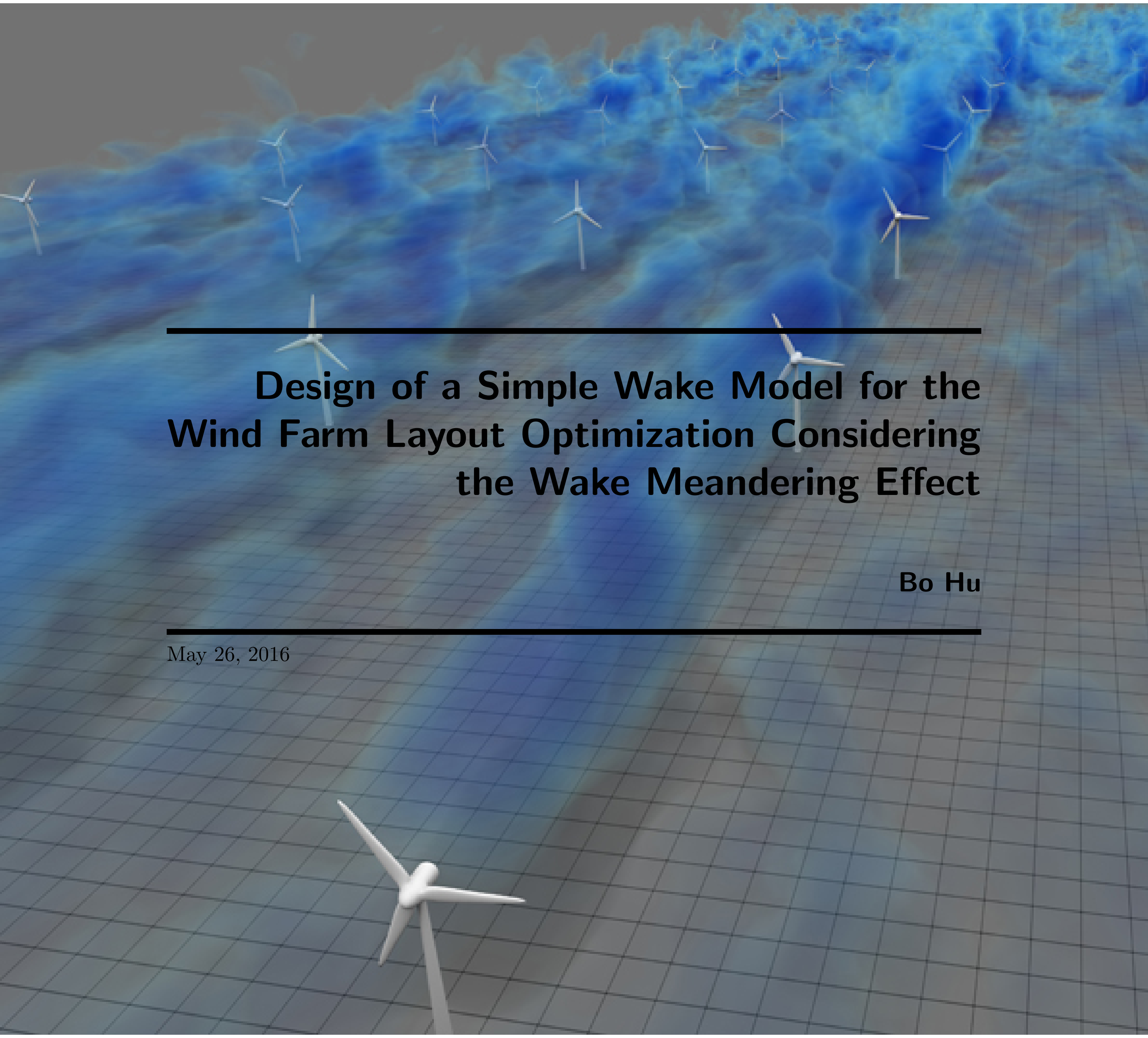

Design of a Simple Wake Model for the Wind Farm Layout Optimization Considering the Wake Meandering Effect

Bo Hu

May 26, 2016

Faculty of Aerospace Engineering · Delft University of Technology

TU Delft Delft University of Technology

Challenge the future

Design of a Simple Wake Model for the Wind Farm Layout Optimization Considering the Wake Meandering Effect

Master of Science Thesis

For obtaining the degree of Master of Science in Aerospace Engineering at Delft University of Technology

Bo Hu

May 26, 2016

Faculty of Aerospace Engineering · Delft University of Technology

Delft University Of Technology
Department Of
Aerodynamcis and Wind Energy

It is recommended to the Faculty of Aerospace Engineering for acceptance a thesis entitled **"Design of a Simple Wake Model for the Wind Farm Layout Optimization Considering the Wake Meandering Effect"** by **Bo Hu** in partial fulfillment of the requirements for the degree of **Master of Science**.

Dated: May 26, 2016

Head of department: ______________________
Prof. Dr. Ir. G. van Bussel

Supervisor: ______________________
Dr. Ir. M. Zaaijer

Reader: ______________________
Dr. Ir. C. J. Simao Ferreira

Reader: ______________________
Dr. Ir. A. H. van Zuijlen

Abstract

The design of the optimal layout of the wind farm is crucial to minimize the cost of energy produced by the wind farm. This requires an accurate wake model to simulate the wake effect on the annual energy yield of the wind farm. On the other hand, the wake model must be very simple in order to limit the duration of the layout optimization process. The initial purpose of this Master thesis project is to develop an improved (simple) wake model for the wind farm layout optimization considering the wake meandering effect. With this purpose, a dynamic wind farm wake model which incorporates the wake meandering motion in the time domain is first developed. Since the dynamic wind farm wake model is very computationally expensive, it is not suitable for the wind farm layout optimization. However, it is discovered with the dynamic wind farm wake model that the wake meandering has very insignificant effect on the annual energy yield of the wind farm. Hence, it is concluded that it is not meaningful to develop such simple wake model that considers the wake meandering effect on the wind farm annual energy yield.

Acknowledgements

I would like to sincerely express my gratitude to my supervisor Dr. Ir. Michiel Zaaijer. His great sense of responsibility, excellent management skill, triggering guidance and care to his students are the keys for me to finishing my thesis successfully. In addition, he has set a perfect example to me as a professional.

Special thanks to Sebastian Sanchez Perez Moreno for generously sharing me the code of his wind farm wake models, which has given me inspirations and ideas in developing my own wind farm wake models.

Many thanks to Dr. Ir. Wim Bierbooms, who helped me with the development of the model used for generating and filtering the atmospheric turbulence velocity.

Finally, I would like to thank my family and friends. They are the constant source of my joy and my strength to overcome the difficulties all the way in this unforgettable journey.

Delft, The Netherlands — Bo Hu
May 26, 2016

Contents

List of Figures

List of Tables

Nomenclature

Latin Symbols

α	wind direction
β	wind farm orientation
ΔC_T	change in the thrust coefficient of the wind turbine due to wake meandering
ΔE_a	change in the annual energy yield of the wind farm/turbine due to wake meandering
Δl	distance between the two spatial points
ΔP	change in the power output of the wind turbine due to wake meandering
ΔU	Velocity deficit in the wake
κ	Von Kármán constant
Λ_1	scale parameter of the longitudinal turbulence
$\overline{uv}$	Reynolds averaged shear stress (Ainslie model)
ρ	air density at the hub height
σ_1	standard deviation of the turbulence velocity component in the longitudinal direction
σ_2	standard deviation of the turbulence velocity component in the lateral direction
σ_3	standard deviation of the turbulence velocity component in the vertical direction
σ_u	standard deviation of the Gaussian-like velocity deficit profiles (BP model)
σ_y	standard deviation of the wake center position in the lateral direction
σ_z	standard deviation of the wake center position in the vertical direction
A	swept area of the wind turbine rotor

a	axial induction factor
a_f	annuity factor
A_s	shadowed area of the wake on the rotor
A_w	cross-sectional area of the wake
C_a	scale parameter of the Weibull distribution
C_{Decom}	decommissioning cost of the wind farm
C_{inv}	total investment cost of the wind farm
C_k	shape parameter of the Weibull distribution
C_{OM}	annual cost for the maintenance and operation of the wind farm
C_T	thrust coefficient of the wind turbine
Coh	coherence function of the turbulence velocity components
D	diameter of the rotor of the wind turbine
D_w	diameter of the wake
dA_j	area of the rotor area element
$E_{a,dynamic}$	annual energy yield of the wind farm/turbine calculated with the dynamic wind farm wake model (with wake meandering)
$E_{a,static}$	annual energy yield of the wind farm/turbine calculated with the static wind farm wake model (no wake meandering)
E_a	annual energy yield of the wind farm
f	frequency in the auto-power spectrum of the atmospheric turbulence velocity
f_c	cut-off frequency of the filter
f_s	sampling frequency
F_T	thrust force of the rotor
$freq$	probability density of wind occurrence
h_H	hub height
I	(total) turbulence intensity
I_+	added turbulence intensity
I_0	ambient turbulence intensity
k	wake decay coefficient
k^*	wake growth rate (BP model)
L_1	turbulence velocity component integral scale parameter in the longitudinal direction
L_2	turbulence velocity component integral scale parameter in the lateral direction
L_3	turbulence velocity component integral scale parameter in the vertical direction
LPC	levelized production cost of the wind farm
N	total number of turbines in the wind farm
N_θ	number of the area elements in the azimuthal direction for the discretization of the rotor

N_r	number of the area elements in the radial direction for the discretization of the rotor
N_t	number of time step in the simulation
P	power output of the wind turbine
$P_{dynamic,avg}$	time-averaged power output of the wind turbine considering wake meandering
P_{static}	power of the wind turbine without considering wake meandering
r	distance/coordinate in the radial direction
R_0	radius of the rotor
r_i	real interest rate
R_w	radius of the wake
s	normalized downstream distance
$S_k(f)$	auto-power spectral density
T	total time of simulation
t	time instant
t_0	initial time
T_a	total time per year
T_e	economic lifetime of the wind farm
U	wind speed in the axial/longitudinal direction
U_0	ambient (free-stream) wind speed at hub height
U_{ci}	cut-in wind speed
U_{co}	cut-out wind speed
$U_{eq,P}$	Equivalent incoming wind speed for the calculation of the wind turbine power output
$U_{eq,T}$	Equivalent incoming wind speed for the calculation of the wind turbine thrust coefficient
U_{eq}	Equivalent incoming wind speed
U_i	wind speed at turbine i
$U_{k,i}$	wind speed in the wake of turbine k at turbine i
V	radial velocity (Ainslie model)
v	filtered turbulence velocity component in the lateral direction
v_n	unfiltered turbulence velocity component in the lateral direction
w	filtered turbulence velocity component in the vertical direction
w_n	unfiltered turbulence velocity component in the vertical direction
x	distance/coordinate in the axial/longitudinal (downstream) direction
y	distance/coordinate in the lateral direction
z	distance/coordinate in the vertical direction
z_0	surface roughness length

Chapter 1

Introduction

1.1 Background Information

A wind turbine wake is a long trail of turbulent wind exiting the turbine with diminished wind speed [13]. In a wind farm where arrays of wind turbines are placed in a cluster, the inflow of some downwind turbines may be affected by the wakes of the turbines upwind and thus have a reduced wind speed. This deficit in the inflow wind speed of the downwind turbines may further lead to a reduction in their power production. Therefore, the total energy output of the wind farm is generally less than the total energy output of the same amount of solitary turbines at the same location with undisturbed inflow conditions. Such loss of energy yield in a wind farm is called wake loss, and it is one of the most significant energy losses for a wind farm.

By placing the wind turbines in different layouts, the turbines will be influenced differently by the wakes of the other turbines in the farm, thus leading to different degrees of wake losses. However, the layout of the wind farm also influences other factors such as the total length of the electrical cables, which is closely related to the electrical losses and the costs of cable installation. Therefore, taking all the influences into account, the optimal layout is to be found during the design phase of a wind farm. A wake model that describes the characteristics of the wake is employed to calculate the wake losses for the optimization of the wind farm layout. Since extensively many different layouts need to be assessed during the optimization, the wake model for the purpose of wind farm layout optimization is required to be not only accurate, but also computationally inexpensive.

1.2 Problem Analysis

Thus far, a handful of categories of wind farm wake models with varying degrees of complexity have been developed. It is generally believed that the models based on solving the full/filtered form of Navier-Stokes equations (hereafter referred to as “the CFD models”) provide the most comprehensive and accurate simulation results. However, the CFD models are also the most complex models that are not suitable for the layout optimization. Instead, the wake models based on simplified aerodynamic equations and empirical relations (hereafter referred to as "the simple models") are commonly used, which simulate the wake effect in a less accurate but much faster manner. Therefore, it would be of great significance to improve the accuracy of these simple models without largely increasing their complexity.

A possible way to do so is by adding the wake meandering effect to the existing simple wake models. As discussed by Bingöl[5] and Trujillo[39], wake meandering is an observed unsteady phenomena that the whole wake oscillates randomly (both laterally and vertically) during its advection downstream. Such behavior of the wake not only influences the loading (mainly in fatigue) of the downstream wind turbines [29], but also causes fluctuation in the power production of the downstream turbines [9]. Yet, at the moment all the well-known simple wake models only attempt to compute the wake speed deficit and wake size expansion, leaving the effect of wake meandering unaccounted for. In order to fill this gap, this Master thesis project aims to design a simple wake model suitable for the wind farm layout optimization while taking the effect of the wake meandering into account. The design of such wake model is not initiated completely from scratch. Instead, the strategy of the design is to study the wake meandering effect in the wind farm and incorporate it with the suitable existing simple wake model. Since in general the objective of wind farm layout optimization is to minimize the *cost of energy*, only the effect of the wake meandering on the *energy production* is considered in this project. The influence of the wake meandering on the wind turbine loading is therefore not in the scope of this thesis.

1.3 Objectives and Methodology

As mentioned in Section 1.2, the main purpose of this thesis is to improve the existing simple wake model used for wind farm layout optimization with wake meandering effect. A straightforward approach is to develop a *dynamic wind farm wake model* by integrating an existing simple wake model with the Dynamic Wake Meandering Model [30]. The dynamic wind farm wake model simulates the wake meandering motion and calculates the wake effect in the wind farm in every instant of the time frame. Therefore, due to the high computational cost, it is not suitable for the wind farm layout optimization. Instead, the ideal solution is to design a *simplified wind farm wake model* which accounts for the *time-averaged* wake meandering effect (hereafter referred to as "simplified wake meandering model").

Owing to the required time-averaging process of the wake meandering effect, the design of the simplified wake meandering model is very tricky. Therefore, for the following reasons, the dynamic wind farm wake model is first developed before the design of the simplified wake meandering model. First of all, it is very crucial to know whether the simplified wake meandering model is really needed. Although the wake meandering causes fluctuation in the power production of the downstream wind turbines, it is unknown how significant this has an influence on the annual energy yield of the wind farm. In this regard, the wake meandering effect on the annual energy yield of the wind farm can be studied with the dynamic wind farm wake model. If the study shows that the wake meandering effect on the wind farm annual energy yield is very insignificant, then there will be no need for the design of the simplified wake meandering model. Secondly, if there is the need to design the simplified wake meandering model, the wake meandering effect studied with the dynamic wind farm wake model can be used as a good design basis. Finally, the dynamic wind farm wake model can be used for the verification of the simplified wake meandering model.

In summary, the first objective of this thesis project is to develop a dynamic wind farm wake model considering the wake meandering effect. Then the second objective is to study the wake meandering effect on the wind farm annual energy yield with this dynamic wind farm wake model. If the wake meandering effect on the annual energy yield is considerable, the third objective is to design a simplified wake meandering model for the wind farm layout optimization.

1.4 Thesis Outline

In Chapter 2, the background of wind farm layout optimization is covered. Then an overview of the wake models for single turbines are presented in Chapter 3. Since the velocity distribution in the wake calculated from the selected wake model is non-uniform, the method to compute the *equivalent velocity* which is in turn used for calculating the power output and thrust coefficient of the turbine is described in Chapter 4. Subsequently, the dynamic wake meandering model which simulates the meandering motion of a single wake is developed in Chapter 5. In order to extend the scope of the study from a turbine in a single wake to a wind farm, the wind farm wake model which incorporates the interactions of multiple wakes and the meandering of the wakes is developed in Chapter 6. With this wind farm wake model, the wake meandering effect on the wind farm annual energy yield is studied in Chapter 7. It is found that the wake meandering has little effect on the wind farm annual energy yield. Hence, the simplified wake meandering model is not designed and the conclusions are drawn in Chapter 8.

Chapter 2

Overview of Wind Farm Layout Optimization

In this chapter, an overview of the wind farm layout optimization will be presented. Firstly, the objective function of the optimization is shortly discussed. Subsequently, the method to calculate the annual energy yield of the wind farm is illustrated. The purpose of this chapter is to identify the link between the wake model and the wind farm layout optimization.

2.1 Objective Function

The optimization process starts with defining the objective function. It is the criterion that the wind farm has to minimise or maximise to be considered optimal. The most commonly used objective functions are *Cost of Energy*, *Energy Production*, *Profit* or a combination of them [36]. The thesis project is intended to work on an existing layout optimization tool (MZ tool [42]), which uses the *Cost of Energy* as the objective function.

Cost of Energy, defined as the cost per kWh of energy produced, takes into account both the energy output of the wind farm and the cost of the installation, maintenance, operation and disposal [36]. Different definitions of the term *Cost of Energy* are presented by different sources. MZ tool uses the levelized production cost (LPC), defined as

$$LPC = \frac{C_{inv}}{a_f \cdot E_a} + \frac{C_{OM}}{E_a} + \frac{C_{Decom}(1+r_i)^{-T_e}}{a_f E_a} \tag{2.1}$$

where C_{inv} is the total investment cost, C_{OM} is the annual cost for the maintenance and operation, C_{Decom} is the decommissioning cost of the wind farm, a_f is the annuity factor, E_a is the annual energy yield, r_i is the real interest rate, and T_e is the economic lifetime of the wind farm [31].

The advantage of using the LPC as the Cost of Energy is that it has accounted for the interest rate and inflation over the whole life time of the wind farm (reflected by the annuity factor). LPC represents the “actualized” cost of energy at the present time.

Hence, in order to minimize the LPC, the annual energy yield of the wind farm and the costs of the wind farm (C_{inv}, C_{OM} and C_{Decom}) need to be calculated. The calculation of the wind farm costs can be achieved with various cost models, but it is not in the scope of this thesis project. Instead, the thesis project gives emphasis on the calculation of the wind farm annual energy yield.

2.2 Calculation of Annual Energy Yield

2.3 Introduction

According to Equation 2.1, the annual energy yield needs to be calculated in order to calculate the LPC. Determined by the wind conditions, the annual energy yield is strongly affected by the wind turbine wakes and therefore the layout of the wind farm. Hence, it is crucial to know how to calculate E_a. This section first describes the calculation of the annual energy yield of a solitary turbine (Section 2.3.1), and then extend the scope to a wind farm (Section 2.3.2).

2.3.1 Annual Energy Yield of a Solitary Turbine

Since the wind farm is composed of a group of solitary wind turbines, it is useful to know how to calculate the annual energy yield of a solitary turbine before extending to the whole wind farm.

The generated power of a wind turbine (P) is a function of the wind speed at hub-height (U). For a specific type of wind turbine, this relation is generally given by the power curve. An example of the power curve is shown in Figure 2.1.

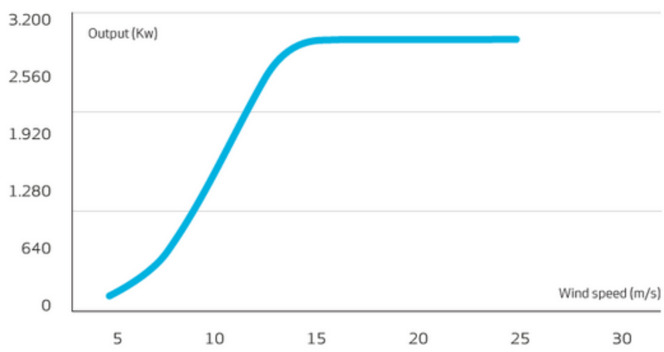

Figure 2.1: The power curve of Vestas V90 [40]

Besides the power curve, the probability density function of the hub-height wind speed at the located site (denoted as $freq(U)$) is required for the calculation. This is usually represented by the Weibull distribution

$$freq(U) = \frac{C_k}{C_a}\left(\frac{U}{C_a}\right)^{C_k-1} \cdot e^{-\left(\frac{U}{C_a}\right)^{C_k}} \tag{2.2}$$

where C_a is the scale parameter and C_k is the shape parameter. These two parameters are determined in such a way that the Weibull distribution fits the histogram of the wind speed distribution obtained from the measurement, as shown in Figure 2.2.

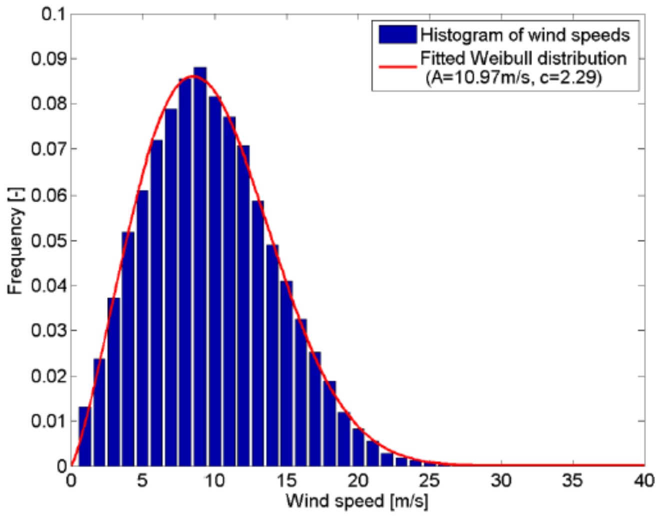

Figure 2.2: The fitted Weibull distribution and the measured wind speed [14]

Finally, the annual energy yield of a wind turbine can be calculated by

$$(E_a)_{turbine} = T_a \int_{U_{ci}}^{U_{co}} P(U) \cdot freq(U) dU \tag{2.3}$$

where T_a is the total time per year, U_{ci} and U_{co} are the cut-in wind speed[1] and cut-out wind speed[2], respectively.

2.3.2 Annual Energy Yield of a wind farm

When it comes to the wind farm, the situation becomes more complicated due to the influences of the wind turbine wakes in the farm. For a given layout, different wind speeds (U) and wind directions (α) will cause different scenarios of wake incidents in the wind farm, leading to different total power production. For this reason, the two-dimensional wind rose has to be taken into account.

As shown in Figure 2.3, a two-dimensional wind rose depicts the probability distribution of the wind speed over the wind direction (denoted as $freq(U, \alpha)$). The wind speed in the wind rose is seen as the undisturbed wind speed in the free stream. The wind speed

[1] The wind speed above which the wind turbine starts to generate power.
[2] The wind speed above which the wind turbine shuts down.

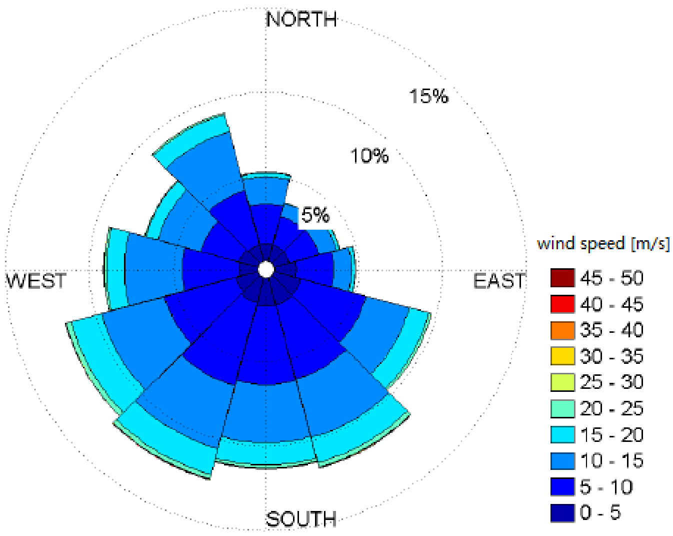

Figure 2.3: An Example of two-dimensional wind rose [14]

within the wind farm shall be calculated by the chosen wake model, with the undisturbed wind speed as an input. Therefore, for a given wind direction and undisturbed wind speed, the actual wind speed 'felt' by the different turbines in the wind farm are different. The power production of each wind turbine in this particular scenario (undisturbed wind speed and direction) can thus be obtained from the power curve. Once the undisturbed wind speed or the wind direction is changed, it becomes a new scenario. Yet, the method to compute the power production of each wind turbine is the same as described. In order to calculate the annual energy yield of the wind farm, all the scenarios have to be taken into account, as can be seen in Equation 2.4.

$$(E_a)_{farm} = T_a \int_{0^\circ}^{360^\circ} \int_{u_{ci}}^{u_{co}} \left(\sum_{i=1}^{N} P_i(U, \alpha) \right) \cdot freq(U, \alpha) \; dU d\alpha \tag{2.4}$$

In this equation, $P_i(U, \alpha)$ is the electrical power of the i-th turbine under the scenario where the undisturbed wind speed is U and the wind direction is α. N is the total number of turbines in the wind farm. T_a is the total time per year. If a dynamic model is used, the annual energy yield of the wind farm can also be calculated using a more general expression:

$$(E_a)_{farm} = \int_0^{T_a} \sum_{i=1}^{N} P_i(t) \; dt, \tag{2.5}$$

where $P_i(t)$ is the electrical power of the i-th turbine at time t. The value of $P_i(U, \alpha)$ in Equation 2.4 and $P_i(t)$ in Equation 2.5 are closely related to the wind farm layout and the wake model chosen for the calculation. Hence, the wake model plays an important role in the wind farm layout optimization.

Chapter 3

Models for Single Wake

3.1 Background

As mentioned in Section 1.3, a dynamic wind farm model which incorporates an existing simple wake model with dynamic wake meandering needs to be developed in this thesis project (the first objective). Therefore, a survey of different simple wake models has been made in the literature study [21] to investigate their suitability for being the basis of the design of the dynamic wind farm wake model. According to the literature study [21], the kinematic wake model developed by Bastankhah and Porté-Agel (hereafter referred to as “the BP model”) is believed to be the most suitable choice. Yet, it is still necessary to present a short overview of the popular wake models in this chapter to provide some background information to the readers.

The simple wake models are classified into two categories (i.e. kinematic models and field models) and are briefly introduced in Section 3.2 and 3.3, respectively. In Section 3.4, the selected simple wake model for this project is presented in detail.

3.2 Kinematic Models

3.2.1 Overview of Kinematic Models

The kinematic models are also known as the explicit models. The origin of the name “explicit models” comes from the fact that the kinematic models calculate the wake expansion and velocity deficit *explicitly* from the analytical expressions, which are derived based on the mass/momentum conservation and turbulence mixing [24] [12]. The kinematic models use self-similar velocity profiles determined semi-empirically [18]. In spite of the simplicity of these models, reasonably accurate results can be obtained if the model parameters are appropriately selected [24]. Based on the chronological order, the major kinematic wake models are Jensen-Katic model [22][23], Larsen model [26][28], Frandsen model [15] and the new analytical model recently proposed by Bastankhah and Porté-Agel

[4]. Because of their simplicity and low computational cost, the kinematic models have been used extensively [12].

3.2.2 Jensen-Katic Model

This model (hereafter referred to as "Jensen model") was initially proposed by N.O. Jensen [22], and further developed by Katic [23]. Implemented in the commercial software WAsP by Risø, this model is also known as the Park model.

Jensen model is essentially built on the mass conservation of the flow. It neglects the near wake region, and assumes that the far wake (turbulent wake) starts directly after the rotor. Furthermore, the model assumes a linear expansion of the wake diameter and a constant velocity deficit across the wake (known as the "top-hat" profile). In order to calculate the wake velocity profile, Jensen model requires incoming wind velocity, thrust coefficient of the turbine, and wake decay coefficient as the inputs of the model. An example of wake velocity profile calculated with Jensen model is shown in Figure 3.1.

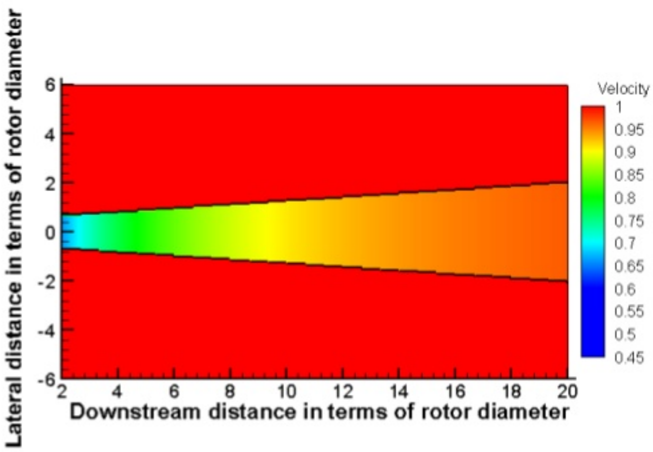

Figure 3.1: Example of wake velocity profile calculated with Jensen model [38]. The "velocity" in the figure is the wind/wake velocity normalized by the free-stream wind velocity.

3.2.3 Larsen Model

This model was initially proposed by Larsen in [26] and [28]. Neglecting the wind shear and thermal effects, and assuming that the wake flow is stationary, incompressible and axisymmetric, Larsen model describes the wake by Prandtl's turbulent boundary layer equations. In Larsen model, the velocity profile over the wake cross-section is not constant but a self-similar polynomial function of the radial distance. Furthermore, Larsen model suggests that the expansion of the wake radius along the downstream direction is proportional to the power of $\frac{1}{3}$ of the downstream distance.

An example of wake velocity profile calculated with Larsen model is shown in Figure 3.2. In order to calculate the wake velocity profile, Larsen model requires incoming wind velocity, thrust coefficient of the turbine, rotor diameter, turbine hub height, and the ambient turbulence intensity as the inputs of the model.

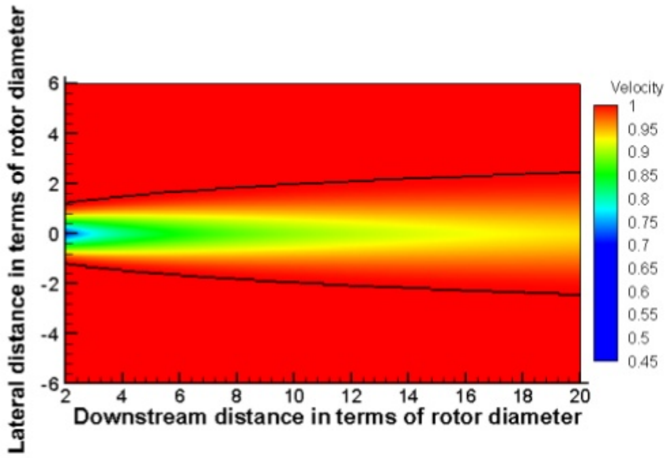

Figure 3.2: Example of wake velocity profile calculated with Larsen model [38]. The "velocity" in the figure is the wind/wake velocity normalized by the free-stream wind velocity.

3.2.4 Frandsen Model

This wake model developed by Frandsen [15] handles the wind farms with specific requirements in their layout:

- A rectangular array geometry with straight rows of wind turbines
- Equidistant spacing between units in each row and equidistant spacing between rows
- Wind direction parallel to the rows

From the upstream end to the downstream end, Frandsen model divides the wind turbine arrays into three regimes as shown in Figure 3.3. The first regime (marked by the green box) is the regime where the turbines are exposed to the multiple wakes. The second regime (marked by the magenta circle) starts when the multiple wakes from neighbouring rows merge and the wakes can only expand vertically upwards (considering the ground as another limitation for the expansion). The third regime (marked by the blue arrows) materializes in the *very large* wind farm where the flow is in balance with the planetary boundary layer. Among the three regimes, Frandsen only derived the analytical models for the wake velocity deficit and wake radius expansion in the *first regime*.

The governing equation for the single-wake model is based on the momentum conservation of the flow in a cylindrical control volume around the wind turbine rotor while neglecting the flow acceleration, pressure force, turbulent shear and gravity. Similar to Jensen model, Frandsen model also assumes a constant velocity profile across the wake. As for the wake expansion, Frandsen model suggests the wake radius to grow in proportion to the power of $\frac{1}{3}$ of the downstream distance, but in different expression compared to Larsen model.

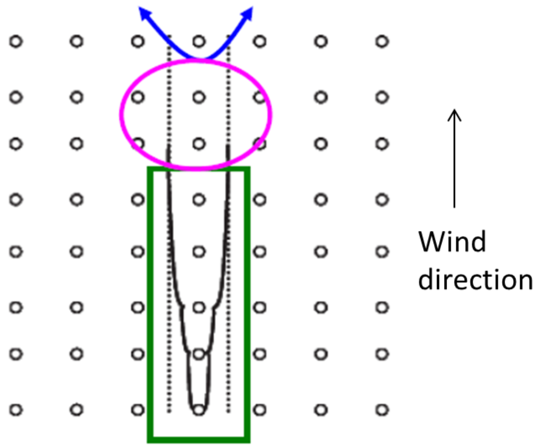

Figure 3.3: Illustration of the regimes of the Frandsen model (modified from [19])

An example of wake velocity profile calculated with Frandsen model is shown in Figure 3.4. In order to calculate the wake velocity profile, Frandsen model requires incoming wind velocity, thrust coefficient of the turbine, wake decay coefficient and rotor diameter as the inputs of the model.

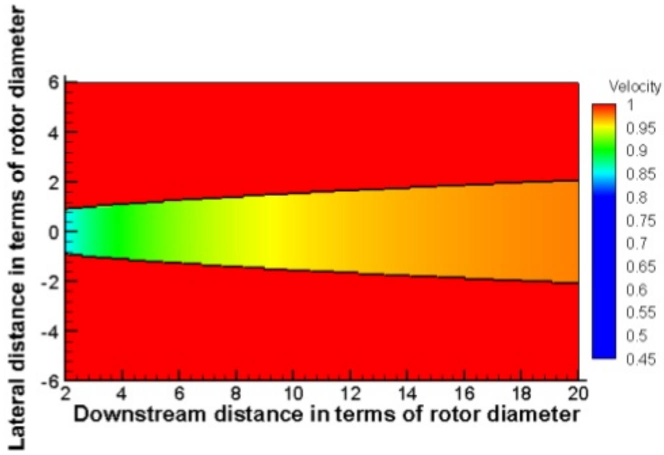

Figure 3.4: Example of wake velocity profile calculated with Frandsen model [38]. The "velocity" in the figure is the wind/wake velocity normalized by the free-stream wind velocity.

3.3 Field Model

3.3.1 Overview of Field Models

Field models, also known as the implicit models, are developed based on approximations of either the Navier-Stokes or vorticity transport equations [18]. In order to solve the differential equations, the field models have to calculate the flow properties numerically at every point of the flow field using a specific marching scheme. Therefore, the field models require a substantially larger calculation power than the kinematic models. However, by making appropriate simplifying assumptions, their requirements can be well within the capabilities of modern computers, not only in the case of single wake but also for multiple wakes occurring in a wind farm [12]. In this section the most commonly used field model, namely the Ainslie model is presented.

3.3.2 Ainslie Model (Eddy Viscosity Model)

Ainslie [2] developed this wake model based on the continuity equation and simplified Navier-Stokes equation[1]. In order to obtain the wind velocity components (U, V) in the defined field containing the wake, these two equations must be solved simultaneously. However, due to the extra unknown namely the Reynolds-averaged shear stress ($\overline{uv}$) in the simplified Navier-Stokes equation, one more equation is needed. The essence of Ainslie Model is expressing the ($\overline{uv}$) by the eddy viscosity, and finally expressing the eddy viscosity by an empirical equation in terms of U. Therefore, Ainslie model is also known as Eddy Viscosity model.

Ainslie model envisaged that the solution (U, V) starts from 2D downstream of the rotor, where the pressure gradient is no longer dominant in the flow[2]. Furthermore, Ainslie model assumes the velocity deficit in the wake cross-section to be of Gaussian distribution. Since U and V are computed in the complete field, the boundary between the wake and the ambient wind is not clearly defined.

An example of wake velocity profile calculated with Ainslie model is shown in Figure 3.5. It should be noted that the wake in Figure 3.5 starts from 0D instead of 2D downstream of the turbine, which is considered to be an error in [37].

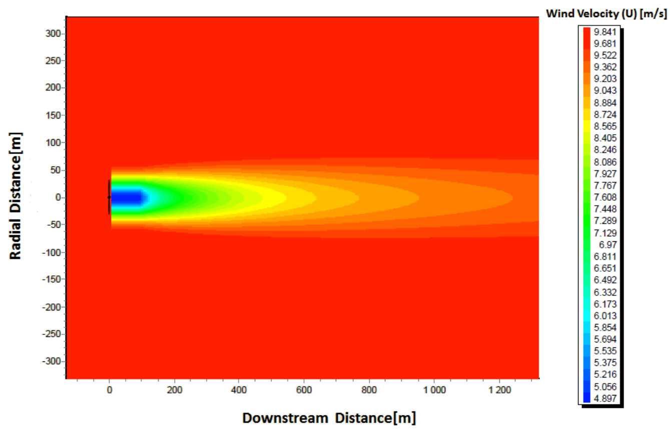

Figure 3.5: Example of wake velocity profile calculated with Ainslie model [37].

[1]The assumptions that are used to simplify the Navier-Stokes equation can be found in the literature study [21]

[2]Neglecting the pressure gradient is one of the assumptions used to simplify the Navier-Stokes equation

3.4 The selected wake model: BP Model

3.4.1 Selection of the wake model

The validation and comparisons of the wake models have been studied by the author in the literature study [21] before the thesis project. According to the literature study, the BP model is selected as the basis to design the required wake model which accounts for the wake meandering effect. The reason is threefold. First, being a kinematic model, the BP model is very computationally inexpensive. Second, the BP model is believed to have very high accuracy in modelling the velocity deficit of the wake. Last but not the least, it is rather easy to implement the BP model in the programming software since it has closed-form solution.

3.4.2 Theory of the BP Model

Presented in the Wake Conference 2015, this model developed by Bastankhah and Porté-Agel [4] is the latest analytical wake model up-to-date. Similar to Frandsen model, the BP model is also derived from the simplified[3] momentum equation:

$$F_T = \int_{A_w} \rho U (U_0 - U) dA_w, \tag{3.1}$$

where F_T is the thrust force of the rotor, A_w is the wake cross-sectional area, U_0 and U are the ambient wind speed and wind speed in the wake, respectively.

However, instead of assuming a uniform velocity profile in the wake cross-section, the BP model considers an axisymmetric Gaussian distribution for the velocity *deficit* in the wake. This is justified by the fact that the (approximately) Gaussian shape of the velocity deficit has been observed in the far wake region by wind tunnel measurements (e.g. [7, 32]), numerical solutions (e.g. [41]) and data from the operating wind farms (e.g. [17, 34]). Furthermore, the Gaussian distribution is self-similar, hence it can lead to a closed-form solution of Equation 3.1. The normalized velocity deficit in the wake is described as

$$\frac{\Delta U}{U_0} = C(x) e^{-\frac{r^2}{2\sigma_u^2}}, \tag{3.2}$$

where $C(x)$ represents the maximum normalized velocity deficit at each downwind location which occurs at the center of the wake, r is the radial distance from the center of the wake, and σ_u is the standard deviation of the Gaussian-like velocity deficit profiles at each axial distance x.

In the meanwhile, the thrust force (F_T) can be expressed by the thrust coefficient (C_T) with the following equation:

$$F_T = \frac{1}{2} C_T \rho A U_0^2, \tag{3.3}$$

where A is the rotor swept area and ρ is the air density at the hub height.

[3] The flow acceleration, pressure force, turbulent shear and gravity, the conservation of momentum in the axial direction are neglected

Substituting Equation 3.3 and 3.2 into Equation 3.1, and integrating from 0 to ∞ yields

$$8\left(\frac{\sigma_u}{D}\right)^2 C(x)^2 - 16\left(\frac{\sigma_u}{D}\right)^2 C(x) + C_T = 0. \tag{3.4}$$

Therefore, $C(x)$ is solved from Equation 3.4:

$$C(x) = 1 - \sqrt{1 - \frac{C_T}{8\left(\sigma_u/D\right)^2}}. \tag{3.5}$$

It should be noted that the other solution which yields wake velocity higher than the free-stream velocity is abandoned. Considering the wake radius as $2\sigma_u$, the BP model uses linear expansion of the wake:

$$\frac{\sigma_u}{D} = k^* \frac{x}{D} + \varepsilon, \tag{3.6}$$

where k^* is the wake growth rate and ε is equivalent to the value of $\frac{\sigma_u}{D}$ as x approaches zero. Inserting Equation 3.5 and 3.6 into Equation 3.2, the final analytical expression for the wake velocity deficit can be obtained:

$$\frac{\Delta U}{U_0} = \left(1 - \sqrt{1 - \frac{C_T}{8\left(k^* x/D + \varepsilon\right)^2}}\right) \cdot exp\left\{-\frac{1}{2\left(k^* x/D + \varepsilon\right)^2}\left(\frac{r}{D}\right)^2\right\}, \tag{3.7}$$

By equating the total mass flow between the BP model and Frandsen model (since they are derived from the same governing equations) and applying empirical correction factor, ε is found to be:

$$\varepsilon = 0.2\sqrt{\gamma}, \tag{3.8}$$

with γ given in Equation 3.9:

$$\gamma = \frac{1}{2} \cdot \frac{1 + \sqrt{1 - C_T}}{\sqrt{1 - C_T}} \tag{3.9}$$

Based on the LES result, Niayifar and Porté-Agel [33] proposed the following empirical equation for the range of conditions ($0.065 < I_0 < 0.15$) to calculate the wake growth rate:

$$k^* = 0.3837I + 0.003678, \tag{3.10}$$

where I_0 is the ambient turbulence intensity and I is the *local* turbulence intensity at the turbine rotor. The turbulence model for the wind farm optimization will be described in detail in Section 6.2.3.

3.4.3 Implementation of the BP Model

The BP model for the single wake is implemented in MATLAB. In order to obtain the wake velocity profile $U(x,r)$ for a turbine located in the free-stream, the normalized wind velocity deficit in the wake $\frac{\Delta U(x,r)}{U_0}$ is first calculated from the BP model. As can be seen from Section 3.4.2, $\frac{\Delta U(x,r)}{U_0}$ is not only a function of spatial coordinates (x,r), but also dependent on parameters[4] C_T, I_0 and D. For a specific wind turbine, the thrust coefficient C_T is generally a known function of the incoming wind speed[5], as shown in Figure 3.6.

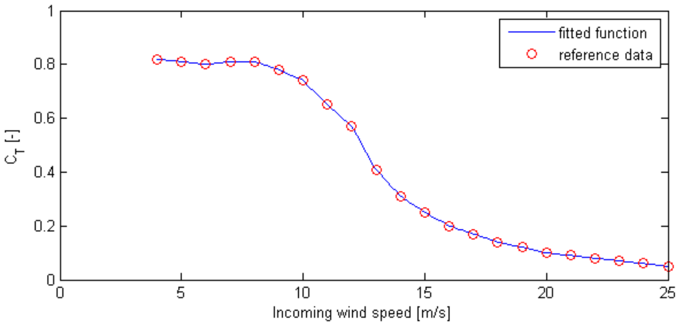

Figure 3.6: The relation between C_T and the incoming wind speed for the turbine Vestas V80. The fitted function is the linear interpolation of the reference data [20].

Using the C_T - U_0 relation depicted in Figure 3.6 and the parameters shown in Table 3.1, the normalized wind velocity deficit in the wake is calculated and shown in Figure 3.7 as an example.

Parameter	Value	Unit
I_0	0.1	$[-]$
D	80	$[m]$
U_0	10	$[m/s]$
Δx	1.6	$[m]$
Δr	0.4	$[m]$

Table 3.1: Parameters used to calculate the wind velocity deficit in the wake

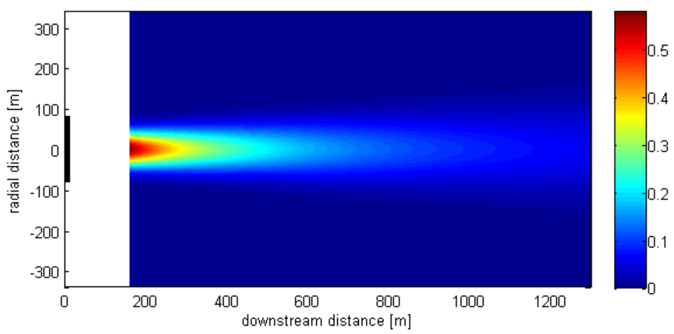

Figure 3.7: Normalized wind velocity deficit in the wake (top view), calculated using the BP model. The black bar represents the rotor of the turbine.

[4]According to Equation 3.9 and 3.8, γ and ε are dependent on C_T. According to Equation 3.10, k^* is dependent on I, which is equal to I_0 in the free-stream

[5]When the turbine is located in the free-stream, the incoming wind speed is U_0. When the turbine is in the incidence of the wake(s), the equivalent incoming wind speed needs to be calculated, as discussed in Chapter 4

The BP model is found to be unstable when modelling the near-wake region (generally less than 2D downstream). Therefore the normalized wind velocity deficit is calculated from 2D downstream of the turbine, as can be seen in Figure 3.7. Since the turbines in the wind farms are generally in the far-wake region of the upstream turbines, this limitation of the BP model does not cause actual problem in the calculation of the wind farm energy yield in the later phase.

Once the normalized wind velocity deficit is calculated, the wake velocity profile can therefore be computed using:

$$U(x, r) = U_0 \cdot \left(1 - \frac{\Delta U}{U_0}\right) \tag{3.11}$$

The wake radius is considered to be $2\sigma_u$ and expands linearly in the BP model. Hence, the wake velocity profile can finally be shown in Figure 3.8.

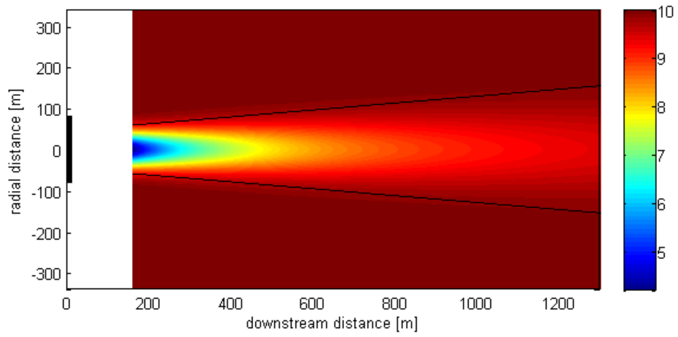

Figure 3.8: wake velocity profile (top view), calculated using the BP model. The black bar represents the rotor of the turbine, and the black lines represents the “boundary” of the wake

Chapter 4

Computation of the Equivalent Incoming Wind Velocity

4.1 Introduction

For a given type of wind turbine, not only the thrust coefficient is a function of the *incoming* wind speed, the power is a function of the incoming wind speed as well. When the incoming wind speed is uniform, it is easy to determine the thrust coefficient and the power output of the turbine. However, what if the incoming wind speed is non-uniform? What would be the *equivalent* incoming wind speed used to calculate the thrust coefficient and power of the wind turbine? It is a common scenario that the turbine is in the full or partial incidence(s) of the wake(s) and perceive non-uniform wind speed over the rotor plane, as depicted in Figure 4.2 and 4.3, respectively. Therefore, three different methods to calculate the wind turbine thrust coefficient and power in such scenarios are tested in this project and will be discussed in this chapter (Section 4.2, 4.3, and 4.4). Finally, the comparison among the three methods is presented in Section 4.5.

4.2 Method 1

As can be seen from Figure 4.2 and 4.3, the rotor plane of the downstream turbine is discretized into many small area elements in order to calculate the non-uniform wind velocity distribution on the plane. The discretization scheme used here is the uniform polar discretization with the origin located at the center of the rotor plane. The number of elements in the radial direction and in the azimuthal direction are represented by N_r and N_θ, respectively. The area of the rotor area element j is denoted by dA_j.

Inspired by [25], the first method calculates the equivalent incoming wind speed as the area weighted average of the wind speed on the rotor plane:

$$U_{eq} = \frac{\sum dA_j \cdot U_j}{\sum dA_j}, \tag{4.1}$$

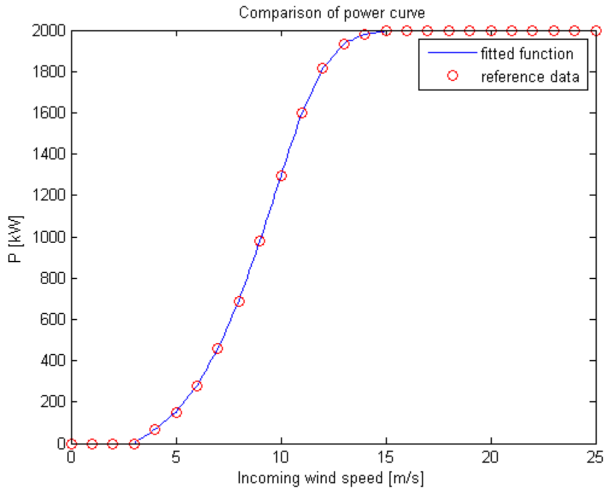

Figure 4.1: The relation between the wind turbine power P and the incoming wind speed for Vestas V80. The fitted function is the linear interpolation of the reference data [20].

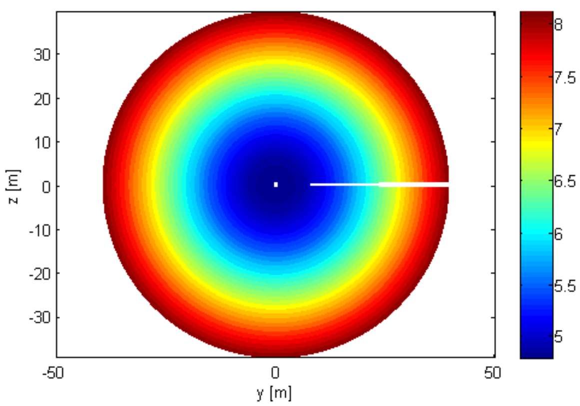

Figure 4.2: The wind velocity profile on the rotor plane of the downstream turbine in the case of full wake incidence. The downstream turbine is located at $3D$ behind the upstream turbine and the free-stream wind speed is 10 m/s. (N_r = 40 and N_θ = 180)

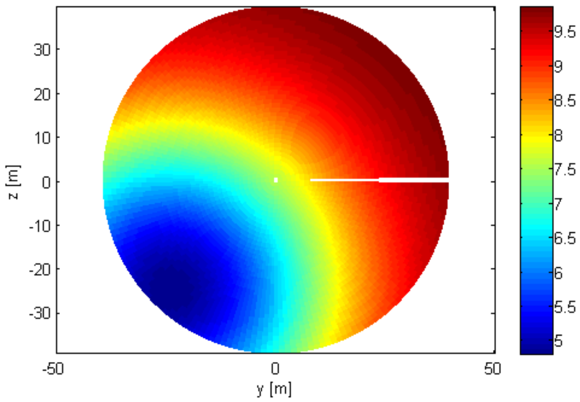

Figure 4.3: The wind velocity profile on the rotor plane of the downstream turbine in the case of partial wake incidence. The downstream turbine is located at $3D$ behind the upstream turbine and the free-stream wind speed is 10 m/s. (N_r = 40 and N_θ = 180)

where U_j is the wind speed on area element j. The equivalent incoming wind speed is then used to determine the turbine thrust coefficient and power through C_T - U and P - U relation, respectively.

This method is very simple. However, it does not appreciate the cubic/quadratic relation between the turbine power/thrust and the wind speed when the turbine is in the partial loading, which will be discussed in the next section.

4.3 Method 2

When the incoming wind speed is in the range between the cut-in wind speed and the rated wind speed[1], the wind turbine is called to be in the *partial loading*. In such case, the power of the wind turbine is generally a *cubic* function of the wind speed (as can be seen in Figure 4.1) and the thrust of the turbine is roughly a *quadratic* function of the wind speed. In the light of these two relations, the following method to calculate the equivalent incoming wind speed is proposed by Choi[8].

For the calculation of the wind turbine thrust T:

$$U_{eq,T} = \sqrt{\frac{\sum dA_j \cdot U_j^2}{\sum dA_j}} \tag{4.2}$$

For the calculation of the wind turbine power:

$$U_{eq,P} = \sqrt[3]{\frac{\sum dA_j \cdot U_j^3}{\sum dA_j}} \tag{4.3}$$

[1]The threshold wind speed that makes the wind turbine reach the rated power.

The $U_{eq,T}$ is then used to determine the thrust coefficient from the C_T - U relation, and the $U_{eq,P}$ is used to find the wind turbine power through P - U relation.

Although this method takes special care of the partial loading regime of the wind turbine, the following drawbacks in this method are anticipated. First, the relation between the wind turbine thrust/power and the incoming wind speed is no more quadratic/cubic when the wind speed is larger than the rated wind speed, namely when the turbine is in the full loading regime. Hence, this method is not accurate when the wind speed spectrum on the rotor plane contains velocities both under and over the rated wind speed. Second, the $U_{eq,T}$ calculated in Equation 4.2 is originally meant to determine the thrust *force* instead of the thrust coefficient. Therefore, inaccuracies may be added in the determination of C_T from $U_{eq,T}$.

4.4 Method 3

In this method, the C_T and P of each area element of the rotor plane (C_{T_j} and P_j) are first determined using the wind speed on the element (U_j). Then the thrust coefficient and power of the complete rotor are calculated as the area weighted average of the C_{T_j} and P_j, respectively. It is mathematically expressed as:

$$C_T = \frac{\sum A_j \cdot C_{T_j}}{\sum dA_j} = \frac{\sum A_j \cdot C_T(U_j)}{\sum dA_j} \tag{4.4}$$

$$P = \frac{\sum A_j \cdot P_j}{\sum dA_j} = \frac{\sum A_j \cdot P(U_j)}{\sum dA_j} \tag{4.5}$$

Similar to Method 2, Method 3 appreciates the quadratic/cubic relation of the thrust/power with respect to the wind speed in the partial loading regime. Besides, this method has solved the problem that is encountered in Method 2 when the wind speed spectrum on the rotor plane contains velocities both under and over the rated wind speed. However, the computational expense of this method is much higher than Method 2. Moreover, in the low wind speed regime, some parts of the rotor plane may experience the wind speed lower than the cut-in wind speed, making the C_{T_j} of these parts being zero. However, the C_{T_j} of the other parts which experience wind speed slightly higher than the cut-in wind speed are very large (around 0.8). Therefore, the overall C_T calculated with Method 3 in such case is very inaccurate due to the discontinuity in the C_T - U relation around the cut-in wind speed. After all, it is not physically reasonable that some parts of the rotor are in operation while the other parts are not.

4.5 Comparison between the three methods

The thrust coefficient/power of the downstream wind turbine are calculated using the three methods mentioned above with $N_r = 40$ and $N_\theta = 180$, and the results are compared. In order to pick a case where the variation of the wind speed on the rotor plane of the downstream turbine is large, the downstream distance of the second turbine with respect to the first turbine is chosen to be as small as $3D$. At first, the scenario of the full wake incidence of the second turbine is examined. The results are shown in Figure 4.4 and 4.5 for the thrust coefficient and power, respectively.

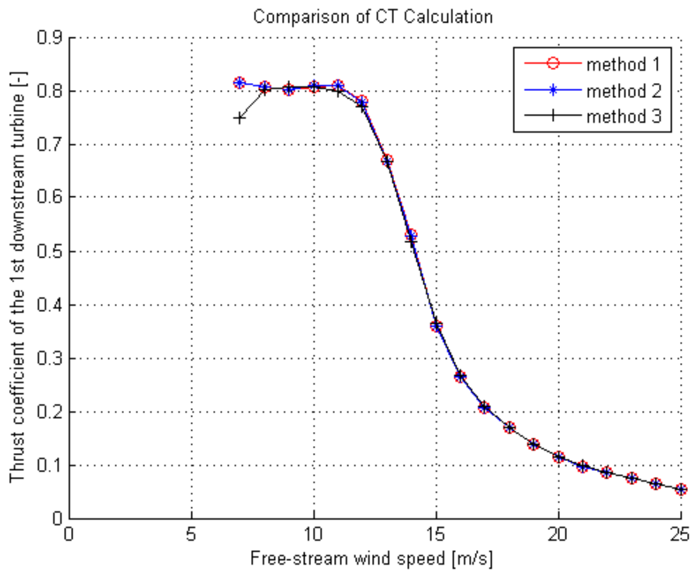

Figure 4.4: Comparison of the three methods to calculate the thrust coefficient of the downstream turbine in the full wake incidence

In general, the three methods yield very close results in this scenario. Besides, three other features are observed from the results. First, in the regime where the free-stream wind speed is very high (i.e. $U_0 \geq 16\ m/s$ in this case), the wind turbine power calculated by the three methods are exactly the same. This feature is corresponding to the situation where the complete wind speed distribution on the rotor plane of the downstream turbine is above the rated wind speed. In this situation both the first and the second method yield the equivalent incoming wind speed larger than the rated wind speed, and the power is constant when the turbine is in the full loading. The second feature is that the values of the thrust coefficient calculated by the three methods are almost the same when the free-stream wind speed is very high (i.e. $U_0 \geq 16\ m/s$ in this case), although the C_T is *not* constant as function of wind speed in the full loading regime. The cause of this feature can be explained by Figure 4.6. Comparing Figure 4.6 with Figure 4.2 (the spans of the colour bar are set to be the same for the comparison), it can be found that the amplitude of the wind speed variation on the rotor plane of the downstream turbine is very small when the free-stream wind speed is very large. This is because the C_T of the upstream turbine is small in the high free-stream wind speed, resulting in a weak wake. Hence, the U_{eq} calculated from Equation 4.1 and the $U_{eq,T}$ calculated form Equation 4.2 are very close, leading to very close values of thrust coefficients. The third feature observed is that the C_T of the downstream turbine calculated using Method 3 in the low wind speed regime (i.e. $U_0 = 7\ m/s$ in this case) notably differs with the C_T calculated using the other two methods. The C_T calculated with Method 3 in this regime is considered to be inaccurate, corresponding to the case discussed at the end of Section 4.4.

Then the scenario where the downstream turbine is in the partial wake incidence is ex-

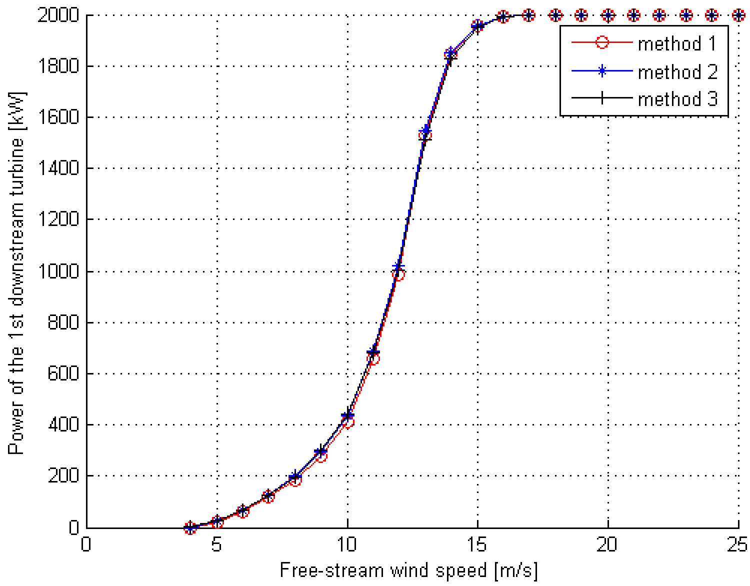

Figure 4.5: Comparison of the three methods to calculate the power of the downstream turbine in the full wake incidence

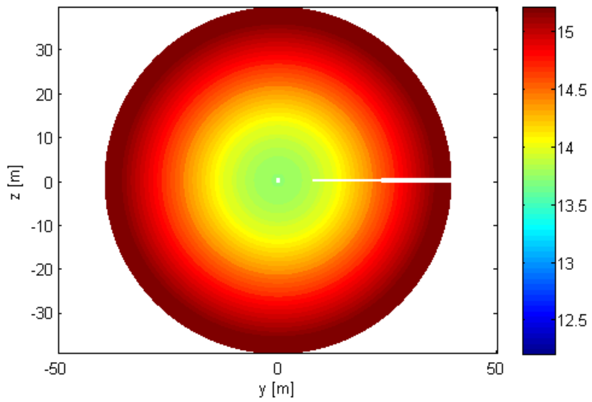

Figure 4.6: The wind velocity profile on the rotor plane of the downstream turbine in the case of full wake incidence. The downstream turbine is located at $3D$ behind the upstream turbine and the free-stream wind speed is 16 m/s. (N_r = 40 and N_θ = 180)

amined. The distance between the two turbines is still $3D$. However, the center of the wake on the rotor plane of the second turbine in this case is at $y = 0.3D$, $z = 0.3D$ w.r.t the center of the rotor plane. The results are shown in Figure 4.7 and 4.8 for the thrust coefficient and power, respectively.

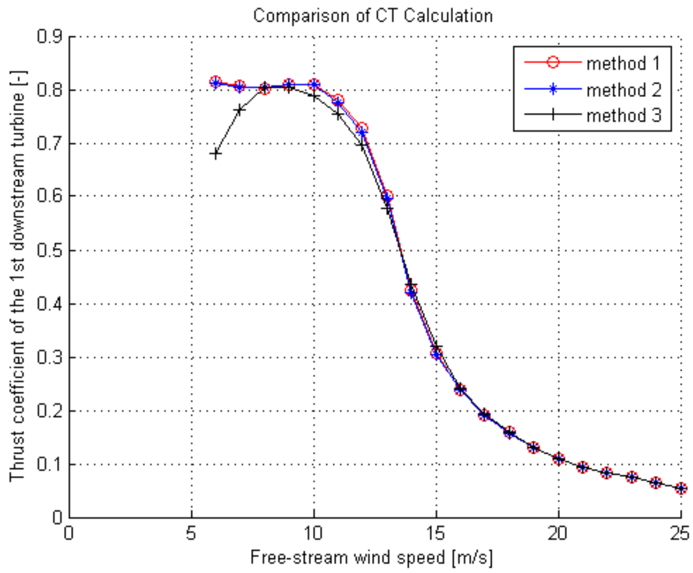

Figure 4.7: Comparison of the three methods to calculate the thrust coefficient of the downstream turbine in the partial wake incidence

The three features observed in the full wake incidence scenario still hold in this case. However, the differences in results between the three methods are slightly more pronounced in the partial wake incidence scenario. This may be due to the collapse of the symmetry of the wind speed distribution on the rotor plane. Nonetheless, the results from the three methods are still very close.

As can be seen from Figure 4.2 and Figure 4.3, the mesh of the rotor plane is very fine with $N_r = 40$ and $N_\theta = 180$. In fact, the sensitivity analysis of the discretization parameters shows that the discretization error becomes acceptably small when $N_r = 8$ and $N_\theta = 36$. Hence, the discretization error in the results of this chapter can be neglected. However, in order to reduce the computational time, $N_r = 8$ and $N_\theta = 36$ are used for the discretization of the rotor plane in the following studies.

It can be concluded that the thrust coefficient and power calculated by the three introduced methods are very close. Hence, choosing any of the methods will not lead to big difference in the results compared to the other two. Since the third method can not calculate the thrust coefficient accurately in the low wind speed regime, this method is not considered to be suitable. Compared to the first method, the second method is slightly more accurate in the partial loading regime, where the wake effects are strongest. Besides, it is not computationally expensive. Therefore the second method will be used in the calculation of the thrust coefficient and the power of the wind turbine.

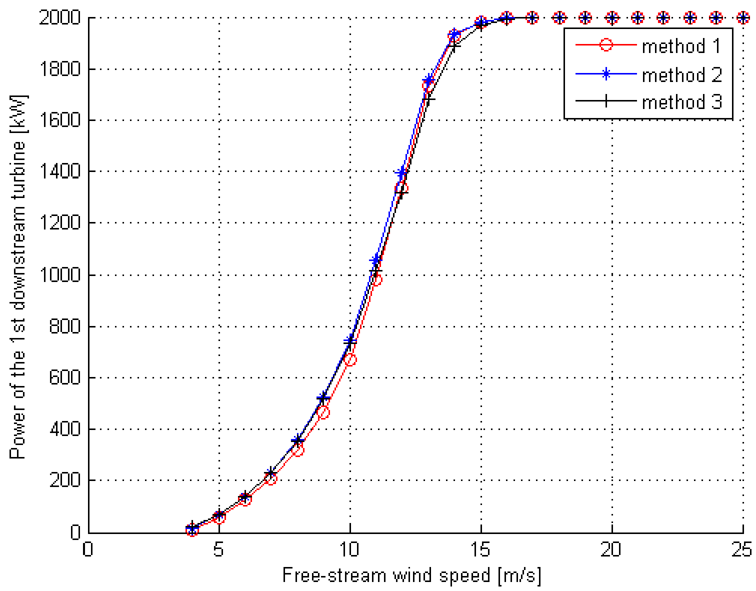

Figure 4.8: Comparison of the three methods to calculate the power of the downstream turbine in the partial wake incidence

Chapter 5

The Dynamic Wake Meandering Model

5.1 Background Theory

The dynamic wake meandering model developed in this project is based on the idea of the Dynamic Wake Meandering Model (DWM) proposed by Larsen et al.[29]. In this section, the background theory of the DWM is presented.

5.1.1 Introduction of DWM

Larsen et al.[30] developed the Dynamic Wake Meandering model which can be coupled with the wake deficit model, turbine aeroelasticity model etc. in order to analyse the energy yield of the wind farm or the fatigue loading of the turbines. The model is based on a fundamental presumption that the meandering of the wake can be modelled by considering the wakes as passive tracers driven by the *large-scale* atmospheric turbulence, while the *small-scale* turbulence is responsible for wake attenuation and expansion as caused by turbulent mixing. Therefore, the modelling of the wake meandering boils down to two aspects: describing the stochastic transport motion and specifying the cut-off frequency of the turbulence which defines the boundary between the large-scale and small-scale turbulence in this context.

5.1.2 Transport Motion Modelling

For modelling the stochastic transport of the wake, the wake is imagined to be constituted by a cascade of wake deficit elements, each released from the turbine at consecutive time instants in agreement with the passive tracer analogy [29].The propagation of each wake cascade element is described, and the collective description of these composes the wake meandering model.

In order to decouple the wake along the longitudinal wind deficit (and its expansion) and the lateral/vertical wake transportation process, the Taylor's hypothesis is adopted, which assumes the downstream advection of these wake cascade elements to be controlled by the (constant) mean wind speed of the ambient wind field. The displacements of each considered wake cascade element in the lateral and vertical directions are calculated based on the large-scale turbulence velocities in these directions at the location of the particular wake cascade element at each time instant. Mathematically, the dynamics of the wake cascade element in the lateral direction (y) and vertical direction (z) are described by:

$$\frac{dy(t,t_0)}{dt} = v(y,z,t,t_0), \tag{5.1}$$

$$\frac{dz(t,t_0)}{dt} = w(y,z,t,t_0), \tag{5.2}$$

where v and w are the *spatially dependent* large-scale turbulent velocities in the lateral and vertical direction, respectively, and t_0 is the time instant when the considered wake cascade element is released from the turbine. The total dynamics of a particular wake cascade element in the lateral direction is illustrated in Figure 5.1, where the red element represents the meandering wake cascade element, the black element depicts the wake position in absence of meandering, and the black box is the boundary of the regime where the large-scale turbulence that drives the wake is modelled. The dynamics in the vertical direction can be illustrated exactly in the same way as Figure 5.1, and is considered to be independent of the dynamics in the lateral direction. A schematic sketch of the complete meandering wake cascade is shown in Figure 5.2.

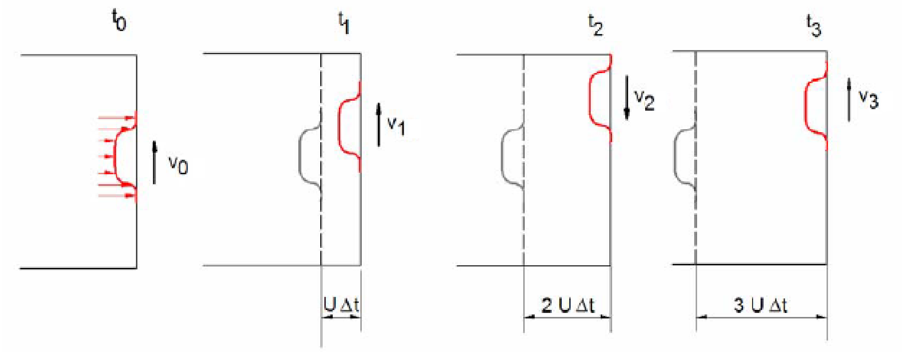

Figure 5.1: Illustration of wake dynamics for a wake cascade element emitted at time t_0. U is the mean wind speed and v_i is the wake transportation velocity at time t_i [30].

5.1.3 Turbulence Filtering

In order to obtain the requested stochastic transportation field, a low pass filter is introduced in the turbulence description, extracting the transport velocities associated with the large-scale turbulence only. The cut-off frequency f_c of the filter is specified as

$$f_c = \frac{U}{2D_w}, \tag{5.3}$$

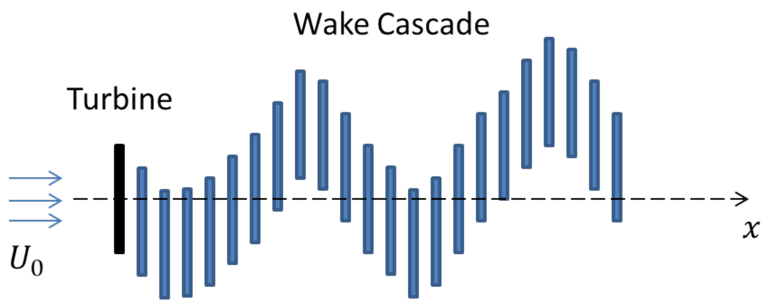

Figure 5.2: Schematic sketch of the complete meandering wake cascade from top view.

where U is the mean wind speed and D_w is the instantaneous wake diameter. The rationale for this choice is explained in [30] as followed: Based on the Taylor's hypothesis, a displacement wave with period T_p has a spatial extend of UT_p. Half of the spatial extend corresponds to the positive displacement and the other half corresponds to the negative displacement. For a spatial structure with a characteristic extend equal to the wake diameter D_w, the minimum wave period which allows for a constant sign displacement of all points on the spatial structure is consequently given by

$$D_w = \frac{UT_p}{2}, \tag{5.4}$$

from which the suggested cut-off frequency (inverse of T_p) is obtained. The selected cut-off frequency corresponds to a length scale of $2D_w$. Therefore, the transport velocities can be obtained by averaging the spatial turbulence field over a circular area (concentric with the advected wake element) which has a characteristic diameter of $2D_w$:

$$v(x, y, z) = \frac{1}{A_f} \iint_{A_f} v_n(x, y, z) dydz, \tag{5.5}$$

$$w(x, y, z) = \frac{1}{A_f} \iint_{A_f} w_n(x, y, z) dydz, \tag{5.6}$$

where A_f is the averaging area, $v_n(x, y, z)$ and $w_n(x, y, z)$ are the unfiltered lateral and vertical turbulent velocities, respectively.

The area-averaging of the velocities described in Equation 5.5 and 5.6 is very computationally expensive. As an alternative, another method of filtering the turbulence velocities (v,w) used by GH Bladed [6] for the dynamic wake meandering is briefly mentioned by [27]. In Bladed, a low pass filter[1] is first applied to the full spectrum of the turbulence velocity in the frequency domain. Then the filtered turbulence velocity governing the meandering motion is obtained from the reverse Fourier transfer of this filtered turbulence spectrum. The method used by GH Bladed is selected for this project, due to its relatively low computational cost compared to the area-averaging method.

[1] The suggested cut-off frequency for the low pass filter is given by Equation 5.3.

5.2 Generation and Filtering of the Turbulence Velocity

In order to implement the dynamic wake meandering model, the turbulence velocity in the lateral (y) and vertical (z) direction as function of time (t) and longtitudinal position (x) needs to be generated. In this project, the Kaimal spectrum specified in the IEC 61400-1 standard (third edition)[10] is used as the auto-power spectral density ($S_k(f)$) function of turbulence:

$$S_k(f) = \sigma_k^2 \frac{4L_k/U_0}{(1+6fL_k/U_0)^{\frac{5}{3}}}, \tag{5.7}$$

where f is the frequency in Hertz, U_0 is the hub height mean wind speed, k is the index referring to the velocity component direction (i.e. 1 = longitudinal, 2 = lateral, 3 = vertical), S_k is the single-sided velocity component spectrum, σ_k is the velocity component standard deviation, L_k is velocity component integral scale parameter, and with:

$$\sigma_k^2 = \int_0^\infty S_k(f)df \tag{5.8}$$

The σ_1 can be determined from the turbulence intensity (I) using the relation described in Equation 5.9:

$$I = \frac{\sigma_1}{U} \tag{5.9}$$

Then the rest of the parameters can be determined by Table 5.1,

Velocity component index k	1	2	3
σ_k	σ_1	0.8 σ_1	0.5 σ_1
L_k	8.1 Λ_1	2.7 Λ_1	0.66 Λ_1

Table 5.1: Turbulence spectral parameters for the Kaimal model

where Λ_1 is the scale parameter of the longitudinal turbulence, given by:

$$\lambda_1 = min\,(0.7 \cdot h_H, 42) \tag{5.10}$$

The spatial coherence of the *lateral/vertical* velocity component needs to be taken into account. However, only the *longitudinal* velocity component coherence values of the Kaimal spectrum are provided in the IEC 61400-1 standard. Therefore the coherence model used by DNV-GL for the simulation software Bladed is applied in this project:

$$Coh(\Delta l, f) = exp\left(-\frac{12f \cdot \Delta l}{U_0}\right), \tag{5.11}$$

where Coh is the coherence function defined by the complex magnitude of the cross-spectral density of the lateral/vertical wind velocity components at two spatially separated points divided by the auto-power spectrum function, Δl is the distance between the two spatial points.

The lateral and vertical components of the turbulence velocity in the time domain are then obtained from the inverse Fourier transform of the auto-power spectrum in conjunction with the coherence model. As mentioned in Section 5.1.3, a low-pass frequency filter is required to be applied on the turbulence signals. Since the diameter of the wake varies with the downstream distance, the cut-off frequency of the low-pass filter also varies with the downstream distance. An example of the generated turbulence velocity in the lateral and vertical direction is shown in Figure 5.3 and 5.4, where the longitudinal location of the turbulence is at 50 m ($x = 50\ m$) behind the wind turbine.

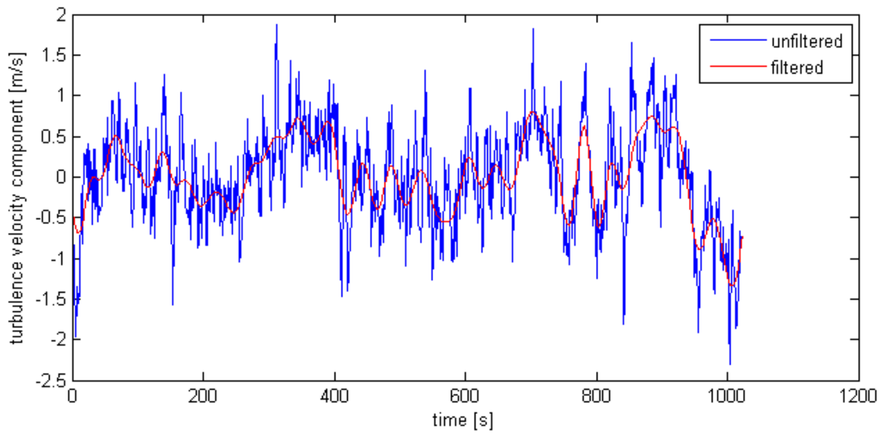

Figure 5.3: The generated turbulence velocity component in lateral (y) direction. $x = 50$ m

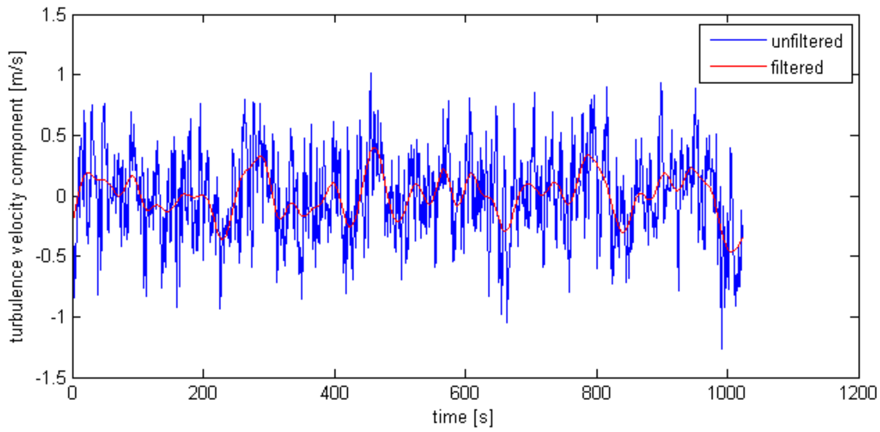

Figure 5.4: The generated turbulence velocity component in vertical (z) direction. $x = 50$ m

It can be seen that the standard deviation of the velocity component in z-direction is slightly smaller than the one in y-direction, which is in compliance with Table 5.1. In order to examine the coherence of the turbulence structures at different longitudinal locations, Figure 5.5 is presented.

It can be seen that turbulence velocity (y-component) generated at $x = 0\ m$ and $x = 10\ m$ are strongly correlated, and they are less correlated with the turbulence velocity generated at $x = 400\ m$. This shows that the coherence between the two turbulence structures decreases with increasing separations, as indicated by Equation 5.11. Furthermore, the

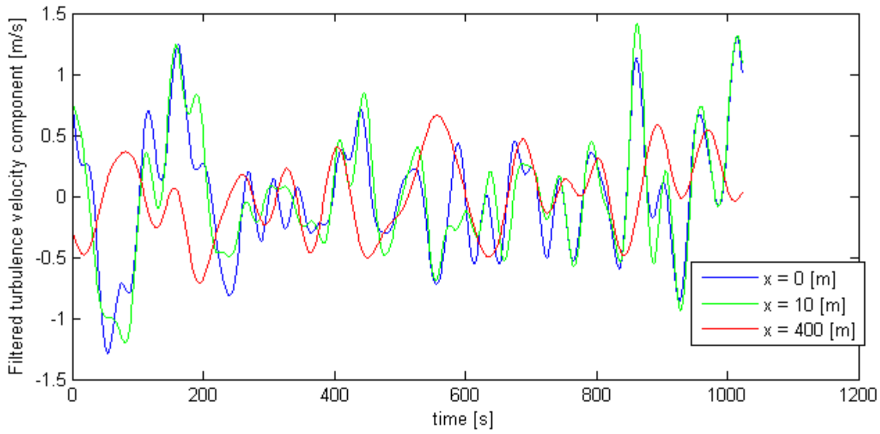

Figure 5.5: Comparison of the filtered lateral turbulence velocity at different longitudinal (x) locations

magnitude of the turbulence velocity at $x = 400$ m appears to be smaller than that of the other two. This is due to the larger wake diameter at further downstream location. According to Equation 5.3, larger wake diameter results in smaller cut-off frequency of the filter, which further engenders less energy content of the turbulence.

5.3 Implementation of the Model

5.3.1 Discritization of Time and Downstream Distance

The generation of turbulence velocity and the dynamics of the wake cascade are both implemented on the discrete time grid with initial time t_0 and constant time step Δt. Hence, the sampling frequency (f_s) of the turbulence velocities is:

$$f_s = \frac{1}{\Delta t} \tag{5.12}$$

By defining the number of time step N_t as a controllable input, the total time of simulation T can also be determined:

$$T = \Delta t \cdot N_t \tag{5.13}$$

Since the wake cascade travels with constant wind speed U_0 in the longitudinal direction, the space in the longitudinal direction is discretized into equidistant grid points with spacing Δx:

$$\Delta x = U_0 \cdot \Delta t. \tag{5.14}$$

Schematically, the mesh grid is illustrated in Figure 5.6. The correspondence between the time discretization and spatial discretization is chosen to avoid the need for interpolation between sampled turbulence velocities for the propagating wake. This makes the computation of wake meandering more efficient.

In the example of Figure 5.6, 11 longitudinal grid points are presented. Not only the turbulence velocity components (v_i, w_i) are generated at these grid points, the locations

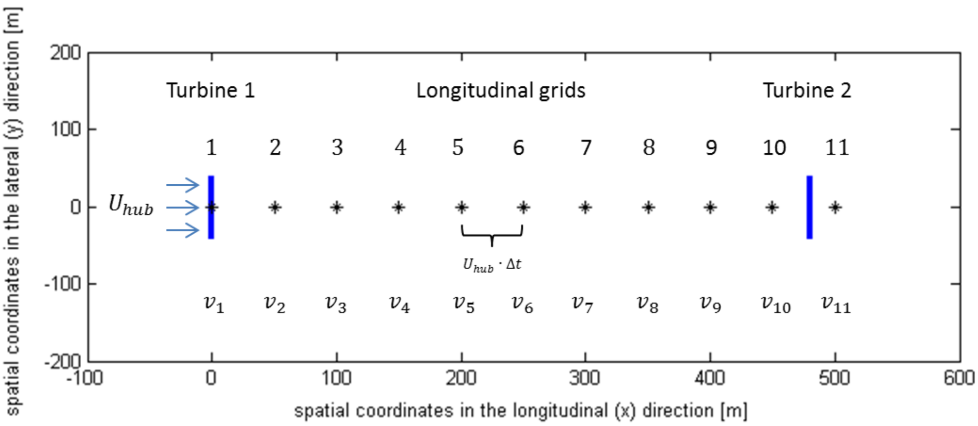

Figure 5.6: Schematic drawing of the longitudinal spatial grids

of the wake cascades are also calculated on these grid points. At grid point i ($i > 1$), the location of the wake cascade j in the lateral direction ($y_{i,j}$) is calculated as:

$$y_{i,j} = \sum_{k=1}^{i-1} v_k(t_0 + (j + k - 2) \cdot \Delta t) \cdot \Delta t \tag{5.15}$$

Similarly, the vertical location of the wake cascade j at longitudinal grid point i ($z_{i,j}$) is:

$$z_{i,j} = \sum_{k=1}^{i-1} w_k(t_0 + (j + k - 2) \cdot \Delta t) \cdot \Delta t \tag{5.16}$$

As can be easily seen, Equation 5.15 and 5.16 are the discretized form of Equation 5.1 and 5.2, respectively.

If the downstream turbine is between the two longitudinal grid points (as in Figure 5.6), the location of the wake cascade on the turbine is calculated as the linear interpolation of the wake locations at the adjacent grid points.

In order to initiate the simulation, the input parameters listed in Table 5.2 need to be specified. There are some requirements for the simulation parameters, which are stated below.

Requirements for dt

Ideally, the highest frequency component needed to be captured in the turbulence signal is the maximum cut-off frequency $f_{c_{max}}$. $f_{c_{max}}$ is defined by Equation 5.3 at the rotor plane, where the wake diameter is smallest. In order to satisfy the Nyquist sampling criterion, the sampling frequency f_s is required to be at least twice of $f_{c_{max}}$. Along with Equation 5.12 and 5.3, the following requirement can thus be derived for dt:

$$\Delta t \leq \frac{1}{2 f_{c_{max}}} = \frac{D_{w_{min}}}{U_0} \tag{5.17}$$

Category	Input parameter	Unit	Value in the example
Simulation parameters	dt	[s]	1
	N_t	[-]	2^{14}
Environmental parameters	U_0	[m/s]	10
	s	[-]	6
	I	[-]	0.08
Turbine parameters	D	[m]	80
	h_H	[m]	80

Table 5.2: The input parameters for the dynamic wake meandering model. The meaning of the symbols can be found in the Nomenclature.

Requirements for Nt

Since the signals of turbulence velocities in the time domain are obtained from the inverse Fourier transform, the total number of points in the turbulence signals (which is equal to N_t) is recommended to be a power of 2 [6] to ensure the accuracy.

$$N_t = 2^k, \qquad k = 1, 2, 3... \tag{5.18}$$

5.3.2 Example of Model Results

With the input parameters specified in Table 5.2, an example of the wake location as a function of time at the downstream wind turbine calculated by the dynamic wake meandering model is shown in Figure 5.7.

It can be seen from Figure 5.7 that the standard deviation of the y_w is larger than that of z_w. This is logical since σ_2 is lager than σ_3. It should be noted that the generated turbulence velocity components are random signals, therefore the results obtained from each run of simulation should not be exactly the same, but *statistically* the same.

Once the location of the wake center is known, the wind velocity distribution on the rotor plane of the downstream turbine can be calculated with the BP wake model. Then the instantaneous power output of the downstream turbine can be calculated using the method described in Section 4.3. With the input parameters specified in Table 5.2, the instantaneous power output of the downstream turbine is shown in Figure 5.8. The green line in this figure represents the time-averaged power output, and the red line represents the power output if the meandering of the wake is not considered. In this very wind turbine layout and wind direction, the downstream turbine will be right in the center of the wake and suffers the highest wind velocity deficit if the meandering of the wake is not considered. Therefore, the wake meandering has a positive effect on the power production of the downstream turbine in this case.

Figure 5.7 is further analysed by plotting the histogram of the wake center locations in the lateral and vertical direction. Then the probability density of the wake center location in these two (y,z) directions are calculated from the histograms, as shown in Figure 5.9 and 5.10, respectively.

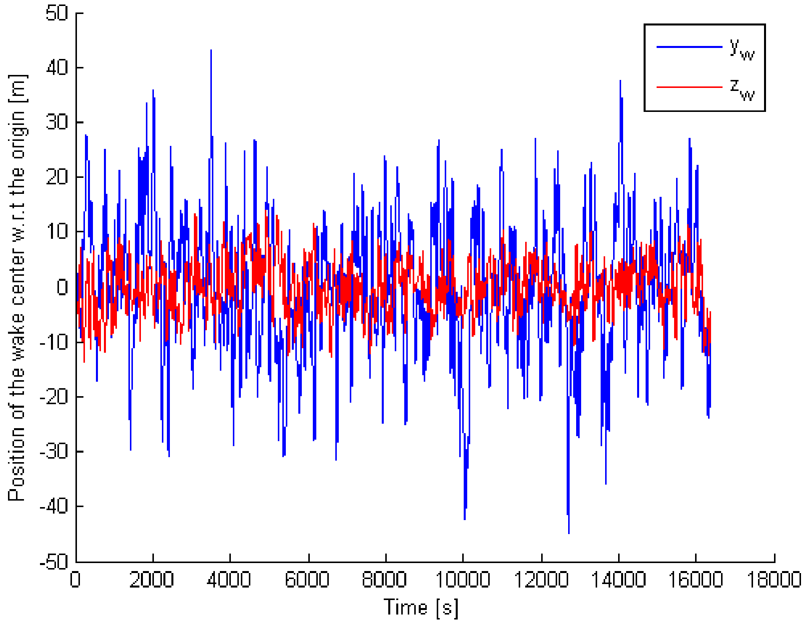

Figure 5.7: The lateral (y_w) and vertical (z_w) location of the wake center at the downstream wind turbine calculated by the dynamic wake meandering model.

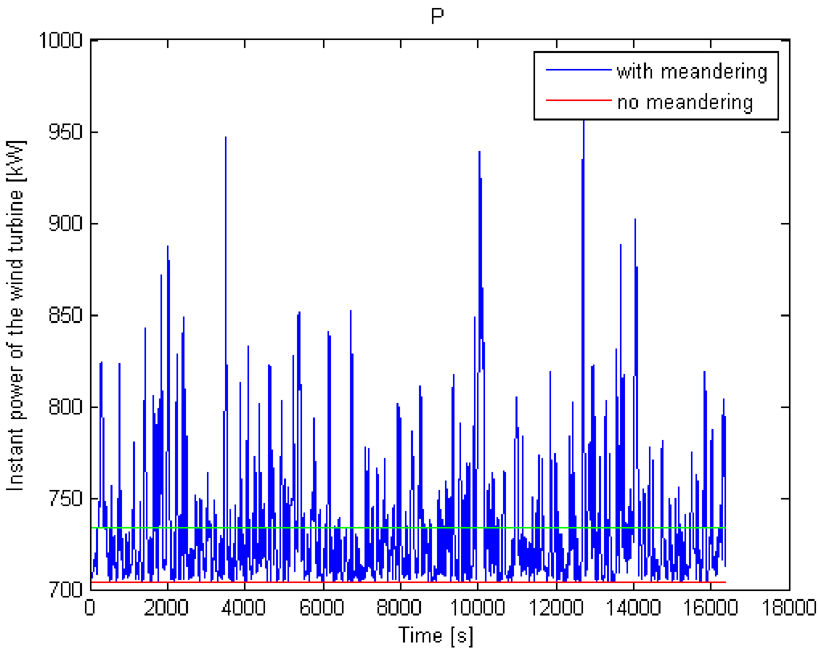

Figure 5.8: The instantaneous power output of the downstream turbine calculated by the dynamic wake meandering model with input parameters specified in Table 5.2

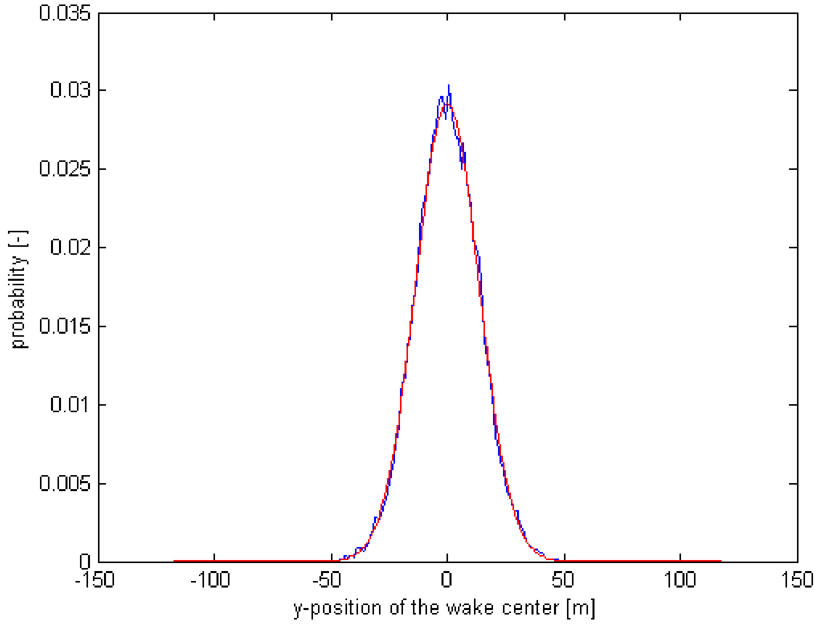

Figure 5.9: The probability density (and its normal distribution fit) of the wake center location in the lateral direction, summarized from Figure 5.7

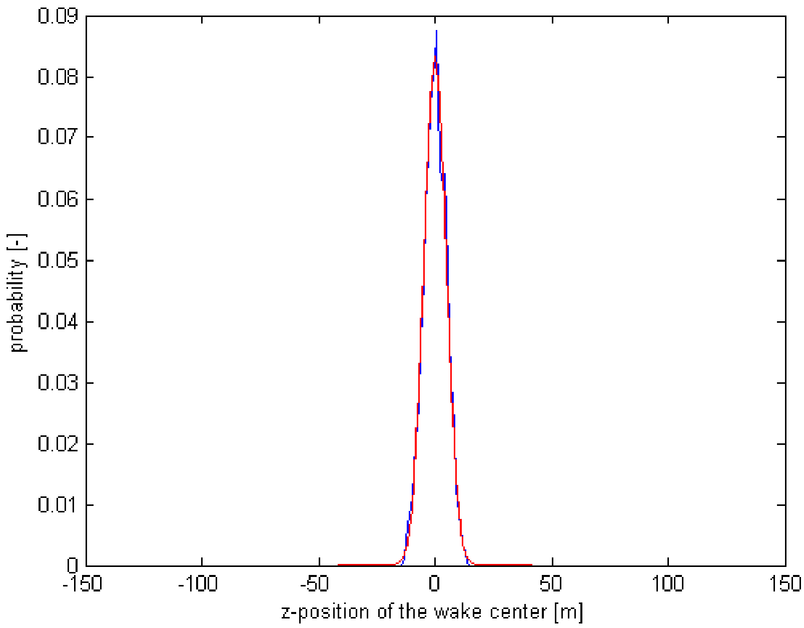

Figure 5.10: The probability density (and its normal distribution fit) of the wake center location in the vertical direction, summarized from Figure 5.7

It can be seen that the probability density of the wake center location can be well fitted by the normal distribution. The mean value (μ) of the normal distribution in both the lateral and vertical direction are approximately zero, and the standard deviation in the lateral direction (σ_y) is larger than that in the vertical direction (σ_z).

5.4 Sensitivity Analysis on the Simulation Parameters

5.4.1 Introduction

In Table 5.2, the environmental parameters define the environmental conditions of the simulated scenario and the turbine parameters are derived from the turbine properties. However, the simulation parameters define the structure of the simulation itself. In order to check how the structure of the simulation influences the results in the same environmental and turbine conditions, a sensitivity analysis is performed for dt and N_t.

5.4.2 Analysis on dt

There are three main reasons for dt to influence the simulation results. Firstly, dt is linked with the sampling frequency of the turbulence velocities by Equation 5.12. Secondly, the spacing between the adjacent turbulence-generation points (dx) are affected by dt according to Equation 5.14 (also see Figure 5.6). If dx is too large, the coherence between the turbulence velocities may not be well captured by the simulation. Thirdly, dt influences the integration of the dynamics of the wake in the discrete framework, as indicated by Equation 5.15 and 5.16. Since the turbulence velocities are assumed to be constant within the time step dt, the smaller dt will make the discrete integration closer to the continuous integration.

In order to see how exactly dt influences the simulation result, the simulation is run with different values of dt while keeping the environmental parameters and turbine parameters constant. Besides, the total time in the simulation T is made constant to eliminate its influence on the simulation result. This is done by adjusting N_t to dt based on the relation described by Equation 5.13, while keeping the requirement described by Equation 5.18 fulfilled. Therefore, the values of dt and N_T listed in Table 5.3 are applied for the sensitivity analysis of dt. On the other hand, the "worst scenario" is used to get the most conservative result. Hence, the cut-out wind speed of the turbine (25 m/s) is used for U_0 to make the largest dx according to Equation 5.14. The other input parameters used here are still the ones specified in Table 5.2.

Input parameter	Values in different cases						
dt [s]	0.125	0.25	0.5	1	2	4	8
N_t [-]	2^{16}	2^{15}	2^{14}	2^{13}	2^{12}	2^{11}	2^{10}

Table 5.3: The values of dt and N_t used to analyse the influence of dt on the simulation results

Since every run of the simulation is a random process, each case defined in Table 5.3 is run 20 times in the simulation so as to reduce the random effect. The result is shown in Figure 5.11.

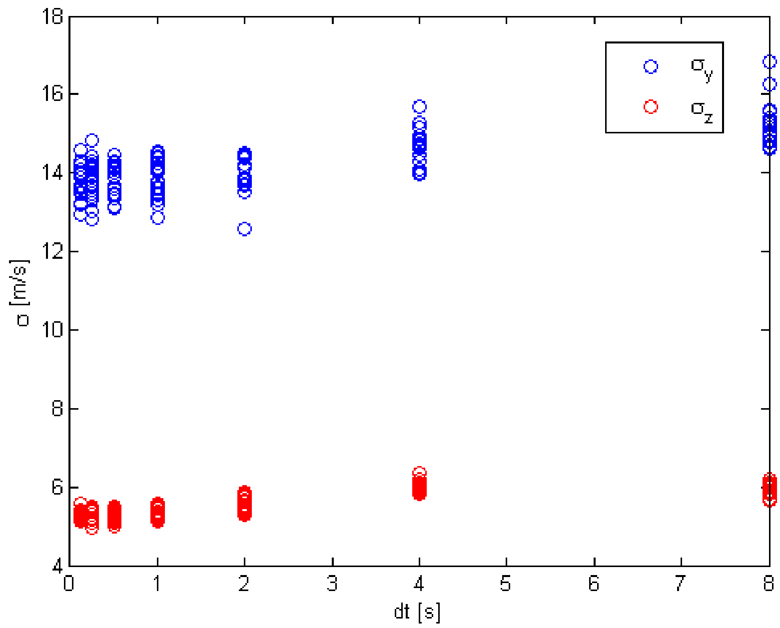

Figure 5.11: Standard deviation of the wake center location as a function of dt.

As can be seen in Figure 5.11, the results of σ_y and σ_z converge to specific values while reducing dt. When dt is less or equal than 1, the mean value of the results are almost constant. Since smaller dt also makes longer computational time, dt is chosen to be 1 in the following simulations to ensure converged results and at the same time keep the computational time as short as possible.

5.4.3 Analysis on Nt

With fixed dt and environmental parameters, changing N_t alone can affect the simulation results because N_t is proportional to the total time in the simulation (T). With longer time in the simulation, the random effect is reduced and therefore the results are more reliable. However, larger N_t also implies longer computational time. Therefore, the minimum N_t that ensures the reliable results needs to be found. For this reason, the simulation is run with varying N_t and the results are compared (as shown in Figure 5.12). For each value of N_t the simulation is run 36 times. In these simulations, the value of the environmental parameters and the turbine parameters are the same as those specified in Table 5.2, and the value of dt is 1.

As can be seen in Figure 5.12, the bandwidth of the results (σ_y and σ_z) reduces with increasing N_t. This indicates that higher reliability of the results is achieved with larger N_t. However, the reduction *rate* of the bandwidth decreases as N_t increases. For $N_t = 2^{16}$ and $N_t = 2^{17}$, the bandwidth of the results are very small and almost the same. Therefore, the value of N_t is chosen to be 2^{16} for the following simulations.

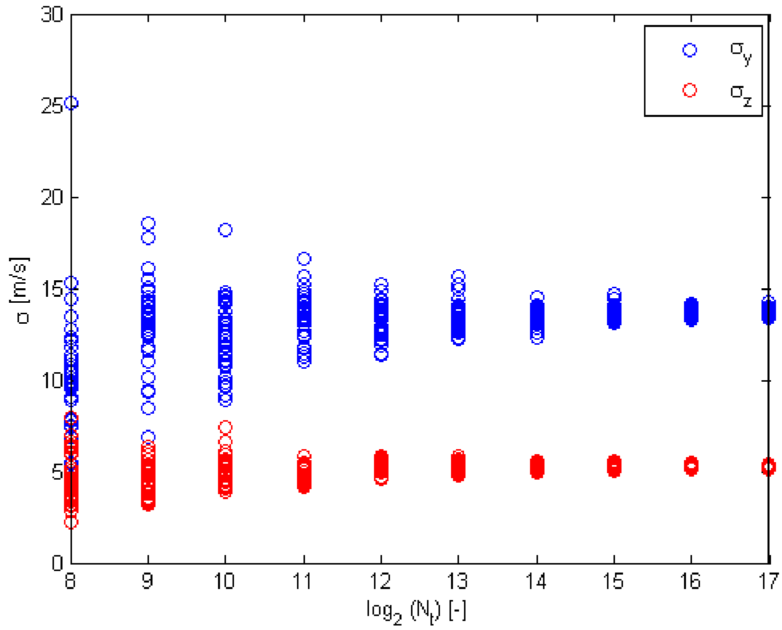

Figure 5.12: Standard deviation of the wake center location as a function of N_t.

5.5 Analysis on the Environmental Parameters

5.5.1 Introduction

In Section 5.4, the influence of dt and N_t on the simulation results are analysed and their recommended values for the simulation ($dt = 1$, $N_t = 2^{16}$) to get the reliable results are presented. On the other hand, the impact of the wake meandering on the downstream turbine is naturally dependent on the environmental conditions (i.e. U_0, s, I in this case). It would be of great value to know how each of these environmental parameters influences the wake meandering effect.

Denoting the power of the downstream turbine calculated without wake meandering as P_{static}, and the average power of the downstream turbine calculated with the dynamic wake meandering model as $P_{dynamic,avg}$, the difference $P_{dynamic,avg} - P_{static}$ is denoted by ΔP. The ΔP is therefore considered to represent the change in the average power output of the downstream turbine due to the wake meandering. Similarly, ΔC_T is defined as $C_{T_{dynamic,avg}} - C_{T_{static,avg}}$, representing the difference in the average thrust coefficient calculated with the dynamic wake meandering model compared to the thrust coefficient calculated with the static wake model where the wake meandering is not considered. Using the recommended values for the simulation parameters and the turbine parameters shown in Table 5.2, the influences of the environmental parameters on the wake meandering effect are studied from the simulation results in this section. More specifically, the wake meandering effect studied here consists of three aspects: σ_y and σ_z of the wake center location on the rotor plane of the downstream turbine, ΔP, and ΔC_T.

5.5.2 The Influence of U_0

In the case of different downstream distances ($s = 6$ and $s = 9$) and longitudinal turbulence intensities ($I = 0.08$ and $I = 0.12$), the simulation is run with various U_0 ranging from cut-in wind speed ($4m/s$) to cut-out wind speed ($25m/s$) with step of $1m/s$. In order to reduce the random effect, the simulation is run 3 times at each wind speed and the results are shown in Figure 5.13, 5.14 and 5.15.

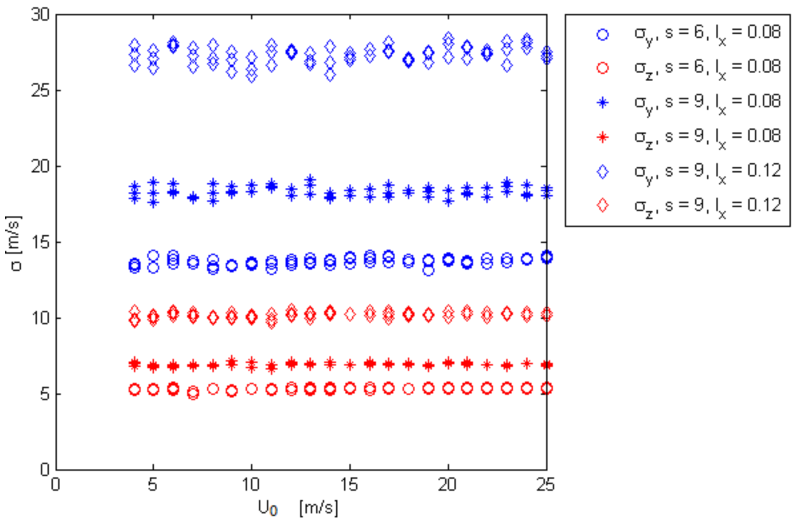

Figure 5.13: Standard deviation of the wake center location as a function of U_0.

From Figure 5.13 it can be seen that σ_y and σ_z are almost constant against U_0 in all three cases, regardless of s and I. Therefore, σ_y and σ_z can be considered independent of U_0 *in the operational range* of the wind speed.

For $I = 0.08$, the U_0 which yields rated wind speed at the downstream turbine is 16.5 m/s for $s = 6$ and 16 m/s for $s = 9$. It can be seen from Figure 5.14 that ΔP is zero when the downstream turbine is in the full loading, since in this case the turbine power is constant with the incoming wind speed and therefore the increase in the incoming wind speed due to the meandering of the wake does not cause increase in the wind turbine power. In the partial loading regime, ΔP first increases with increasing U_0. In this region, higher U_0 gives rise to higher $U_{eq,P}$ (equivalent incoming wind speed) of the *downstream* turbine, and the *increase* in $U_{eq,P}$ due to the wake meandering ($\Delta U_{eq,P}$) is almost constant with U_0. Since the wind turbine power is proportional to the cube of the wind speed in this region, ΔP is larger at higher $U_{eq,U}$ with the same amount of $\Delta U_{eq,P}$. Then ΔP decreases with increasing U_0 after the peak value of ΔP occurring at around $U_0 = 11m/s$ for both cases, corresponding to $U_{eq,P} = 9.07$ m/s for $s = 6$ and $U_{eq,P} = 9.66$ m/s for $s = 9$, respectively. The reasons why ΔP decreases with U_0 in this region are twofold. Firstly, when U_0 is above $10m/s$, the C_T of the upstream turbine starts to drop significantly (can be seen in Figure 3.6). This results in weaker velocity deficit in the wake, and therefore the increase in $U_{eq,P}$ of the downstream turbine due to the wake meandering becomes smaller. Secondly, the cubic relation between the wind turbine power and wind speed starts to collapse when the wind speed is approaching the rated wind speed and the slope of the $P - U$ curve decreases in this region.

As for the thrust coefficient, ΔC_T is almost constant at low U_0 (up to $U_0 = 9m/s$) because in this region C_T is theoretically constant against the incoming wind speed. After that, ΔC_T first decreases and then increases with increasing U_0, making a valley shape in Figure 5.15. The reason for this valley-shape behaviour is believed to be analogous to the peak-shape behaviour of ΔP against U_0 in Figure 5.14, which is explained in the previous paragraph.

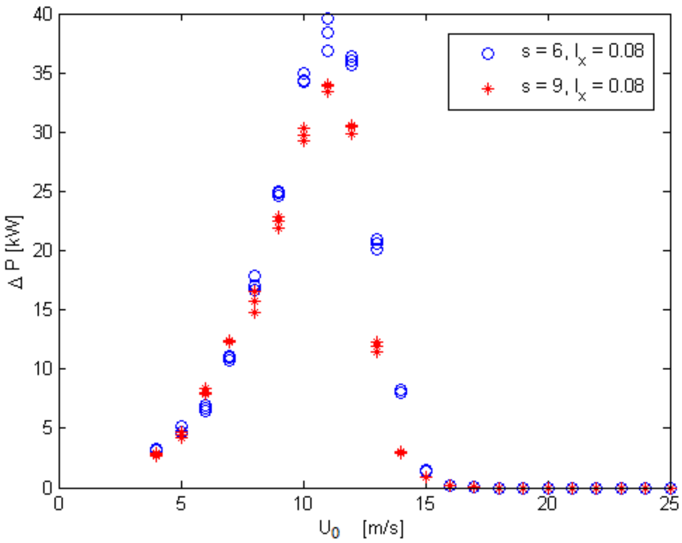

Figure 5.14: The change in the average power output of the downstream turbine due to the meandering of the wake as a function of U_0.

5.5.3 The Influence of s

In order to study the influence of s on the wake meandering effect, the simulation is run with various s ranging from 2 to 30 with step of 1. Two different values of I (0.08 and 0.12) are used to make the analysis more universal. Since σ_y and σ_z are considered to be independent of U_0, only one value of U_0 ($11m/s$) is used in this study. This specific value of U_0 is chosen on the purpose of maximizing ΔP and ΔC_T. The results are shown in Figure 5.16, 5.17 and 5.18.

As can be seen in Figure 5.16, σ_y and σ_z first exhibit parabolic-like behaviour with s and then increases linearly with s. The boundary between these two region is approximately at $s = 12$. The reason for σ_y and σ_z to increase with s is rather simple. With larger downstream distance, the wake cascade travels for longer time. Therefore the wake can also be transported to larger distance in the lateral and vertical direction by the turbulence. However, since the turbulence velocity components (v, w) are random signals with mean value of zero, the integration of v and w in time (i.e. the wake location in y and z direction, respectively) are more likely to be confined in a limited range as time increases. This explains why the slope of $\sigma - s$ curve decreases with increasing s in region I. On the other hand, the cut-off frequency of the turbulence velocity component decreases as s increases, making v and w more consistent and less vibrant in the time domain. This

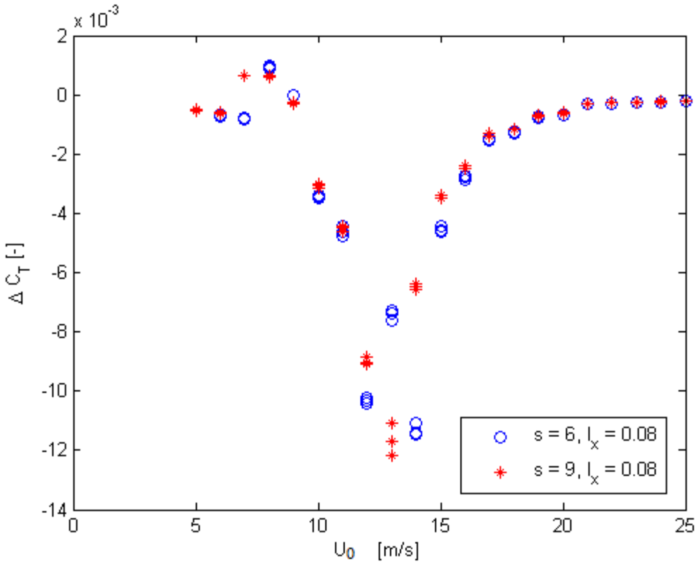

Figure 5.15: The change in the thrust coefficient of the downstream turbine due to the meandering of the wake as a function of U_0.

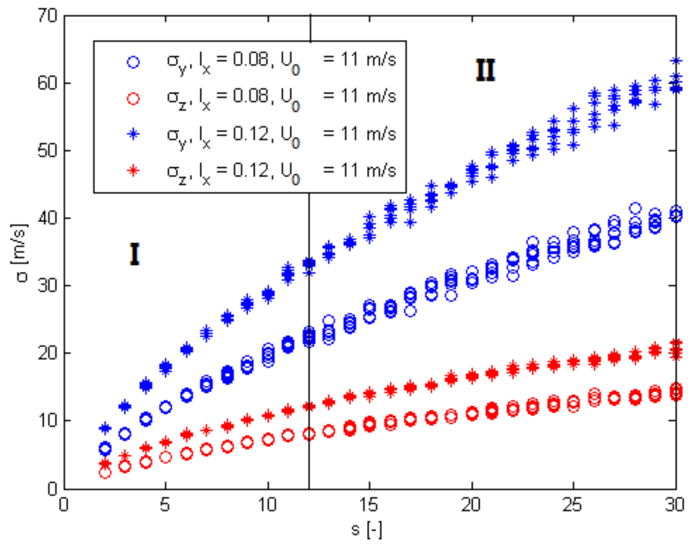

Figure 5.16: Standard deviation of the wake center location as a function of s.

may be the reason why σ does not approach to a limit but increase linearly with s in region II.

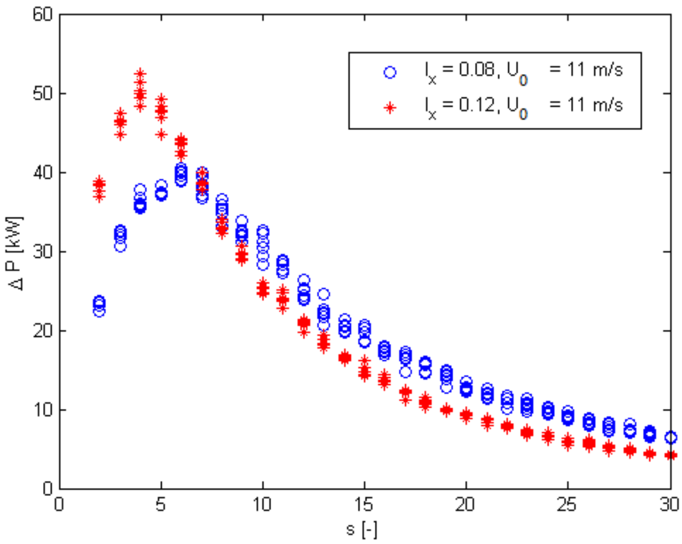

Figure 5.17: The change in the average power output of the downstream turbine due to the meandering of the wake as a function of s.

Figure 5.17 shows that ΔP at first increases with s. This is mainly due to the increase of σ_y and σ_z, which causes larger $\Delta U_{eq,P}$. Then ΔP decreases as s becomes even larger, mainly because that the velocity deficit in the wake reduces with s, making the wake meandering effect less influential. It can also be seen that the peak value of ΔP is higher when I is larger. Besides, the peak occurs at smaller s when I is larger, because the wind velocity in the wake recovers faster with higher I due to the stronger mixing between the wake and the ambient atmosphere.

The influence of s on ΔC_T is analogous to the influence of s on ΔP but in the opposite manner, as C_T decreases with incoming wind speed.

5.5.4 The Influence of I

The influence of I on the wake meandering effect can be studied from Figure 5.19, 5.20 and 5.21.

It can be seen from Figure 5.19 that σ_y and σ_z increases linearly with I, because the standard deviation of v and w increases linearly with I. In the case of larger s, not only the overall values of σ become larger (as also shown in Figure 5.16), the slope of the $\sigma - I$ line is also increased.

The influence of I on the wake meandering effect on the downstream turbine is twofold. On one hand, σ_y and σ_z become larger when I increases, which promotes the wake meandering effect. On the other hand, higher I makes the wind speed in the wake recover faster, which reduces the wake effect, and therefore also the difference between the meandering wake model and the static wake model. Which of these two aspects dominates is dependent on

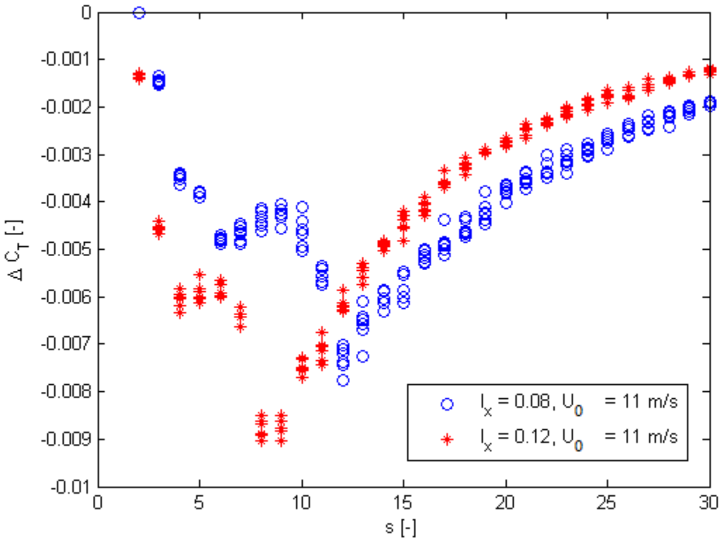

Figure 5.18: The change in the thrust coefficient of the downstream turbine due to the meandering of the wake as a function of s.

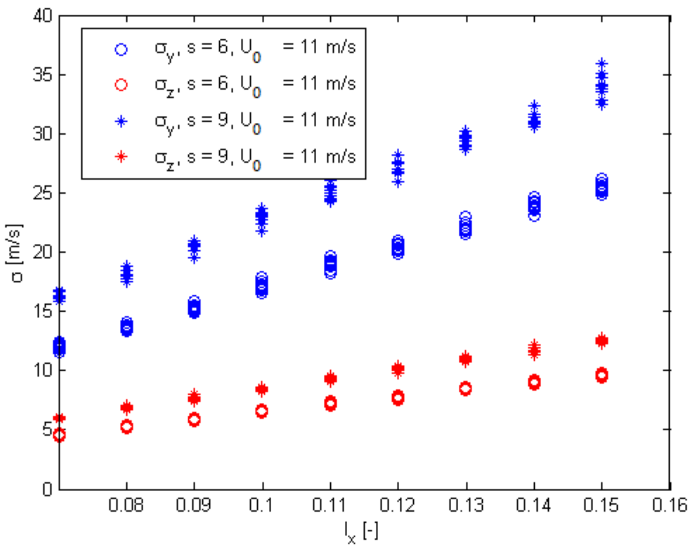

Figure 5.19: Standard deviation of the wake center location as a function of I.

the s and U_0. Therefore, Figure 5.20 and Figure 5.21 show very different behaviours of ΔP and ΔC_T against I, respectively, at different downstream distances.

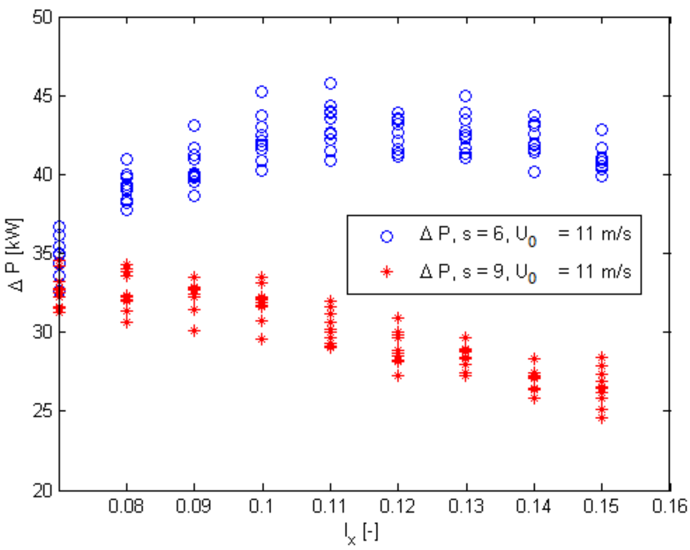

Figure 5.20: The change in the average power output of the downstream turbine due to the meandering of the wake as a function of I.

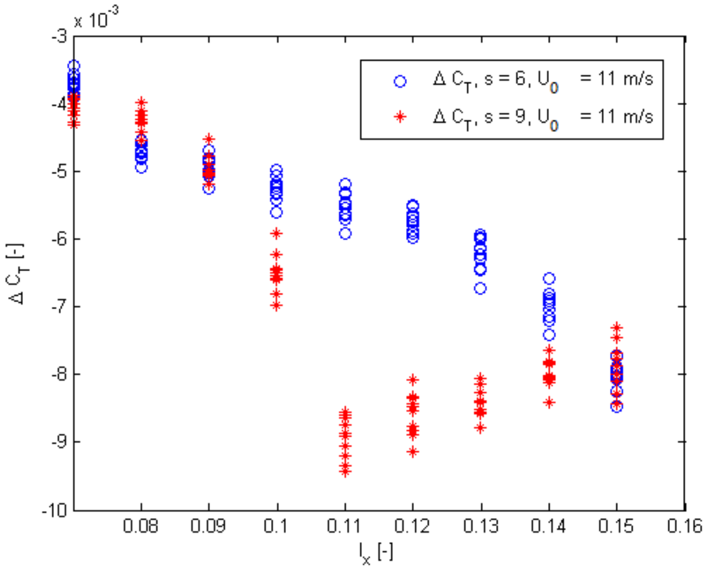

Figure 5.21: The change in the thrust coefficient of the downstream turbine due to the meandering of the wake as a function of I.

Chapter 6

Wind Farm Wake Model with Dynamic Wake Meandering

6.1 Introduction

Chapter 5 has developed a wake model with wake meandering for the wake of a *solitary* turbine. It is used in a simple and special case where the wind farm only consists of two turbines, and the downstream turbine is affected by the *single* wake from the upstream turbine. However, in reality the wind farms are usually composed of more than two turbines. In these wind farms, the downstream turbine may be affected by *multiple* wakes from the upstream turbines. Furthermore, the wakes of different turbines may sometimes overlap/mix with each other as shown in Figure 6.1. Hence, the wake effect on the turbines in the wind farm (hereafter the word "wind farm" represents the wind farm consisting of more than two turbines) is much more complicated.

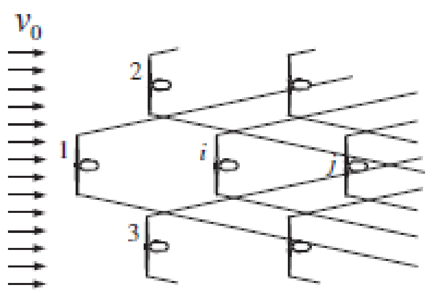

Figure 6.1: An example of multiple wakes in the wind farm [18].

The BP model discussed in Section 3.4.2 is a *single-wake model*. In order to study the wake meandering effect on the annual energy yield of the whole wind farm, the *wind farm wake model* which considers the interactions of wakes needs to be developed. Therefore, in this chapter, the static wind farm wake model which does not consider the wake meandering is firstly developed and verified in Section 6.2 and Section 6.3, respectively. Subsequently, the static wind farm wake model is coupled with the dynamic wake meandering model in Section 6.4 and verified in Section 6.5.

6.2 Static Wind Farm Wake Model

6.2.1 Overview

In general, the static wind farm wake model aims to model the wind velocity deficit in the wind farm wakes including the wake mixing phenomenon. This is achieved by combining the single-wake model (i.e. the BP model) with a wake mixing model. Since the turbulence intensity is an input of the BP model, the influence of the wake(s) on the turbulence intensity also needs to be considered. In this regard, a turbulence model is also integrated into the static wind farm wake model. It should be noted that the wake of the wind turbines are assumed to be static in the static wind farm wake model, therefore the wake meandering is not considered yet.

6.2.2 Wake Mixing Model

The wake mixing model combines the velocity deficits in the individual wakes to calculate the total velocity deficit in the overlapping area of multiple wakes. Different wake mixing models are summarized and compared in the literature study [21]. According to the literature study, the most suitable wake mixing model to be coupled with the BP single-wake model is the linear superposition model proposed by Niayifar and Porté-Agel [33]. It assumes the total velocity deficit in the overlapping wakes is the linear summation of the *relative* deficit in each wake:

$$U_i = U_0 - \sum_k \left(U_k - U_{k,i}\right), \tag{6.1}$$

where U_i is the wind speed at turbine i and $U_{k,i}$ is the wind speed in the wake of turbine k at turbine i, U_k is the wind speed at turbine k and U_0 is the free stream wind velocity.

In order to adapt Equation 3.7 to the wind farm wake model, U_0 in Equation 3.7 is replaced by U_k, and ΔU represents $U_k(x,r) - U_k$ for the wake of turbine k, leading to:

$$\frac{U_k(x,r) - U_k}{U_k} = \left(1 - \sqrt{1 - \frac{C_T}{8\left(k^* x/D + \varepsilon\right)^2}}\right) \cdot exp\left\{-\frac{1}{2\left(k^* x/D + \varepsilon\right)^2}\left(\frac{r}{D}\right)^2\right\} \tag{6.2}$$

Since the output of Equation 6.2 is the *normalized* velocity deficit, Equation 6.1 can be rewritten into the following form so as to be compatible with Equation 6.2:

$$U_i = U_0 - \sum_k \left[\left(\frac{U_k - U_{k,i}}{U_k}\right) \cdot U_k\right], \tag{6.3}$$

where the normalized velocity deficit $\frac{U_k - U_{k,i}}{U_k}$ can be calculated by Equation 6.2.

6.2.3 Turbulence Model

As has been considered in many single-wake models (e.g. Larsen model, BP model), the growth of the wake is strongly dependent on the turbulence intensity of the local environment. In general, the wake recovers faster with higher ambient turbulence intensity, since the flow mixing between the wake and the outside air is enhanced.

Due to the turbulence created by the shear in the wake and that created by the turbine itself, the turbulence intensity in the wind turbine wake (I) is different from the ambient turbulence intensity (I_0) [12]. Therefore, in a wind farm where many turbines are in the wakes of the others, the local turbulence intensity experienced by different turbines are most likely different. In order to extend the BP model into a wind farm wake model, it is necessary to calculate the local turbulence intensity for each wind turbine in the wind farm, which requires modelling the turbulence intensity in both the single wake and the mixing wakes.

According to [3], the turbulence intensity in the wake can be modelled as

$$I = \sqrt{I_+^2 + I_0^2}, \tag{6.4}$$

where I_+ is the added turbulence intensity in the wake. Among the various models to model the I_+, the literature study [21] suggests that the Crespo - Hernandez model shall be used in this project. Crespo and Hernandez [11] introduced the following empirical expression for I_+ based on their numerical data:

$$I_+ = 0.73a^{0.8325} I_0^{0.0325} \left(\frac{x}{D}\right)^{-0.32}, \tag{6.5}$$

where a is the induction factor. It should be note that Equation 6.5 is proposed for the following range of conditions: $5 < x/d_0 < 15$, $0.07 < I_0 < 0.14$ and $0.1 < a < 0.4$.

Extensive experimental and numerical studies have shown that the turbulence intensity inside a wind farm increases and quickly reaches an equilibrium after 2-3 rows [35, 1]. Frandsen and Thøgersen [16] suggested that only the influence of neighbouring turbines is important to predict the turbulence intensity on a given turbine in the wake(s). In this regard, for every turbine in the farm, Niayifar et al. [33] suggest to consider only the added turbulence intensity resulting from the closest upstream turbine, and picked up the one who has the largest impact. Mathematically it is defined as:

$$I_{+_i} = max\left(\frac{A_{s_{k,i}}}{A} I_{+_{k,i}}\right), \tag{6.6}$$

where I_{+_i} is the added turbulence intensity at turbine i, A_s is the shadowed area of the wake on the rotor, A is the swept area of the rotor, and $I_{+_{k,i}}$ is the added turbulence intensity induced by the turbine k at the turbine i.

6.2.4 Implementation of the Static Wind Farm Wake Model

The static wind farm wake model is developed by integrating the BP model with the wake mixing model and the turbulence model presented above. The detailed structure of the static wind farm wake model is shown in Appendix A. At first, the turbines are sorted from upstream to downstream based on the wind direction and the wind farm layout. Subsequently, a loop of calculations is run from the upstream turbine to the downstream turbine. In each iteration of the loop (i.e. for each of the turbine), the incoming wind speed at the current turbine (U_i) is calculated from the normalized wake velocity deficit ($\frac{U_k - U_{k,i}}{U_k}$) of all the upstream turbines (calculated in the former iterations) using the wake mixing model[1]. The total turbulence intensity at the current turbine (I_{total_i}) is calculated from the added turbulence intensity ($I_{+_{k,i}}$) and the wake incidence area ($A_{s_{k,i}}$) of all the upstream turbines (calculated in the former iterations) using Equation 6.6. With U_i and I_{total_i}, the non-dimensional wake velocity deficits and the incidence areas of the wake of the current turbine on the downstream turbines are calculated using the BP model, and the added turbulence intensities in the wake of the current turbine on the downstream turbines are calculated using the Crespo - Hernandez model. Then the loop goes to the next iteration (the next turbine).

6.3 Verification of the Static Wind Farm Model

As mentioned in the literature study [21], the idea of developing the static wind farm wake model by integrating the BP model with the linear superposition wake mixing model and the Crespo - Hernandez turbulence model is originated from Niayifar and Porté-Agel [33]. Therefore, the results shown in [33] are used as benchmarks to verify the static wind farm wake model developed in this project.

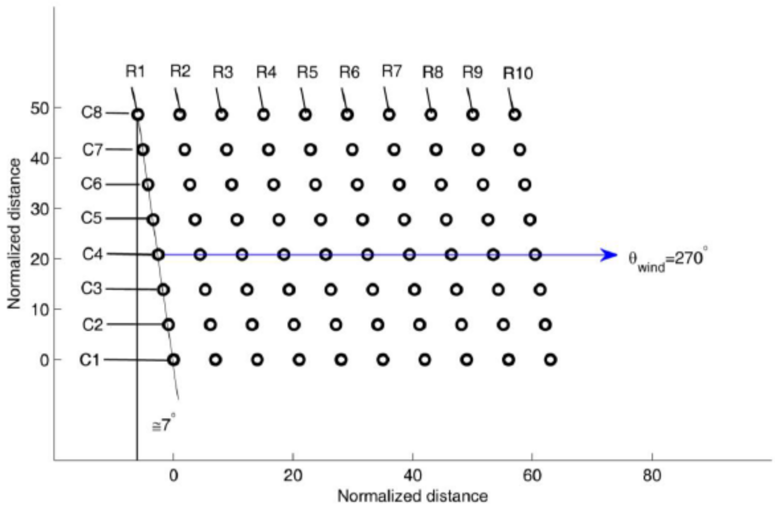

Figure 6.2: Layout of Horns Rev wind farm. Distances are normalized by the rotor diameter [33].

Consisting of 80 turbines, the layout of the Horns Rev wind farm is shown in Figure 6.2. The turbines in Horns Rev are Vestas V80, which is the turbine type used in all the studies of this project. First, the normalized wind farm power output which is weighted-averaged over all wind speeds is calculated with the static wind farm wake model in different

[1] The *normalized* deficit is calculated with Equation 6.2

wind directions (Figure 6.4) and compared with the reference results (Figure 6.3). The normalized wind farm power output is the total power of the wind farm normalized by the power of an equivalent number of stand-alone wind turbines operating in the free-stream wind condition. It can be seen that the normalized wind farm power calculated with the static wind farm wake model very well matches the global pattern in the reference. Comparing the normalized power at each wind direction, the result obtained from the static wind farm wake model is slightly higher than the result in the reference (blue circles). This small discrepancy can be originated from the difference in the input data used in the two studies, such as the power curve of the wind turbine, the thrust curve of the wind turbine and the parameters of the Weibull distribution. The above mentioned data is not clearly given in the reference.

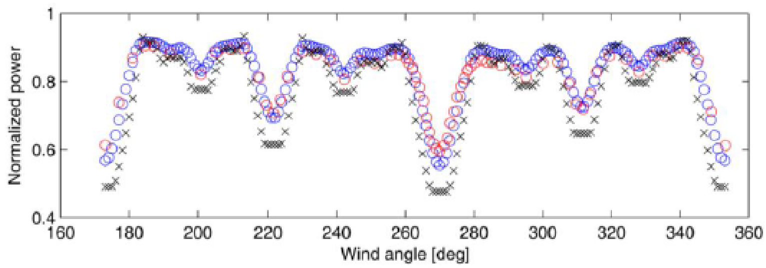

Figure 6.3: Reference result: distribution of the normalized Horns Rev wind farm power output obtained with the BP model (blue circles), Jensen-Katic model (black crosses) and Large Eddy Simulation (red circles) for different wind directions [33]. I = 7.7%.

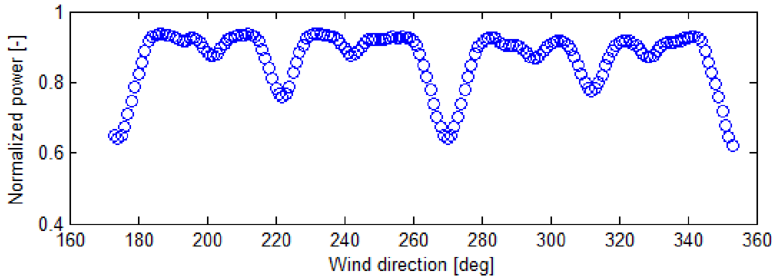

Figure 6.4: Distribution of the normalized Horns Rev wind farm power output obtained with the static wind farm wake model developed in this chapter. $I_0 = 7.7\%$

Subsequently, the normalized power output at wind direction of $270 \pm 5°$ as a function of turbine row (averaged over columns 2, 3 and 4) is compared, as shown in Figure 6.5 and Figure 6.6. The result obtained from the static wind farm wake model developed in this project is compared with the results obtained from the "New analytical Model" in the reference. The last two rows (row 9 and row 10) are not shown in Figure 6.5 and 6.6 because they are not given in the reference. It can be seen that the global trend of the two results are very similar, except for the part from row 2 to row 3. In fact, compared to the results calculated by the BP model (the "New analytical Model") in the reference, the result obtained from the static wind farm wake model is closer to the observed data in the reference.

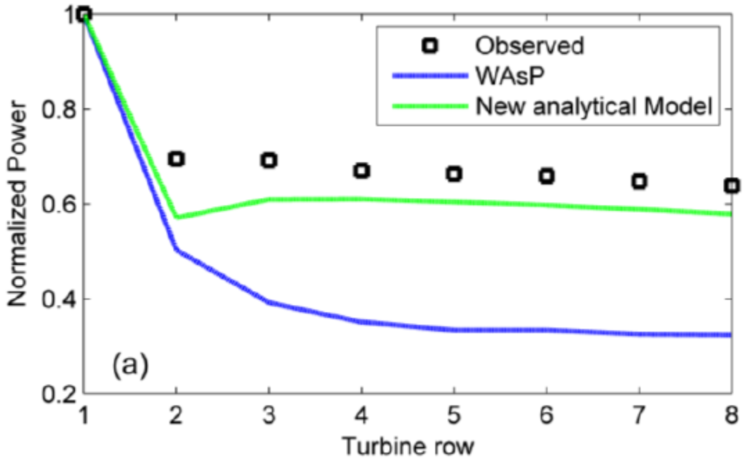

Figure 6.5: Reference result: the normalized power output at wind direction of $270 \pm 5°$ as a function of turbine row (averaged over columns 2, 3 and 4) [33]. I $= 7.7\%$. The "New analytical Model" (green line) represents the wind farm wake model developed with BP model.

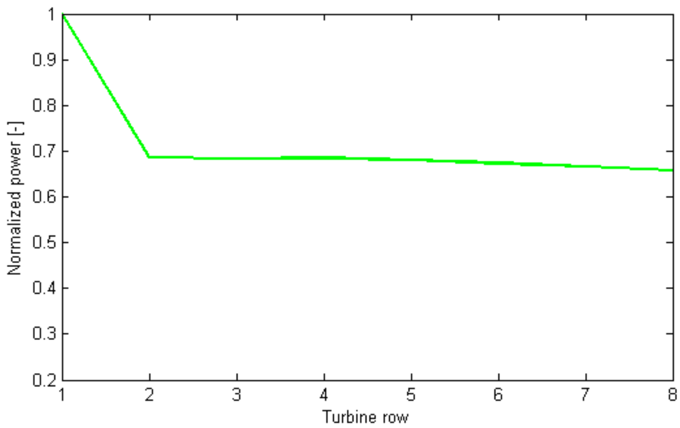

Figure 6.6: The normalized power output at wind direction of $270 \pm 5°$ as a function of turbine row (averaged over columns 2, 3 and 4), calculated from the static wind farm wake model. I $= 7.7\%$

Finally, the total turbulence intensity at wind direction of 270° as a function of turbine row is compared, as shown in Figure 6.7 and Figure 6.8. The calculated result shows a very good match with the reference results that are obtained with the Crespo - Hernandez model and LES (large eddy simulation). Only a very small difference is observed at row 2.

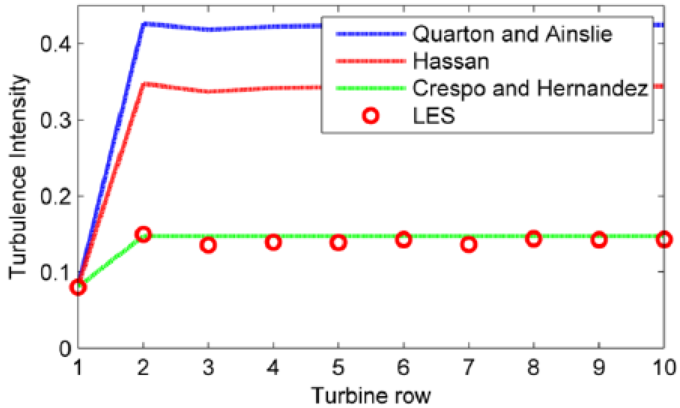

Figure 6.7: Reference result: the observed and simulated (total) turbulence intensity at hub height [33])

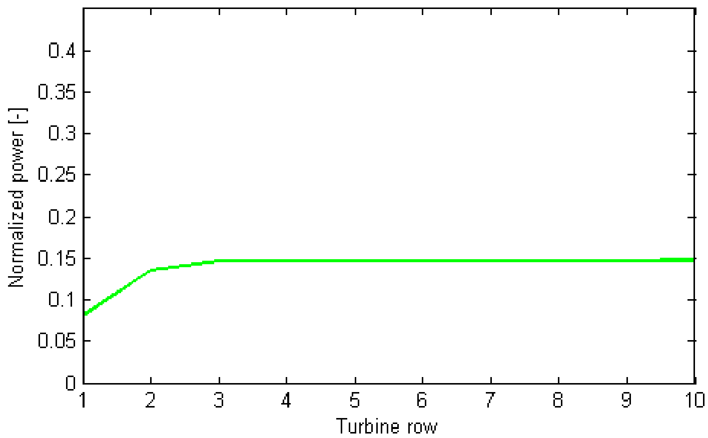

Figure 6.8: The calculated total turbulence intensity at hub height using the static wind farm wake model

In summary, the developed static wind farm wake model yields very similar results as the reference. As mentioned earlier, the small discrepancy can be originated from the differences in the input data.

6.4 Dynamic Wind Farm Wake Model

The dynamic wind farm wake model is developed by integrating the static wind farm wake model with the dynamic wake meandering model. The detailed structure of the dynamic wind farm wake model is presented in Appendix B. At first, the coordinate system and the longitudinal grids used for the wake meandering are established. As shown in Figure 6.9, the wind direction adapted coordinate system (hereafter referred to as the "WD coordinate system") is used in the dynamic wind farm wake model. In the WD coordinate system, the positive x-direction (longitudinal direction) points to the downstream wind direction, the y-direction (lateral direction) is perpendicular to the x-direction in the horizontal plane, and the positive z-direction points vertically upward. For a geographically fixed wind farm, the WD coordinates of the wind turbines are different in different wind directions. However, there are two major benefits of using the WD coordinate system. First, it is easy to sort the turbines from upstream to downstream in this coordinate system, even for the complicated wind farm layout. Moreover, the wake will always propagate in the x-direction and meander in the y and z-direction in the WD coordinate system. Using the method described in Section 5.3 and Figure 5.6, the longitudinal grids are created for the wake of each turbine in the wind farm except for the most downstream one, as shown in Figure 6.9.

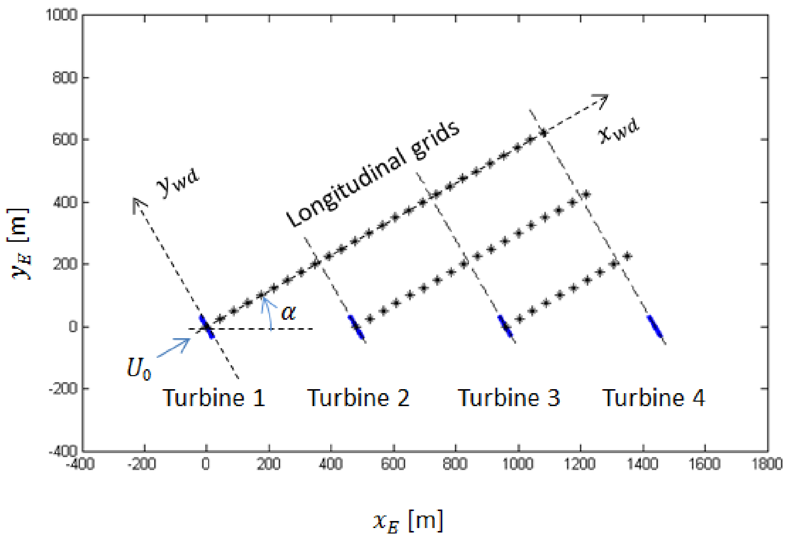

Figure 6.9: Set-up of the longitudinal grids in the wind farm of four turbines in a row. α defines the wind direction. $[x_{wd}, y_{wd}]$: wind direction adapted coordinate system. $[x_E, y_E]$: Fixed geographical coordinate system.

Subsequently, the static wind farm wake model is employed to calculate the wind turbine coordinates in the WD coordinate system, the turbulence intensity at every turbine location, and the diameter of the wake at its longitudinal grids. The turbulence intensity is used to generate the time series of the lateral and vertical turbulence velocity components (i.e. v and w, respectively) for the wake meandering, and the wake diameter is used to develop the low-pass filter for the spectrum of the turbulence velocity components in the frequency domain. The time series of v and w are generated at all the longitudinal grids. In every time step, the wake cascade of each turbine propagates along the longitudinal grids and meanders in the lateral and vertical directions as described in Section 5.3. Therefore, the time series of the location of the wake cascade on the (extended) rotor plane[2] of the wind turbines (i.e. y_w and z_w) can be determined. It can be easily

[2]It is the infinitely large vertical plane in which the wind turbine rotor lies. In Figure 6.9, it is represented by the dash line coinciding with the turbine rotor and normal to the longitudinal direction.

seen that at initialisation the wake cascade needs some travelling time before reaching the rotor plane of the downstream wind turbines, and the longest travelling time (denoted by $T_{tra,max}$) occurs to the wake cascade of the most upstream turbine to reach the rotor plane of the most downstream turbine. In order to make sure that *all* the wakes have reached *all* the rotor planes, the data in the time series y_w and z_w that are obtained during the period $T_{tra,max}$ at the beginning of the meandering process are dismissed. In this manner, the time series y_w and z_w on the rotor plane of all the turbines are synchronized in the time domain and have the same data length.

Finally, taking y_w and z_w as inputs, the static wind farm wake model is again employed to calculate the instant power output (time series) of each wind turbine in the wind farm. Hence, the time-averaged power output of the wind turbines P_{avg} in the meandering wakes can then be determined.

As mentioned in Section 5.2, the coherence between the turbulence velocity components generated at different longitudinal grids is considered for the single meandering wake. In the wind farm, the coherence of the turbulence velocity components does not only exist in the longitudinal direction, but also in the lateral direction (i.e. between the two grid points of different wakes). It is actually unknown in this project how exactly the turbulence velocities are correlated in the two-dimensional space. Hence, two extreme scenarios are simulated in this project with the dynamic wind farm wake model. First, the wake of each turbine in the wind farm is assumed to meander independently, therefore the lateral coherence is not considered. However, the coherence in the longitudinal direction is still considered for the meandering of each *individual* wake in the wind farm. In the second scenario, the wakes of all the turbines are assumed to meander with the same velocity at the same time. Moreover, the time series of turbulence velocities at all the grid points are assumed to be the same (full coherence in both lateral and longitudinal direction).

For the single turbine in the free-stream, the turbulence velocity components are generated with the ambient turbulence intensity (I_0) as input. However, for the turbines in the wind farm, it is unknown if the turbulence velocity components should be generated with the ambient turbulence intensity or the total turbulence intensity (I) at the wind turbine locations. Hence, both cases are simulated in the scenario where the wakes meander independently. In the other scenario where all the wakes meander identically, the turbulence velocity components must be generated with the same turbulence intensity for all the wakes, therefore I_0 is used in this scenario.

In summary, three versions of the dynamic wind farm wake model are developed, as described in Table 6.1.

Version of the Dynamic Wind Farm Wake Model	A	B	C
Meandering of Different Wakes	Indep.	Indep.	Ident.
Longitudinal Coherence	Yes	Yes	Yes
Lateral Coherence	No	No	Yes
Turbulence Intensity Used for Generating v & w	I	I_0	I_0

Table 6.1: Characteristics of the three versions of the dynamic wind farm wake model. (Indep.: Independent; Ident.: Identical)

6.5 Verification of the Dynamic Wind Farm Wake Model

A wind farm of six turbines in a row with turbine spacing of 6D is used for the verification of the dynamic wind farm wake model. The standard deviation of the time series y_w and z_w (i.e. σ_y and σ_z, respectively) is calculated with the dynamic wind farm wake model for (the wake of) all the upstream turbines at all positions of the downstream turbines. Then they are compared with the σ_y and σ_z obtained from the single dynamic wake meandering model using the same environmental parameters (s and I) and turbine parameters. In both the wind farm and the single wake models, the wind direction is set to be $\alpha = 0°$ and the free-stream wind speed at hub height is set to be $U_0 = 11$ m/s.

The verification is carried out for all the three versions mentioned above. Therefore, three sets of result are presented in this section, namely in Table 6.2, Table 6.3 and Table 6.4. In the top half of these tables, the (σ_y, σ_z) of all the wakes at all the downstream turbine positions are calculated in a single simulation using the dynamic wind farm wake model. On the other hand, the (σ_y, σ_z) in the bottom half of these tables is calculated one by one with the single dynamic wake meandering model using the environmental parameters and turbine parameters corresponding to the wind farm case. Due to the size limit of the tables, the values of the turbulence intensity at the turbine locations and the thrust coefficient of the turbines are only shown in the bottom half of the tables, but they are the same in the top half of the tables, correspondingly.

On	T2	T3	T4	T5	T6
Wake of					
Turbine 1 (T1)	(13.5, 5.2)	(21.5, 8.0)	(28.2, 10.3)	(33.6, 12.3)	(39.7, 14.4)
Turbine 2 (T2)	-	(21.5, 8.3)	(34.6, 13.2)	(44.7, 16.8)	(53.9, 19.8)
Turbine 3 (T3)	-	-	(25.3, 9.8)	(40.1, 15.6)	(52.9, 20.3)
Turbine 4 (T4)	-	-	-	(25.7, 9.7)	(40.9, 14.5)
Turbine 5 (T5)	-	-	-	-	(25.2, 9.8)

I	C_T	s = 6	s = 12	s = 18	s = 24	s = 30
8%	0.650	(13.3, 5.4)	(21.1, 8.1)	(27.6, 10.7)	(34.9, 12.4)	(40.3, 14.5)
12.88%	0.778	-	(21.4, 8.8)	(35.5, 12.8)	(45.0, 16.2)	(54.4, 19.5)
14.85%	0.786	-	-	(24.7, 9.5)	(40.4, 14.5)	(54.1, 19.3)
15.01%	0.786	-	-	-	(24.8, 9.6)	(41.0, 15.1)
14.98%	0.785	-	-	-	-	(24.8, 9.7)

Table 6.2: The value of (σ_y, σ_z) calculated with the dynamic wind farm wake model - Version A (top), and with the single dynamic wake meandering model (bottom) in the same conditions.

It can be seen that, for all the three versions, the σ_y and σ_z calculated with the dynamic wind farm wake model are very close to the σ_y and σ_z obtained from the single dynamic wake meandering model. Since the meandering of the wake is a random process, the values of σ_y and σ_z from the two models can not be exactly the same. Comparing version A with

On	T2	T3	T4	T5	T6
Wake of					
Turbine 1 (T1)	(13.5, 5.2)	(21.5, 8.0)	(28.2, 10.3)	(33.6, 12.3)	(40.6, 14.4)
Turbine 2 (T2)	-	(13.5, 5.2)	(21.4, 8.2)	(29.7, 10.4)	(33.5, 12.3)
Turbine 3 (T3)	-	-	(13.6, 5.3)	(21.6, 8.4)	(28.5, 10.9)
Turbine 4 (T4)	-	-	-	(13.7, 5.2)	(21.8, 7.7)
Turbine 5 (T5)	-	-	-	-	(13.4, 5.3)

I	C_T	s = 6	s = 12	s = 18	s = 24	s = 30
8%	0.650	(14.0, 5.0)	(22.1, 8.1)	(28.6, 10.4)	(35.5, 12.7)	(39.7, 13.9)
8%	0.778	-	(13.3, 5.1)	(22.2, 8.1)	(29.3, 10.4)	(33.7, 12.9)
8%	0.786	-	-	(13.2, 5.2)	(22.4, 8.2)	(28.6, 10.4)
8%	0.786	-	-	-	(13.9, 5.3)	(21.5, 8.2)
8%	0.785	-	-	-	-	(13.5, 5.4)

Table 6.3: The value of (σ_y, σ_z) calculated with the dynamic wind farm wake model - Version B (top), and with the single dynamic wake meandering model (bottom) in the same conditions.

On	T2	T3	T4	T5	T6
Wake of					
Turbine 1 (T1)	(15.5, 5.9)	(24.3, 8.8)	(30.9, 11.1)	(36.7, 13.1)	(42.4, 14.8)
Turbine 2 (T2)	-	(15.5, 5.9)	(24.3, 8.8)	(30.9, 11.1)	(36.7, 13.1)
Turbine 3 (T3)	-	-	(15.5, 5.9)	(24.3, 8.8)	(30.9, 11.1)
Turbine 4 (T4)	-	-	-	(15.5, 5.9)	(24.3, 8.8)
Turbine 5 (T5)	-	-	-	-	(15.5, 5.9)

I	C_T	s = 6	s = 12	s = 18	s = 24	s = 30
8%	0.650	(15.6, 5.8)	(24.7, 8.7)	(30.0, 10.5)	(38.0, 11.3)	(40.9, 13.7)

Table 6.4: The value of (σ_y, σ_z) calculated with the dynamic wind farm wake model - Version C (top), and with the single dynamic wake meandering model (bottom) in the same conditions.

version B of the dynamic wind farm wake model, the values of the σ_y and σ_z in version A are larger than those in version B[3], because the turbulence intensities at the locations of the downstream turbines are larger in version A. Comparing version B with version C, the values of σ_y and σ_z are higher in version C. This shows that higher coherence of the turbulence velocities in the longitudinal direction leads to larger σ_y and σ_z. In Table 6.4

[3]Except for the wake of the first turbine on the downstream turbines.

the values of σ_y and σ_z in the diagonal are the same, because the meandering of all the wakes are identical in version C.

Chapter 7

Wake Meandering Effect on Wind Farm Power and Energy Yield

7.1 Introduction

Once the dynamic wind farm wake model is developed, it is used to study the wake meandering effect on the wind farm power and annual energy yield in this chapter. First, the case of a single downstream turbine is studied in Section 7.2 with a 2-turbine wind farm. Subsequently, the study is extended to a small wind farm of six turbines in a row, as presented in Section 7.3. Finally, the two cases are compared in Section 7.4 in order to extrapolate the trend of wake meandering effect for the wind farm with even more turbines.

7.2 Case Study I: A Single Downstream Turbine

Using the wind farm of two turbines depicted in Figure 7.1, the influence of the wake meandering on the annual energy yield of the downstream turbine will be studied in this section. In order to do so, the power of the downstream turbine needs to be calculated with the dynamic wake meandering model for all the wind directions and all the operational wind speeds as mentioned in Section 2.3.2. Two aspects are taken into account while choosing the environmental parameters in this study. First, the scenario described by the chosen parameters needs to be realistic. Second, it is aimed to get an idea of the largest possible difference between the results calculated with the dynamic wake meandering model and the results calculated with the static wake model. In these regards, $s = 6$ and $I = 0.08$ are used in this study, based on the results obtained from Section 5.5.

In this study, the range of the wind direction is from $0°$ to $360°$ with a step of $1°$, and the range of U_0 is from 4 m/s (cut-in wind speed) to 25 m/s (cut-off wind speed) with a step of 1 m/s. The ΔP (defined in Section 5.5.1) is calculated in the complete range of the

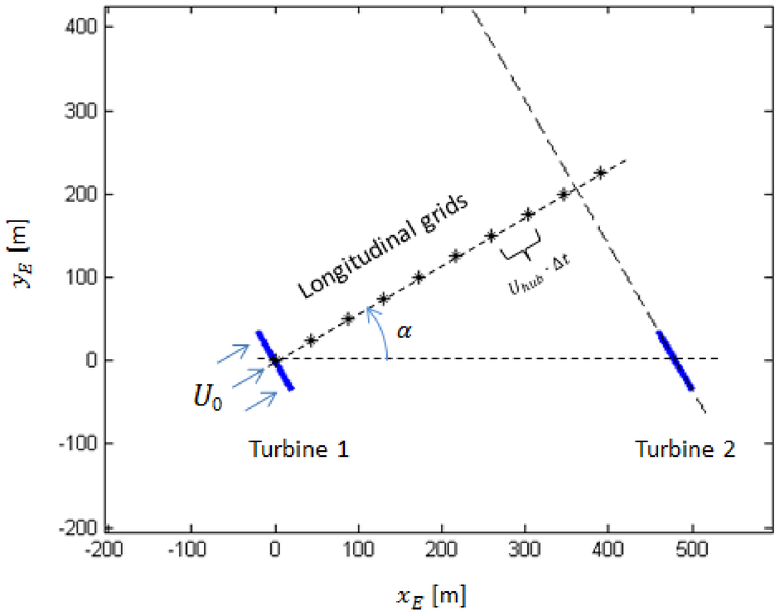

Figure 7.1: Set-up of the longitudinal grids in a wind farm of two turbines.

wind direction and wind speed. Figure 7.2 and 7.3 show the result for some representative free stream wind speed at hub height (U_0).

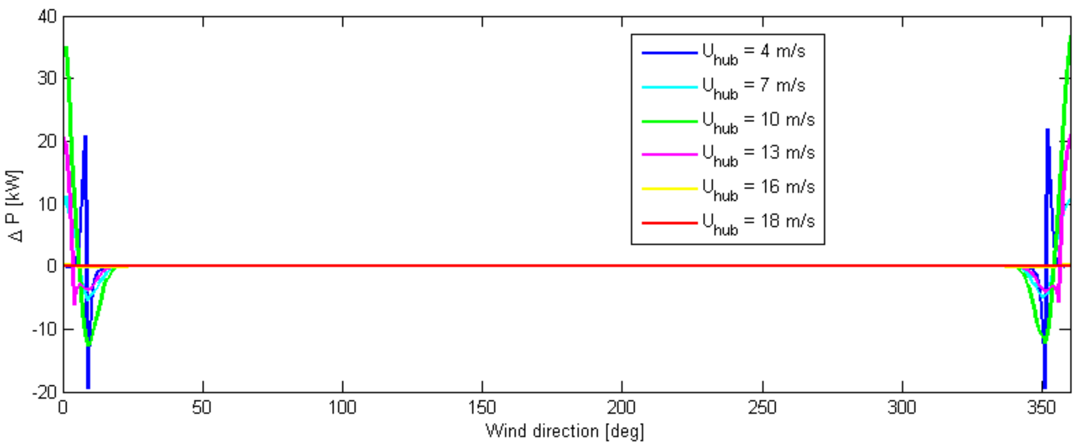

Figure 7.2: ΔP of Turbine 2 at different wind directions

It can be seen that, when the wind direction is parallel to the line of the wind turbines (i.e. $\alpha = 0°$), the meandering behaviour of the upstream turbine wake helps *increase* the power of the downstream turbine. It is because the wake is "led away" from the downstream turbine by the meandering in this case. As α increases, the wake of the upstream turbine moves away from the downstream turbine in general. At a particular wind direction, the meandering behaviour will bring the wake towards the turbine more than lead the wake away from the turbine. In this case, the wake meandering will lead to a *reduction* in the power of the downstream turbine hence a negative ΔP. As α further increases, the upstream wake will be too far away from the downstream turbine and even

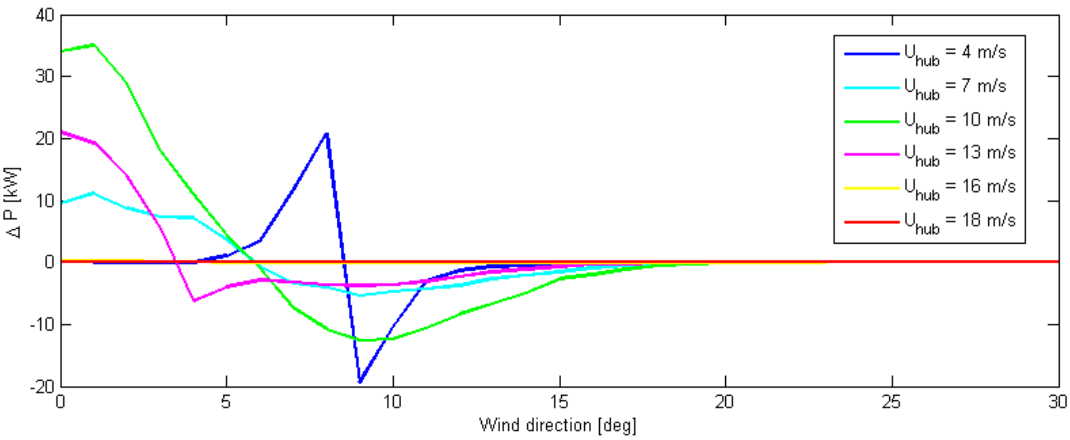

Figure 7.3: ΔP of Turbine 2 at different wind directions (zoom in of Figure 7.2

the meandering is not able to bring the wake into the downstream turbine. In this case the wake meandering will not have any influence on the power of the downstream turbine. Therefore, the ΔP generally follows the pattern "positive - decrease - negative - increase - zero" when α increases from $0°$ to $180°$.[1] The wind direction is opposite between α and $360°$ - α. Due to the symmetry of the wind farm layout, the wake meandering effect is the same for the opposite wind directions as shown in Figure 7.2. Since the ΔP for α and 360 - α are calculated from different runs of simulation, the symmetry depicted in Figure 7.2 also indicates a good converge in results of the dynamic wake meandering model with the system parameters chosen in Section 5.4.

The cut-in wind speed of the turbine is 4 m/s. In the given power curve data (as shown in Figure 4.1), the power at $U = 4\ m/s$ is 66.3 kW and the power at $U = 3\ m/s$ is 0 kW. It is not completely clear how the turbine actually starts up from $U = 3\ m/s$ to $U = 4\ m/s$. Therefore in this study it is assumed that the turbine starts up at $U = 3.8\ m/s$. When the wind speed is between $U = 3.8\ m/s$ and $U = 4\ m/s$, the wind turbine power is assumed to be the linear interpolation between 0 kW and 66.3 kW. When U_0 is 4 m/s and α is smaller than $4°$, the $U_{eq,P}$ of the downstream turbine is below 3.8 m/s no matter if the wake meanders or not, hence the ΔP is zero. As α increases, the meandering of the wake will make the $U_{eq,P}$ of the downstream turbine sometimes lager than 3.8 m/s. This explains why ΔP increases from $\alpha = 4°$ to $\alpha = 8°$ for $U_0 = 4\ m/s$.

When U_0 is above 16.5 m/s, the downstream turbine operates in the rated wind speed and therefore ΔP is zero. In Figure 7.2 and 7.3, the plot for $U_0 = 16\ m/s$ almost coincides with the plot for $U_0 = 18\ m/s$.

Two different two-dimensional wind roses are used in the calculation of the annual energy yield of the downstream turbine. The first one is the actual wind rose at the site Horns Rev, as described in Table 7.1. The second one is a hypothetical wind rose with uniform probability density over the wind directions while using the same Weibull distribution as listed in Table 7.1. For the first wind rose, the frequency of occurrence (f [%]) of the wind direction is plotted in Figure 7.4, based on Table 7.1

[1] The special case is when U_0 is 4 m/s, which will be discussed later separately.

θ Direction	0° N	30° NNE	60° ENE	90° E	120° ESE	150° SSE	180° S	210° SSW	240° WSW	270° W	300° WNW	330° NNW
C_k [m/s]	8.89	9.27	8.23	9.78	11.64	11.03	11.50	11.92	11.49	11.08	11.34	10.76
C_a [-]	2.09	2.13	2.29	2.30	2.67	2.45	2.51	2.40	2.35	2.27	2.24	2.19
f [%]	4.82	4.06	3.59	5.27	9.12	6.97	9.17	11.84	12.41	11.34	11.70	9.69

Table 7.1: Parameters of Weibull distribution (C_k: shape parameter, C_a: scale parameter) and frequency of occurrence (f) for 12 sectors [14].

The annual energy yield of the 2-turbine wind farm is calculated from Equation 2.4. When the wake meandering is considered, the P_i in Equation 2.4 is the average power $P_{dynamic,avg}$ of Turbine i. It should be noted that either Turbine 1 or Turbine 2 can be the downstream turbine in the wind farm, depending on the wind direction and the wind farm orientation. Denoted by β, the wind farm orientation is defined and illustrated in Figure 7.5.

It is obvious that the orientation of the wind farm affects the annual energy yield, especially with the non-uniform wind rose. As for the uniform wind rose described above, β still plays a role in the annual energy yield. It is because the Weibull distributions over the wind directions are still different. In this regard, E_a is calculated for different wind farm orientations, ranging from 0° to 359° with a step of 1°.

Finally, the annual energy yield of the 2-turbine wind farm is calculated and plotted as a function of the wind farm orientation in Figure 7.6 and Figure 7.7. It can be seen that, in both cases (the uniform wind rose and the wind rose of Horns Rev), the wake meandering has very little effect on the annual energy yield of the 2-turbine wind farm. Denoting the annual energy yield calculated with the static wake model (in which the wake meandering is not considered) as $E_{a,static}$, and that calculated with the dynamic wake meandering model as $E_{a,dynamic}$, the difference $E_{a,dynamic}$ - $E_{a,static}$ is denoted as ΔE_a. To have a closer look at the result, the relative change in the annual energy yield due to the wake meandering $\Delta E_a/E_{a,static}$ (in percentage) is calculated and shown in Figure 7.8. It can be seen that the wake meandering generally causes a very insignificant increase in the annual energy yield of the 2-turbine wind farm. Besides, the variation of $\Delta E_a/E_{a,static}$ as a function of β is much larger in the non-uniform wind roses than in the uniform wind roses.

7.3 Case Study II: A Wind Farm of Six Turbines

In this section, a wind farm composed of six turbines in a row is used to study the wake meandering effect on the wind farm annual energy yield. The computational time of the

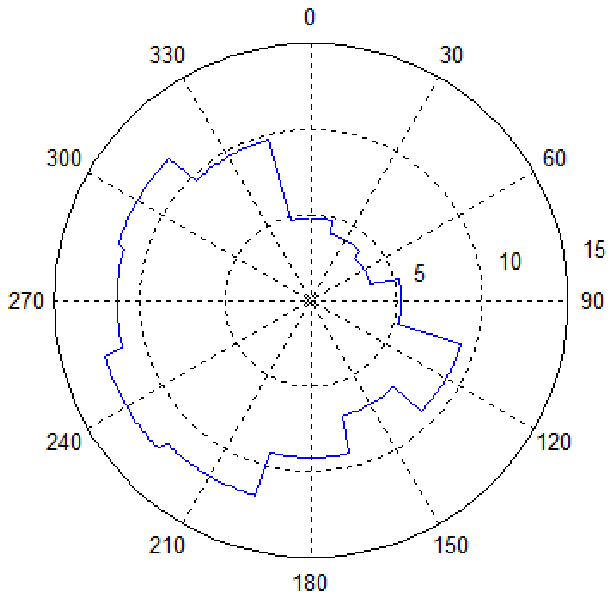

Figure 7.4: The frequency of occurrence (f [%]) of the wind direction at Horns Rev

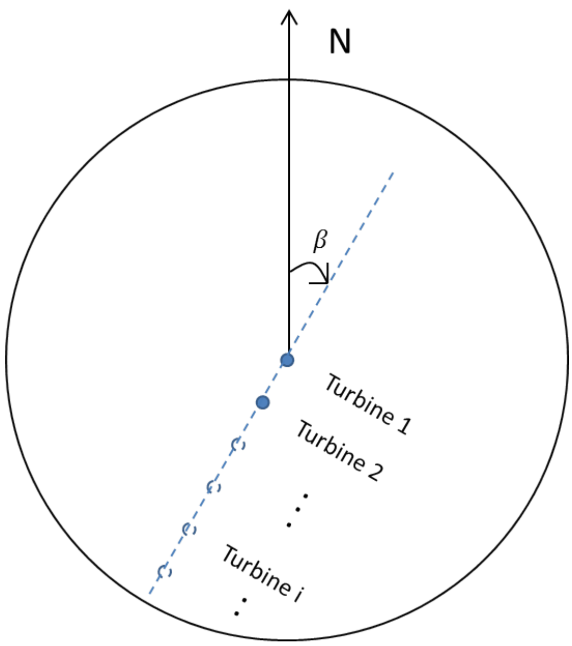

Figure 7.5: The definition of the wind farm orientation (β)

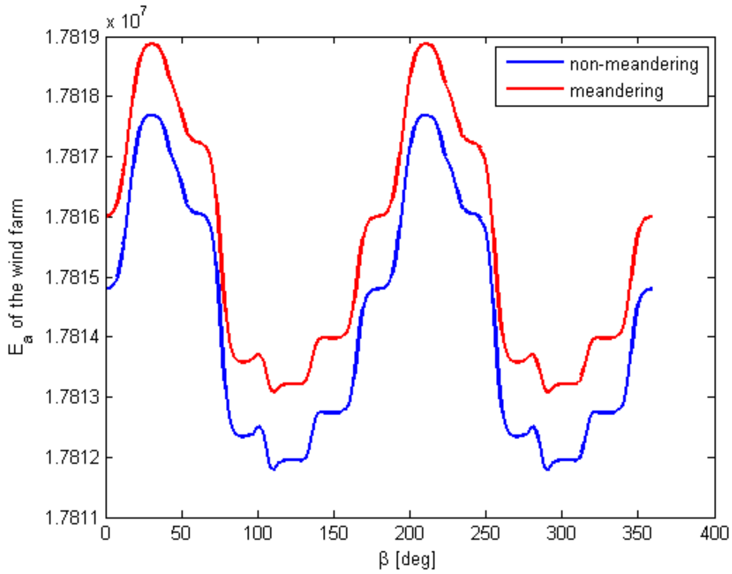

Figure 7.6: The annual energy yield of the 2-turbine wind farm as a function of the wind farm orientation in the Uniform Wind Rose

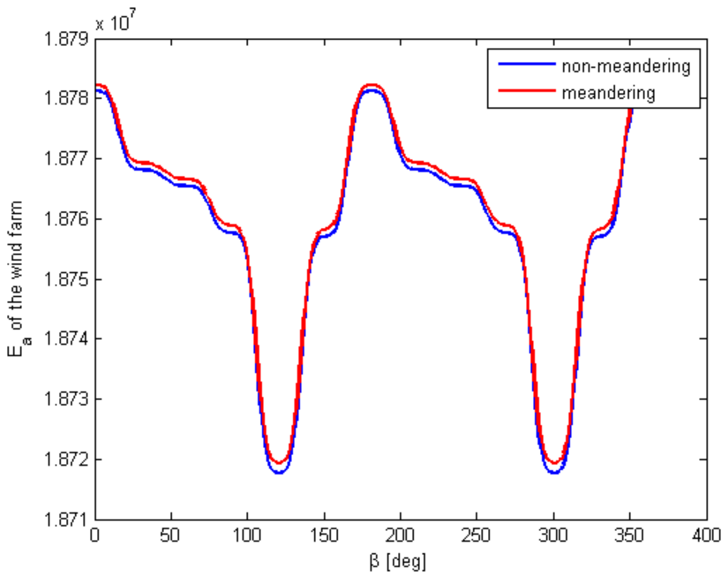

Figure 7.7: The annual energy yield of the 2-turbine wind farm as a function of the wind farm orientation in the Wind Rose of Horns Rev

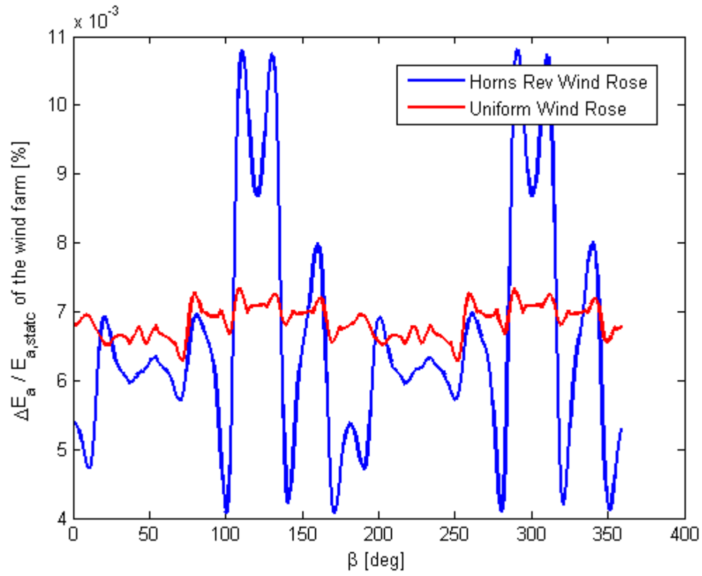

Figure 7.8: The relative change of the annual energy yield of the 2-turbine wind farm due to the wake meandering as a function of the wind farm orientation.

dynamic wind farm wake model increases significantly with the number of turbines in the wind farm. The number of six turbines is believed to be the upper limit for this project constrained by the duration of the project. In order to maximize the wake effect for the study, the six turbines are placed in a row with equal spacings instead of other layouts.

Similar to the Section 7.2, the time-averaged power output ($P_{dynamic,avg}$) of the turbines in the wind farm is computed with the dynamic wind farm wake model for all the wind directions ($0°$ to $360°$ with a step of $1°$) and operational wind speeds (4 m/s to 25 m/s with a step of 1 m/s). Since the power output of the wind turbine without considering the wake meandering is calculated by the static wind farm wake model (P_{static}), the *change* in the turbine power output due to the wake meandering (ΔP) is calculated by $P_{dynamic,avg} - P_{static}$. Besides, the turbine spacing and ambient turbulence intensity used in the 6-turbine wind farm are the same as those in the previous study of the 2-turbine wind farm ($s = 6$, $I = 0.08$).

For a specific wind farm layout, the ΔP of each turbine in the wind farm is influenced by the free-stream wind speed (U_0), the wind direction (α) and the relative position of the turbine in the wind farm. For the wind farm used in this study, it is found that the maximum ΔP of the turbines generally occurs at free-stream wind speed of 10 m/s to 14 m/s. In Figure 7.9 to 7.14, the ΔP of the turbines in the wind farm as a function of wind direction are plotted for the case U_0 is 10 m/s and 13 m/s, calculated with different versions of the dynamic wind farm wake model. Globally, it can be seen that the turbines ranked more in the downstream generally have larger magnitude of ΔP, although the values of ΔP are very small compared to the rated power of the wind turbine (2000 kW). Besides, the symmetry in the geometry of the wind farm layout is clearly reflected in these figures. Comparing Figure 7.12 with Figure 7.14 (or Figure 7.11 with Figure 7.13), it can be seen that the magnitude of ΔP is slightly higher in version C than version B of the dynamic wind farm wake model. It indicates that the wake meandering has slightly larger effect on the *power output* of the wind turbines in the wind farm if the correlation of the meandering motion is larger. This can also be reflected by the larger σ_y and σ_z in the version C compared to version B, as shown in Table 6.3 and Table 6.4. Comparing Figure 7.9 with Figure 7.11 (or Figure 7.10 with Figure 7.12), it can be found that the magnitude of ΔP is much larger in version A than in version B. It indicates that the influence of wake meandering on the power output of the wind turbines in the wind farm increases with larger turbulence intensity.

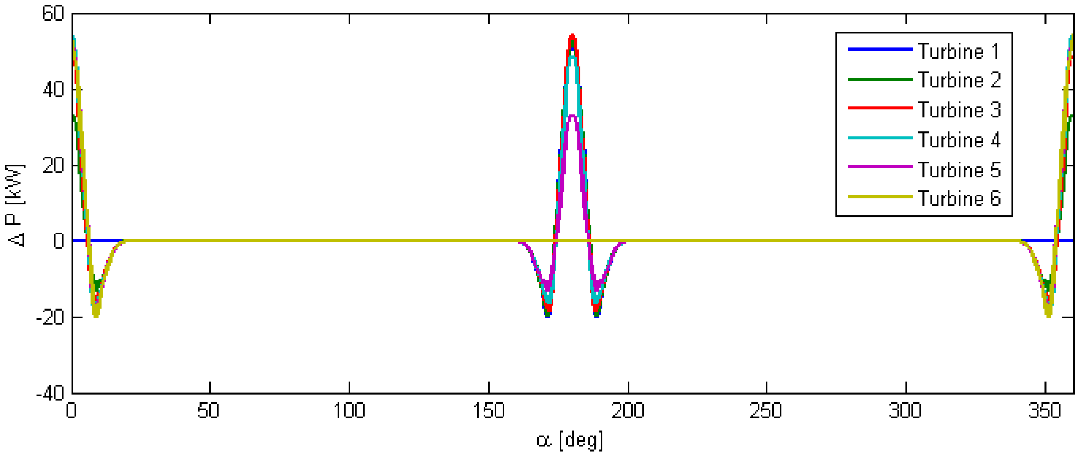

Figure 7.9: ΔP as a function of α for the turbines in the wind farm at U_0 = 10 m/s, calculated with the version A of the dynamic wind farm wake model.

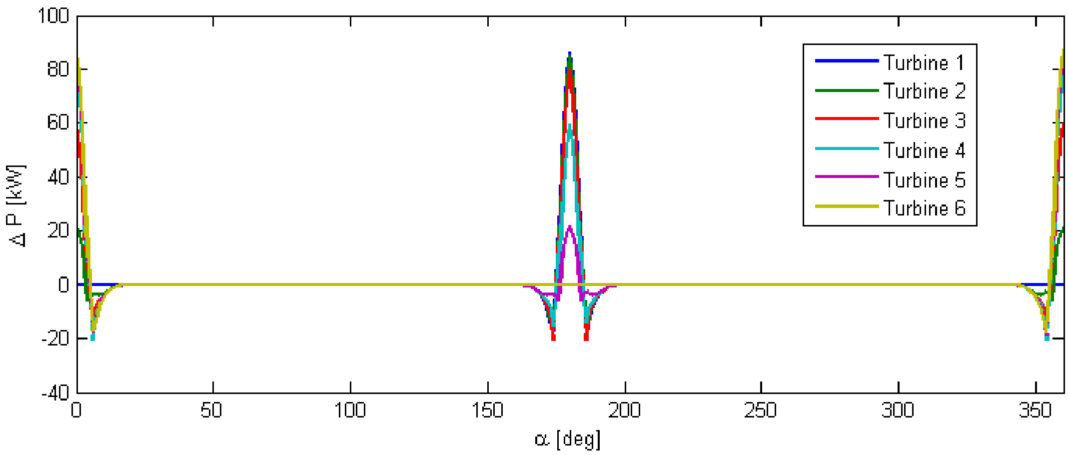

Figure 7.10: ΔP as a function of α for the turbines in the wind farm at U_0 = 13 m/s, calculated with the version A of the dynamic wind farm wake model.

With the $P_{dynamic,avg}$ obtained from the dynamic wind farm wake model, the *annual energy yield* (E_a) of the wind farm is calculated with the two wind roses described in Section 7.2 using Equation 2.4. The study is performed with all the three versions of the dynamic wind farm wake model and for different wind farm orientations (β form 0° to 360° with a step of 1°).

The annual energy yield of the wind farm calculated with different versions of the dynamic

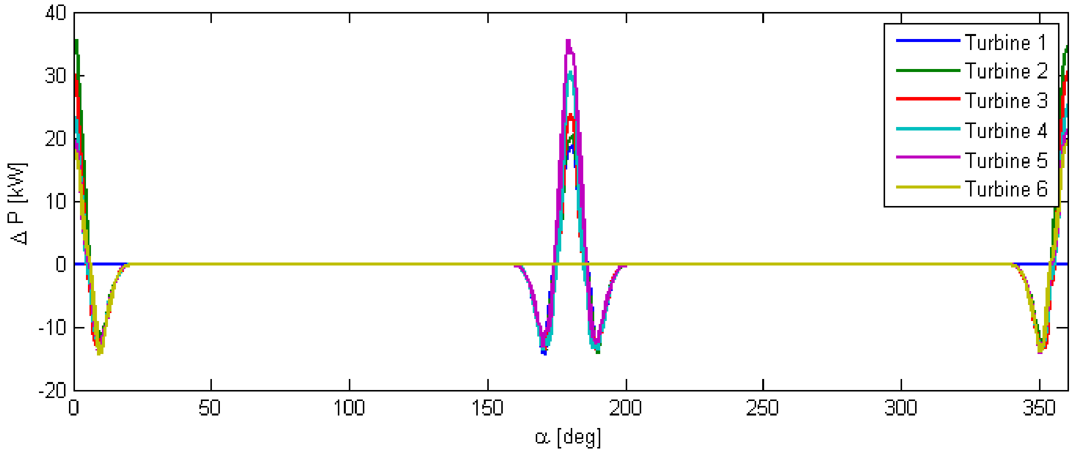

Figure 7.11: ΔP as a function of α for the turbines in the wind farm at U_0 = 10 m/s, calculated with the version B of the dynamic wind farm wake model.

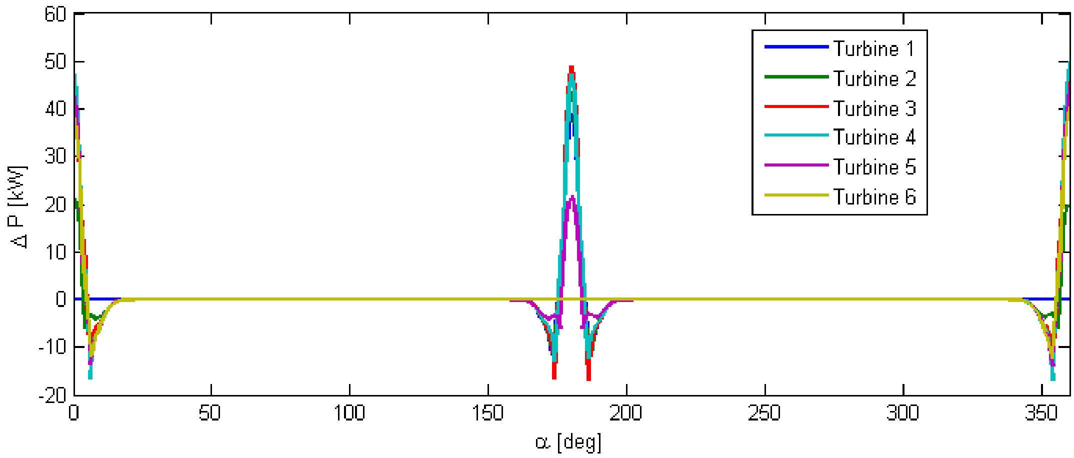

Figure 7.12: ΔP as a function of α for the turbines in the wind farm at U_0 = 13 m/s, calculated with the version B of the dynamic wind farm wake model.

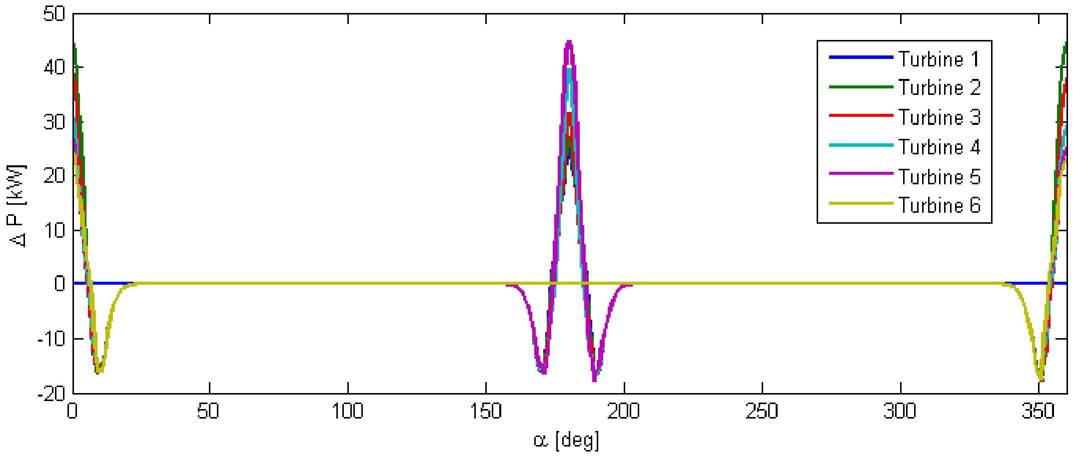

Figure 7.13: ΔP as a function of α for the turbines in the wind farm at U_0 = 10 m/s, calculated with the version C of the dynamic wind farm wake model.

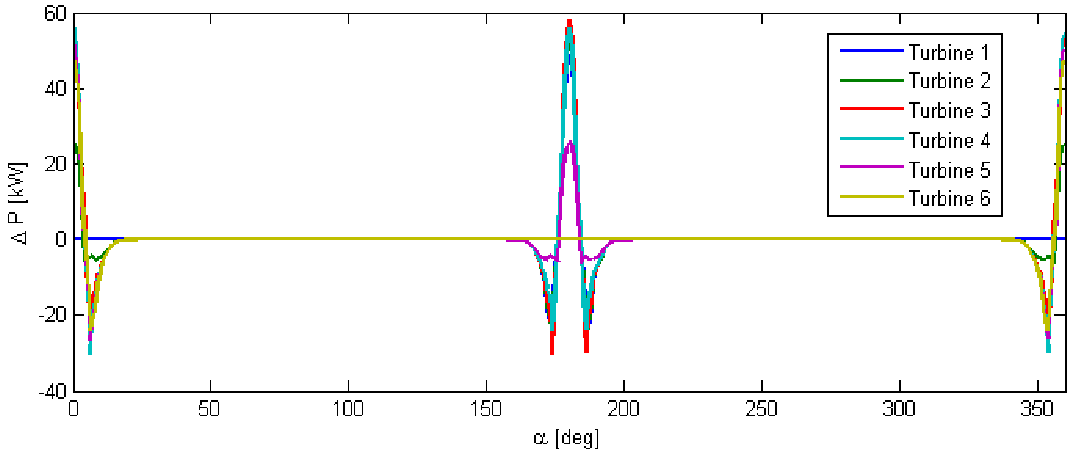

Figure 7.14: ΔP as a function of α for the turbines in the wind farm at U_0 = 13 m/s, calculated with the version C of the dynamic wind farm wake model.

wind farm wake model are compared with the E_a calculated with the static wind farm wake model in Figure 7.15. It shows that version A of the dynamic wind farm wake model delivers much larger wake meandering effect on the annual energy yield of the wind farm than the other two versions. In order to compare version B and version C, the $\Delta E_a/E_{a,static}$ (in percentage) is computed and shown in Figure 7.16. It can be seen that the difference in $\Delta E_a/E_{a,static}$ calculated by the two versions are very small. Version C yields slightly less increase (or more decrease, dependent on the wind farm orientation) in the wind farm annual energy yield than version B. Figure 7.17 shows the $\Delta E_a/E_{a,static}$ calculated with the version A of the dynamic wind farm wake model using different wind roses. It can be seen that the extreme value of $\Delta E_a/E_{a,static}$ is larger with the non-uniform wind rose. Figure 7.15, 7.16 and 7.17 collectively show that wake meandering generally causes an increase in the wind farm annual energy yield, especially when the turbulence intensity is large (version A). However, the increase (or decrease) in the wind farm annual energy yield due to wake meandering is so small (less than 0.1% in this case) that it can be neglected.

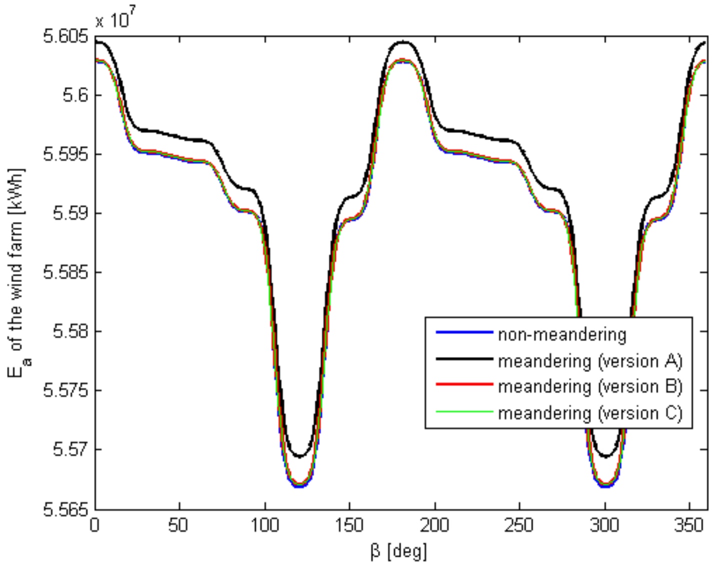

Figure 7.15: The annual energy yield of the wind farm as a function of wind farm orientation, calculated with the wind rose of Horns Rev.

7.4 Comparison of the Two Cases

Comparing Figure 7.8 with Figure 7.16, it can be seen that the relative change of the wind farm annual energy yield due to the wake meandering (i.e. $\Delta E_a/E_{a,static}$) is larger in the 2-turbine wind farm than in the 6-turbine wind farm with version B and version C of the dynamic wind farm wake model. However, comparing Figure 7.8 and Figure 7.17, it shows that the $\Delta E_a/E_{a,static}$ is larger in the 6-turbine wind farm than in the 2-turbine wind farm with version A of the dynamic wind farm wake model. In order to get an insight of this contradicting result, the $\Delta E_a/E_{a,static}$ of *each downstream turbine* in the 6-turbine wind farm (as used in the case II) is examined with all the three versions of the dynamic

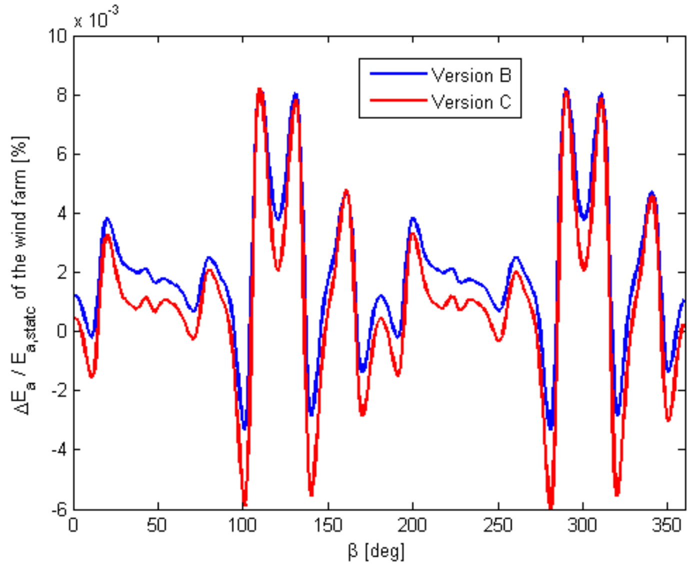

Figure 7.16: The relative change of the annual energy yield of the wind farm due to the wake meandering as a function of the wind farm orientation, calculated with the wind rose of Horns Rev.

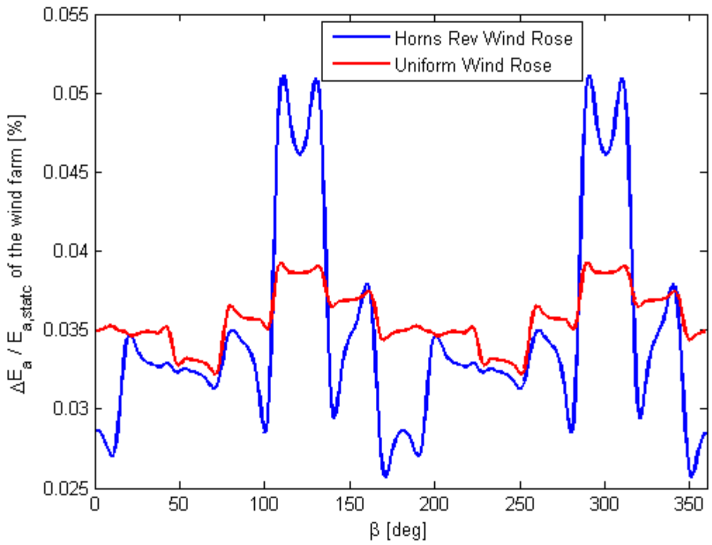

Figure 7.17: The relative change of the annual energy yield of the wind farm due to the wake meandering as a function of the wind farm orientation, calculated with the version A of the dynamic wind farm wake model.

wind farm wake model. It should be noted that, with a specific wind farm orientation, the rank of the wind turbine in the downstream position can be different with different wind directions. For instance, with $\beta = 270°$, Turbine 2 is the first downstream turbine when $\alpha = 0°$, while it becomes the fourth downstream turbine when $\alpha = 180°$. Therefore, instead of examining the $\Delta E_a / E_{a,static}$ of the specific turbine (Turbine 2, Turbine 3, etc.), it is more meaningful to examine the $\Delta E_a / E_{a,static}$ of the turbine at a specific rank of the downstream position (the first downstream turbine, the second downstream turbine, etc.). The results are shown in Figure 7.18, 7.19 and 7.20, which are calculated with version A, B, and C of the dynamic wind farm wake model, respectively. The results are presented with two wind farm orientations. The first wind farm orientation ($\beta = 111°$) is the one that yields the highest value of the $\Delta E_a / E_{a,static}$ of the wind farm. The second wind farm orientation ($\beta = 0°$) is a random pick. The wind rose at Horns Rev is used in this calculation.

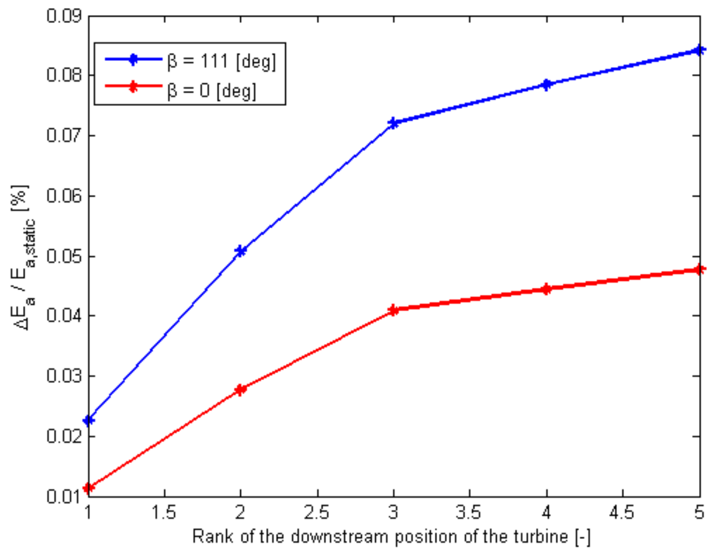

Figure 7.18: The $\Delta E_a / E_{a,static}$ [%] of the downstream wind turbines in the wind farm considered in Case II, calculated with version A of the dynamic wind farm wake model.

It can be seen from Figure 7.19 and Figure 7.20 that, the $\Delta E_a / E_{a,static}$ of the turbine calculated with version B and version C initially decreases with the rank of the downstream position of the turbine and then reaches an equilibrium at approximately the fourth downstream turbine. This phenomenon can be explained by the following reason. In the low wind speed regime ($U_0 < 12$ m/s, approximately), the ΔP of the turbine ranked further downstream is generally lower, as can be seen in Figure 7.11 and Figure 7.13. This corresponds to the decrease of the P_{static} along the downstream position in a row of turbines, as indicated in Figure 6.6. On the other hand, in the high wind speed regime, the ΔP of the turbine ranked further downstream is higher, as can be seen in Figure 7.12 and Figure 7.14. This is because the incoming wind speed of the more upstream turbines are closer to the rated wind speed, making the ΔP caused by the wake meandering diminishes as the incoming wind speed approaches the rated wind speed. In overall, the decrease of ΔP in the low wind speed regime outweighs the increase of ΔP in the high wind speed

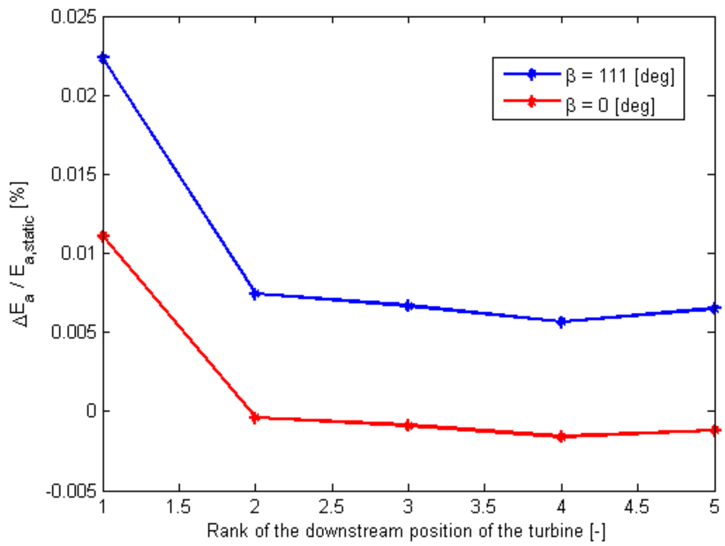

Figure 7.19: The $\Delta E_a/E_{a,static}$ [%] of the downstream wind turbines in the wind farm considered in Case II, calculated with version B of the dynamic wind farm wake model.

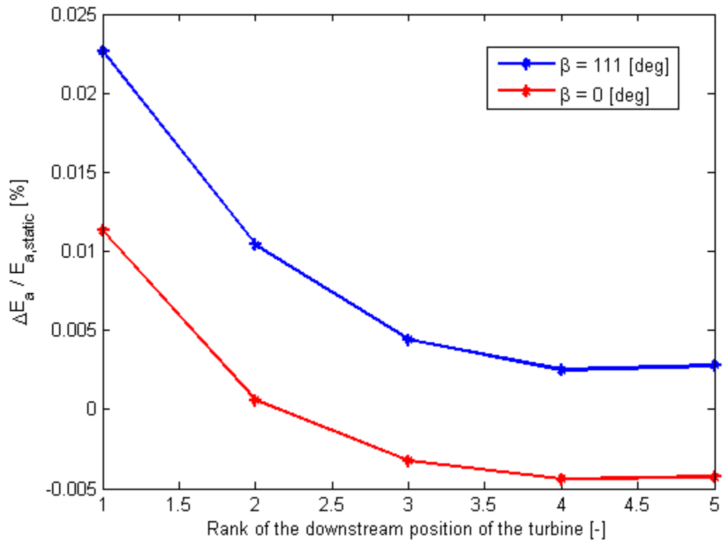

Figure 7.20: The $\Delta E_a/E_{a,static}$ [%] of the downstream wind turbines in the wind farm considered in Case II, calculated with version C of the dynamic wind farm wake model.

regime for the downstream turbine. Therefore, the turbine ranked further downstream generally has lower ΔE_a than its upstream turbines.

However, the situation is the opposite if the version A of the dynamic wind farm wake model is used, as shown in Figure 7.18. The $\Delta E_a/E_{a,static}$ of the turbine increases with the rank of the downstream position of the turbine, while the increasing *rate* reduces and reaches an equilibrium at the third downstream turbine. This can be explained by the fact that the ΔP of the turbine ranked further downstream is globally increased due to the larger σ_y and σ_z (as can be seen in Figure 7.9 and Figure 7.10), which are in turn caused by the larger turbulence intensity used to generate the turbulence velocity components in version A.

Hence, for the wind farm composed of a single row of turbines, the following conclusion can be drawn. If I_0 is used to generate the turbulence velocity components for the wake meandering (as in version B and version C), the $\Delta E_a/E_{a,static}$ of the wind farm will decrease as the number of turbines increases. On the contrary, if I is used to generate the turbulence velocity components for the wake meandering (as in version A), the $\Delta E_a/E_{a,static}$ of the wind farm will increase as the number of turbines increases. However, the increasing rate of $\Delta E_a/E_{a,static}$ with the number of turbines in the latter case is expected to be very low, which is deduced from Figure 7.18.

Chapter 8

Conclusions

8.1 Conclusions

The initial purpose of this Master thesis project is to develop a simple wind farm wake model suitable for the wind farm layout optimization considering the wake meandering effect. However, with the dynamic wind farm wake model developed in Chapter 6, it is found that the wake meandering effect on the wind farm annual energy yield is very insignificant. For a wind farm consisting of six turbines in a row, the change in the annual energy yield of the wind farm caused by wake meandering is less than 0.1% based on the developed dynamic wind farm wake model. Therefore, it can be concluded that it is not meaningful to develop such simple wake model for the wind farm layout optimization that takes the wake meandering effect on the wind farm annual energy yield into account.

The dynamic wind farm wake model developed in this project is very computationally expensive, hence it is not suitable for the wind farm layout optimization. Instead, the static wind farm wake model developed based on the BP model is recommended for this purpose. Although the static wind farm wake model does not consider the meandering motion of the wake, it has very high accuracy benchmarking against the dynamic wind farm wake model in terms of the wake meandering effect on the wind farm annual energy yield. It is believed that one of the main reasons for the high accuracy of the static wind farm wake model is the Gaussian profile of the velocity deficit in the wake used in the BP model. The dynamic wake meandering model has shown that the position of the wake center falls into the two-dimensional Gaussian distribution in the y-z plane during meandering. Hence, the Gaussian profile of the velocity deficit is considered to be more accurate than the top-hat profile (as used in the Jensen-Katic model and Frandsen model) for the static wake.

As for the wake meandering effect on the annual energy yield of the wind farm, it can be concluded that wake meandering generally causes an increase in the wind farm annual energy yield, especially when the turbulence intensity is large. Besides, the coherence of the atmospheric turbulence velocity components does not play an import role in the wake meandering effect on the annual energy yield. For a wind farm composed of a single row of turbines, the relative difference between the wind farm annual energy yield calculated with and without the wake meandering ($\Delta E_a/E_{a,static}$) will decline as the number of turbine increases if the ambient turbulence intensity is used to generate the turbulence velocity for the wake meandering. On the contrary, if the total turbulence intensity at the turbine location is used to generate the turbulence velocity for the wake meandering, the $\Delta E_a/E_{a,static}$ of the wind farm will incline with increasing number of turbines, but in a very slow rate.

8.2 Recommendations for the Future Work

Due to the time limit in this thesis project, only a very simple wind farm layout (i.e. a row of six turbines) is studied with the dynamic wind farm wake model. In order to verify the conclusion in the generic wind farm, it is recommended to perform the same study on a larger wind farm with multiple rows and columns.

Besides, the static wind farm wake model and the dynamic wind farm wake model developed in this project are based on the BP single-wake model. It is recommended to compare the BP model with other single-wake models in the study of the wake meandering effect on the wind farm annual energy yield.

Last but not the least, it is highly recommended to validate the static wind farm wake model and the dynamic wind farm wake model developed in this project with the actual wind farm measurements.

References

[1] Abkar, M., and Porté-Agel, F. A new wind-farm parameterization for large-scale atmospheric models. *Journal of Renewable and Sustainable Energy 7*, 1 (2015), 013121.

[2] Ainslie, J. F. Calculating the flowfield in the wake of wind turbines. *Journal of Wind Engineering and Industrial Aerodynamics 27*, 1 (1988), 213–224.

[3] Barthelmie, R. J., Frandsen, S. T., Nielsen, M., Pryor, S., Rethore, P.-E., and Jørgensen, H. Modelling and measurements of power losses and turbulence intensity in wind turbine wakes at middelgrunden offshore wind farm. *Wind Energy 10*, 6 (2007), 517–528.

[4] Bastankhah, M., and Porté-Agel, F. A new analytical model for wind-turbine wakes. *Renewable Energy 70* (2014), 116–123.

[5] Bingöl, F., Mann, J., and Larsen, G. C. Light detection and ranging measurements of wake dynamics part i: one-dimensional scanning. *Wind energy 13*, 1 (2010), 51–61.

[6] Bossanyi, E. Gh bladed theory manual. *GH & Partners Ltd* (2003).

[7] Chamorro, L. P., and Porté-Agel, F. A wind-tunnel investigation of wind-turbine wakes: boundary-layer turbulence effects. *Boundary-layer meteorology 132*, 1 (2009), 129–149.

[8] Choi, J., and Shan, M. Advancement of jensen (park) wake model. In *Proceedings of the European Wind Energy Conference and Exhibition* (2013), pp. 1–8.

[9] Churchfield, M. J., Moriarty, P. J., Hao, Y., Lackner, M. A., Barthelmie, R., Lundquist, J. K., and Oxley, G. S. A comparison of the dynamic wake meandering model, large-eddy simulation, and field data at the egmond aan zee offshore wind plant.

[10] Commission, I. E., et al. Iec 61400-1: Wind turbines part 1: Design requirements. *International Electrotechnical Commission* (2005).

[11] Crespo, A., Herna, J., et al. Turbulence characteristics in wind-turbine wakes. *Journal of wind engineering and industrial aerodynamics 61*, 1 (1996), 71–85.

[12] Crespo, A., Hernandez, J., and Frandsen, S. Survey of modelling methods for wind turbine wakes and wind farms. *Wind energy 2*, 1 (1999), 1–24.

[13] Diamond, K. E., and Crivella, E. J. Wind turbine wakes, wake effect impacts, and wind leases: Using solar access laws as the model for capitalizing on wind rights during the evolution of wind policy standards. *Duke Envtl. L. & Pol'y F. 22* (2011), 195.

[14] Feng, J., and Shen, W. Z. Modelling wind for wind farm layout optimization using joint distribution of wind speed and wind direction. *Energies 8*, 4 (2015), 3075–3092.

[15] Frandsen, S., Barthelmie, R., Pryor, S., Rathmann, O., Larsen, S., Højstrup, J., and Thøgersen, M. Analytical modelling of wind speed deficit in large offshore wind farms. *Wind energy 9*, 1-2 (2006), 39–53.

[16] Frandsen, S. T., and Thøgersen, M. L. Integrated fatigue loading for wind turbines in wind farms by combining ambient turbulence and wakes. *Wind Engineering 23* (1999), 327–339.

[17] Gaumond, M., Réthoré, P.-E., Ott, S., Peña, A., Bechmann, A., and Hansen, K. S. Evaluation of the wind direction uncertainty and its impact on wake modeling at the horns rev offshore wind farm. *Wind Energy 17*, 8 (2014), 1169–1178.

[18] González-Longatt, F., Wall, P., and Terzija, V. Wake effect in wind farm performance: Steady-state and dynamic behavior. *Renewable Energy 39*, 1 (2012), 329–338.

[19] Guillén, F. B. Development of a design tool for offshore wind farm layout optimization. Master's thesis, Delft University of technology, 2009.

[20] Hansen, K. S., Barthelmie, R., Jensen, L. E., and Sommer, A. Power deficits due to wind turbine wakes at horns rev wind farm. *Torque* (2010).

[21] Hu, B. Literature study for the design of a simple wake model considering the wake meandering effect. Unpublished article in Delft University of Technology, 2015.

[22] Jensen, N. O. *A note on wind generator interaction.* 1983.

[23] Katic, I., Højstrup, J., and Jensen, N. A simple model for cluster efficiency. In *European Wind Energy Association Conference and Exhibition* (1986), pp. 407–410.

[24] Kiranoudis, C., and Maroulis, Z. Effective short-cut modelling of wind park efficiency. *Renewable Energy 11*, 4 (1997), 439–457.

[25] Lange, B., Waldl, H.-P., Guerrero, A. G., Heinemann, D., and Barthelmie, R. J. Modelling of offshore wind turbine wakes with the wind farm program flap. *Wind Energy 6*, 1 (2003), 87–104.

[26] Larsen, G. C. *A simple wake calculation procedure.* 1988.

[27] Larsen, G. C., Aagaard Madsen, H., Troldborg, N., Larsen, T. J., Réthoré, P.-E., Fuglsang, P., Ott, S., Mann, J., Buhl, T., Nielsen, M., et al. Topfarm-next generation design tool for optimisation of wind farm topology and operation. Tech. rep., Danmarks Tekniske Universitet, Risø Nationallaboratoriet for Bæredygtig Energi, 2011.

[28] Larsen, G. C., Højstrup, J., and Aagaard Madsen, H. Wind fields in wakes. In *1996 European Wind Energy Conference and Exhibition* (1996), pp. 764–768.

[29] Larsen, G. C., Madsen, H. A., Thomsen, K., and Larsen, T. J. Wake meandering: a pragmatic approach. *Wind energy 11*, 4 (2008), 377–395.

[30] Larsen, G. C., Madsen Aagaard, H., Bingöl, F., Mann, J., Ott, S., Sørensen, J. N., Okulov, V., Troldborg, N., Nielsen, N. M., Thomsen, K., et al. Dynamic wake meandering modeling. Tech. rep., Risø National Laboratory, 2007.

[31] Martínez, J. E. G. Layout optimisation of offshore wind farms with realistic constraints and options. Master's thesis, Delft University of technology, 2014.

[32] Medici, D., and Alfredsson, P. Measurements on a wind turbine wake: 3d effects and bluff body vortex shedding. *Wind Energy 9*, 3 (2006), 219–236.

[33] Niayifar, A., and Porté-Agel, F. A new analytical model for wind farm power prediction. In *Journal of Physics: Conference Series* (2015), vol. 625, IOP Publishing, p. 012039.

[34] Nygaard, N., Jensen, L., Downey, R., and Méchali, M. Construction and validation of a new offshore wake model. In *Proceedings of the International Conference on Aerodynamics of Offshore Wind Energy Systems and Wakes (ICOWES) Conference, Lyngby, Danmark* (2013), vol. 1719.

[35] Porté-Agel, F., Wu, Y.-T., and Chen, C.-H. A numerical study of the effects of wind direction on turbine wakes and power losses in a large wind farm. *Energies 6*, 10 (2013), 5297–5313.

[36] Tesauro, A., Réthoré, P.-E., and Larsen, G. C. State of the art of wind farm optimization. In *EWEA 2012-European Wind Energy Conference & Exhibition* (2012).

[37] Thogersen, M. L., Sorensen, T., Nielsen, P., Grotzner, A., and Chun, S. Introduction to wind turbine wake modelling and wake generated turbulence. *DNV/Risø, 2nd ed.: Risø National Laboratory, EMD International A/S* (2006).

[38] Tong, W., Chowdhury, S., Zhang, J., and Messac, A. Impact of different wake models on the estimation of wind farm power generation. In *12th AIAA Aviation Technology, Integration, and Operations (ATIO) Conference and 14th AIAA/ISSMO Multidisciplinary Analysis and Optimization Conference, American Institute of Aeronautics and Astronautics* (2012).

[39] Trujillo, J.-J., Bingöl, F., Larsen, G. C., Mann, J., and Kühn, M. Light detection and ranging measurements of wake dynamics. part ii: two-dimensional scanning. *Wind Energy 14*, 1 (2011), 61–75.

[40] Vestas. Vestas V90 Power Curve, July 2015. Available at http://www.vestas.com/en/products_and_services/turbines/v90-3_0_mw#!power-curve.

[41] Wu, Y.-T., and Porté-Agel, F. Atmospheric turbulence effects on wind-turbine wakes: An les study. *energies 5*, 12 (2012), 5340–5362.

[42] Zaaijer, M. B. *Great expectations for offshore wind turbines: Emulation of wind farm design to anticipate their value for customers*. PhD thesis, Delft University of Technology, 2013.

Appendix A

Structure of the Static Wind Farm Wake Model (Without Wake Meandering)

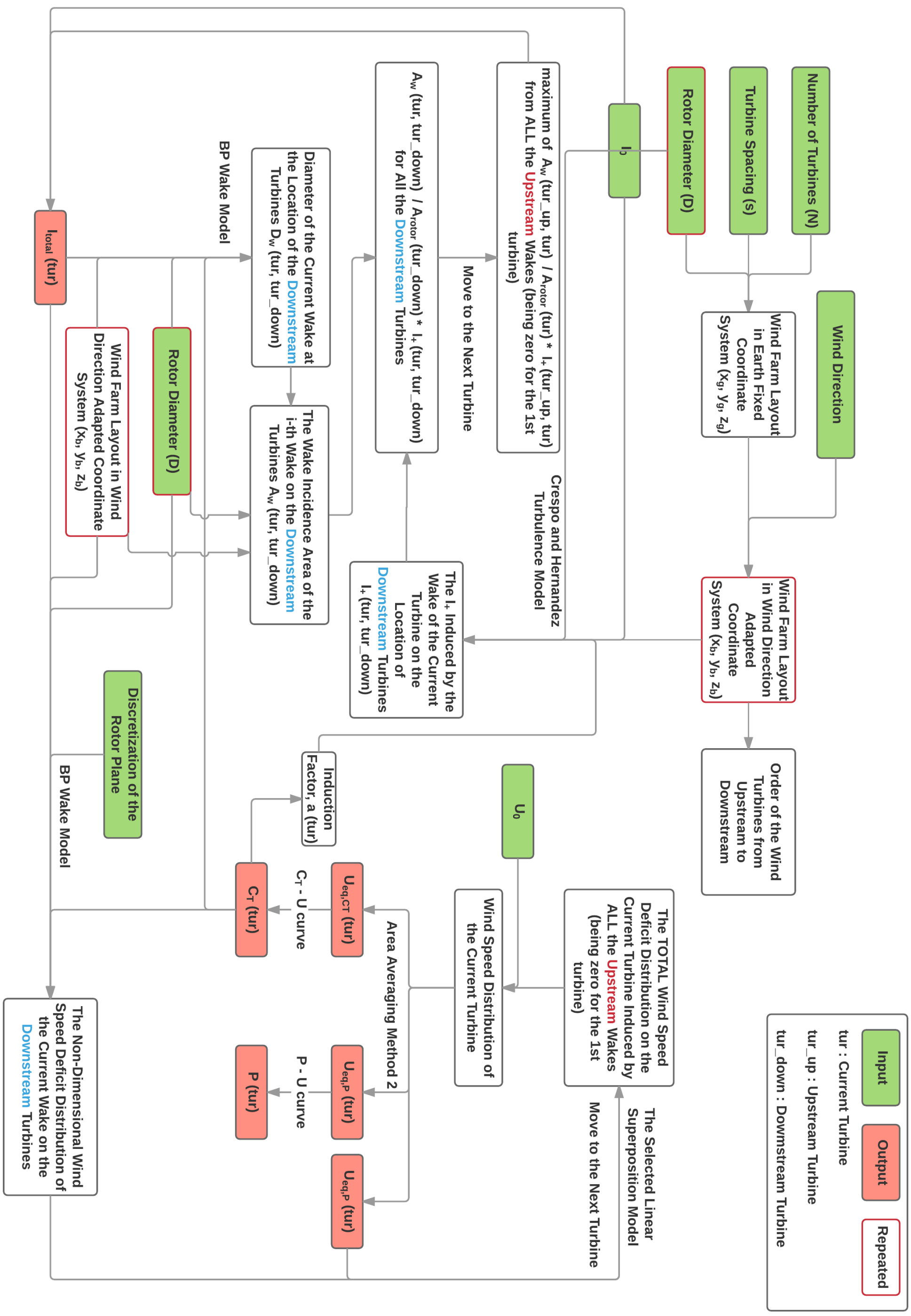

Number of Turbines (N)
Turbine Spacing (s)
Rotor Diameter (D)
I0
Wind Direction
Wind Farm Layout in Earth Fixed Coordinate System (xg, yg, zg)
Wind Farm Layout in Wind Direction Adapted Coordinate System (xb, yb, zb)
Order of the Wind Turbines from Upstream to Downstream
maximum of Aw (tur_up, tur) / Arotor (tur) * I+ (tur_up, tur) from ALL the Upstream Wakes (being zero for the 1st turbine)
Move to the Next Turbine
Aw (tur, tur_down) / Arotor (tur_down) * I+ (tur, tur_down) for All the Downstream Turbines
Crespo and Hernandez Turbulence Model
The I+ Induced by the Wake of the Current Turbine on the Location of Downstream Turbines I+ (tur, tur_down)
Itotal (tur)
Diameter of the Current Wake at the Location of the Downstream Turbines Dw (tur, tur_down)
BP Wake Model
The Wake Incidence Area of the i-th Wake on the Downstream Turbines Aw (tur, tur_down)
Rotor Diameter (D)
Wind Farm Layout in Wind Direction Adapted Coordinate System (xb, yb, zb)
Discretization of the Rotor Plane
BP Wake Model
Induction Factor, a (tur)
U0
CT (tur)
CT - U curve
Ueq,CT (tur)
Area Averaging Method 2
Wind Speed Distribution of the Current Turbine
The TOTAL Wind Speed Deficit Distribution on the Current Turbine Induced by ALL the Upstream Wakes (being zero for the 1st turbine)
The Selected Linear Superposition Model
Move to the Next Turbine
Ueq,P (tur)
P - U curve
P (tur)
Ueq,P (tur)
The Non-Dimensional Wind Speed Deficit Distribution of the Current Wake on the Downstream Turbines
Input
Output
Repeated
tur : Current Turbine
tur_up : Upstream Turbine
tur_down : Downstream Turbine

Figure A.1: .

Appendix B

Structure of the Dynamic Wind Farm Wake Model (Including Wake Meandering)

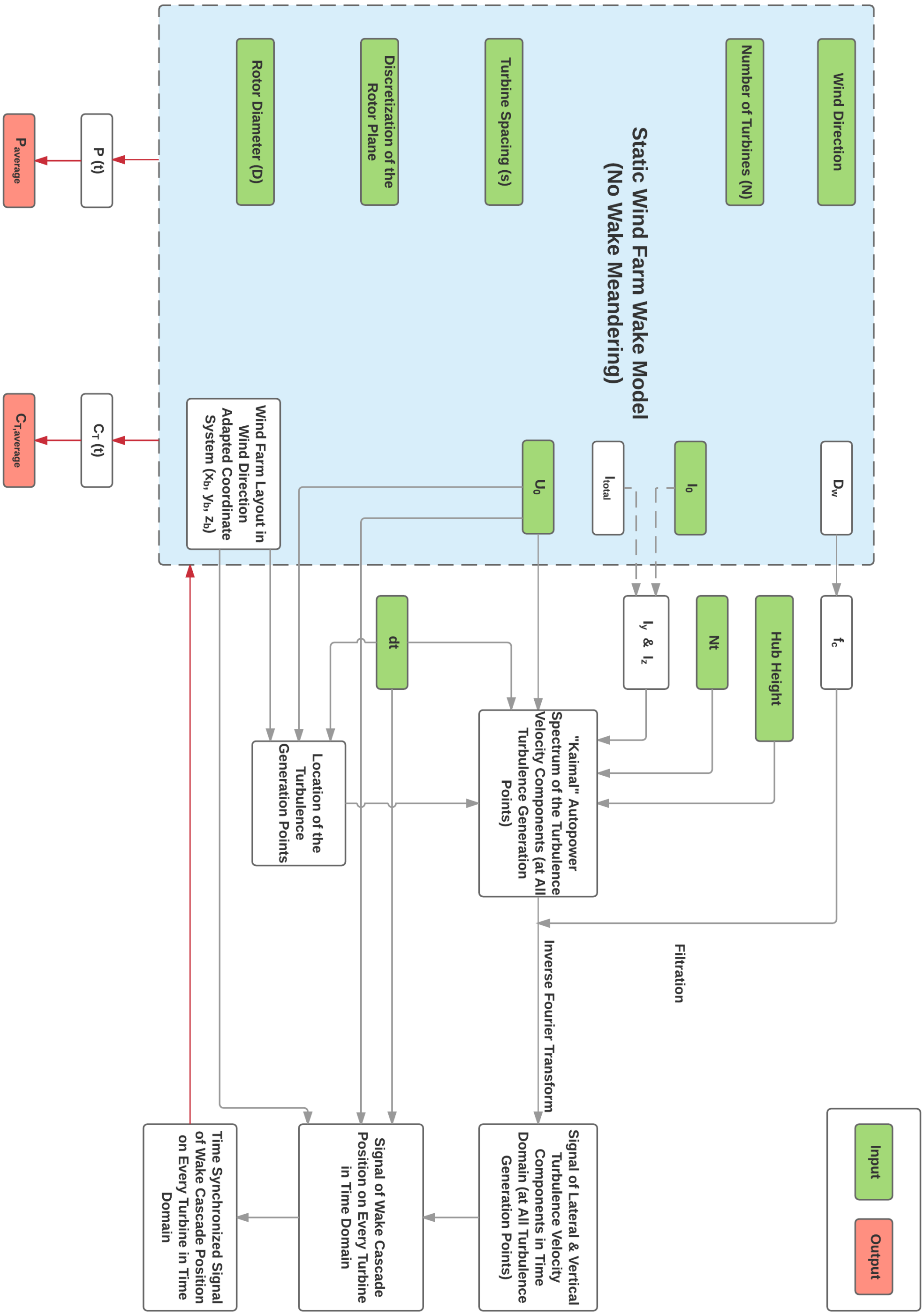

Static Wind Farm Wake Model
(No Wake Meandering)
Wind Direction
Number of Turbines (N)
Turbine Spacing (s)
Discretization of the Rotor Plane
Rotor Diameter (D)
P (t)
P average
Dw
I0
Itotal
U0
Wind Farm Layout in Wind Direction Adapted Coordinate System (xb, yb, zb)
CT (t)
CT,average
fc
Hub Height
Nt
Iy & Iz
dt
"Kaimal" Autopower Spectrum of the Turbulence Velocity Components (at All Turbulence Generation Points)
Location of the Turbulence Generation Points
Filtration
Inverse Fourier Transform
Signal of Lateral & Vertical Turbulence Velocity Components in Time Domain (at All Turbulence Generation Points)
Signal of Wake Cascade Position on Every Turbine in Time Domain
Time Synchronized Signal of Wake Cascade Position on Every Turbine in Time Domain
Input
Output

Figure B.1: .